The relation between cold dust and star formation in nearby galaxies

George J. Bendo
(with the Herschel Local Galaxies Guaranteed-Time Surveys and the Herschel Virgo Cluster Survey)

Outline

- Analyses before Herschel (IRAS and Spitzer)
- Work with Herschel data on M81, M83, NGC 2403
- Other Herschel analyses (including M31 and M33)
- New work with more nearby galaxies (because showing old data by itself would get boring)


Before Herschel

IRAS results

Early IRAS analyses produced conflicting interpretations:

- Some groups found that IRAS fluxes were correlated with star formation tracers.
- Other groups found that older stars could explain at least part of the infrared emission.

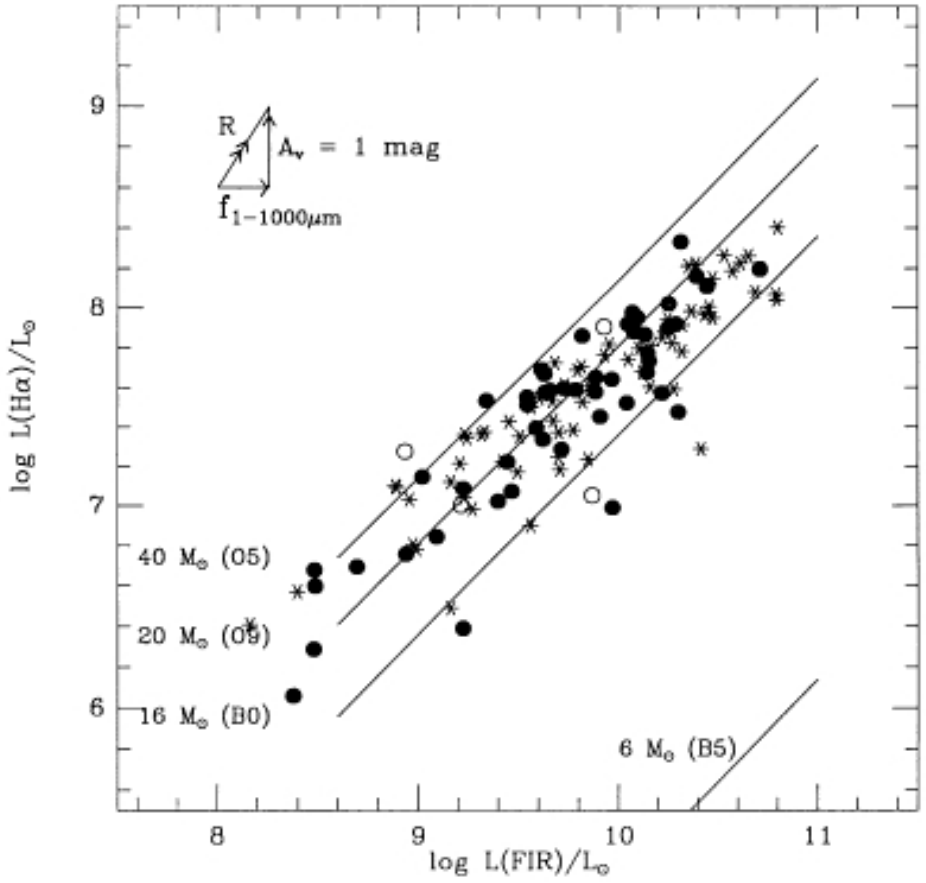

Devereux & Young
1990, ApJ, 350, L25

IRAS results

Early IRAS analyses produced conflicting interpretations:

- Some groups found that IRAS fluxes were correlated with star formation tracers.
- Other groups found that older stars could explain at least part of the infrared emission.

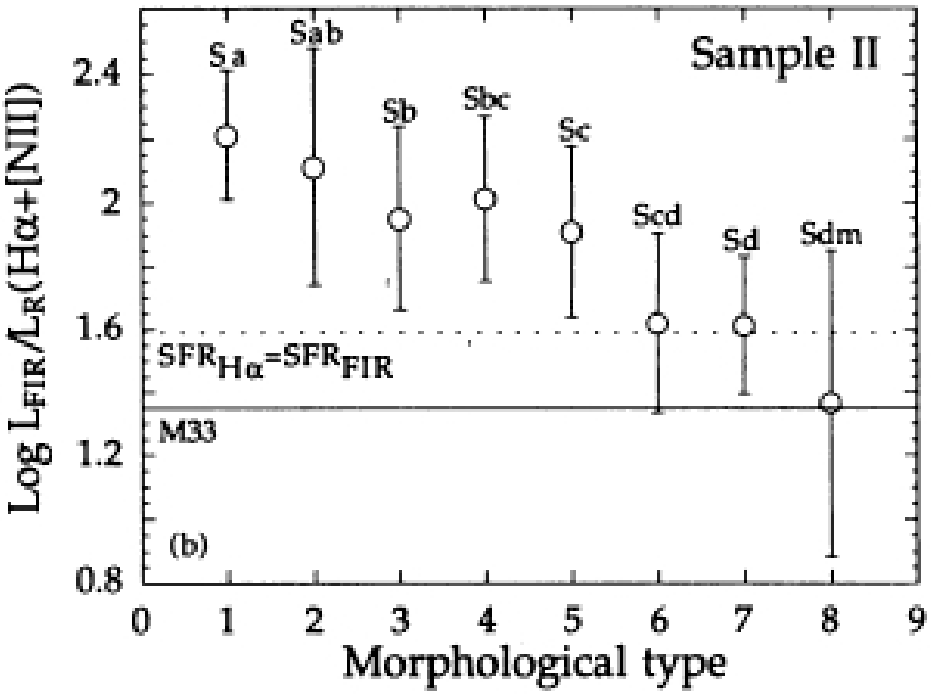

Sauvage & Thuan
1992, ApJ, 396, L69

Spitzer results

- The relation between infrared emission and other star formation tracers showed more scatter as the infrared wavelength increased.
- Other analyses indicated that emission at 160 μm could be tied to older stellar populations.

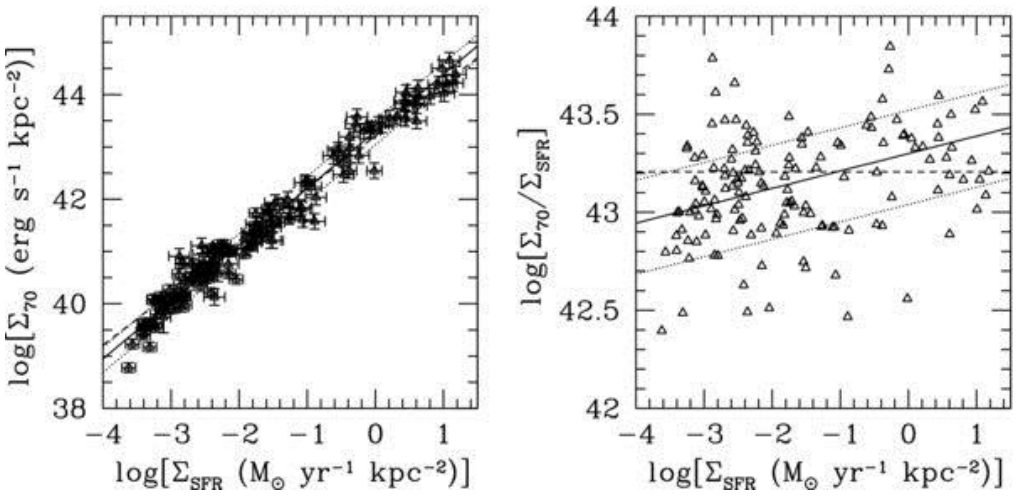

Calzetti et al.
2010, ApJ, 714, 1256

Spitzer results

- The relation between infrared emission and other star formation tracers showed more scatter as the infrared wavelength increased.
- Other analyses indicated that emission at 160 μm could be tied to older stellar populations.

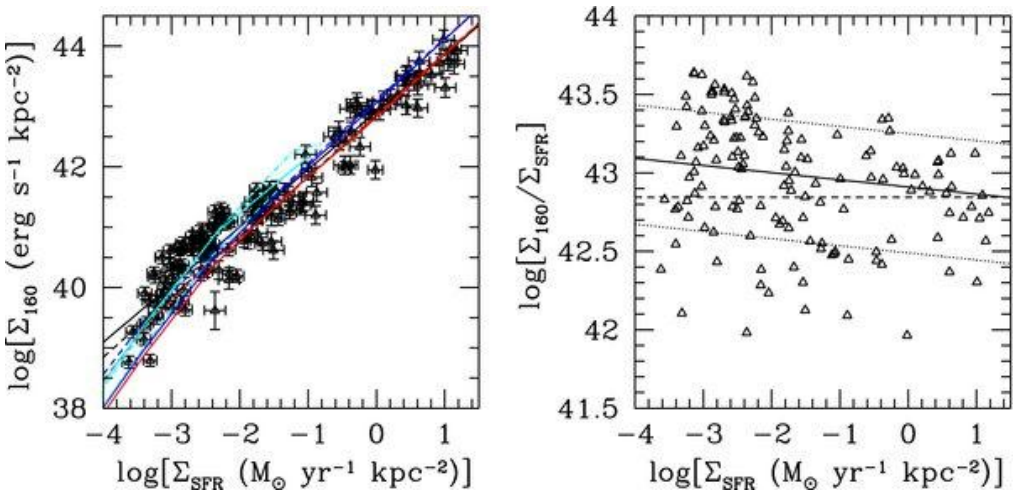

Calzetti et al.
2010, ApJ, 714, 1256

Spitzer results

- The relation between infrared emission and other star formation tracers showed more scatter as the infrared wavelength increased.
- Other analyses indicated that emission at 160 μm could be tied to older stellar populations.

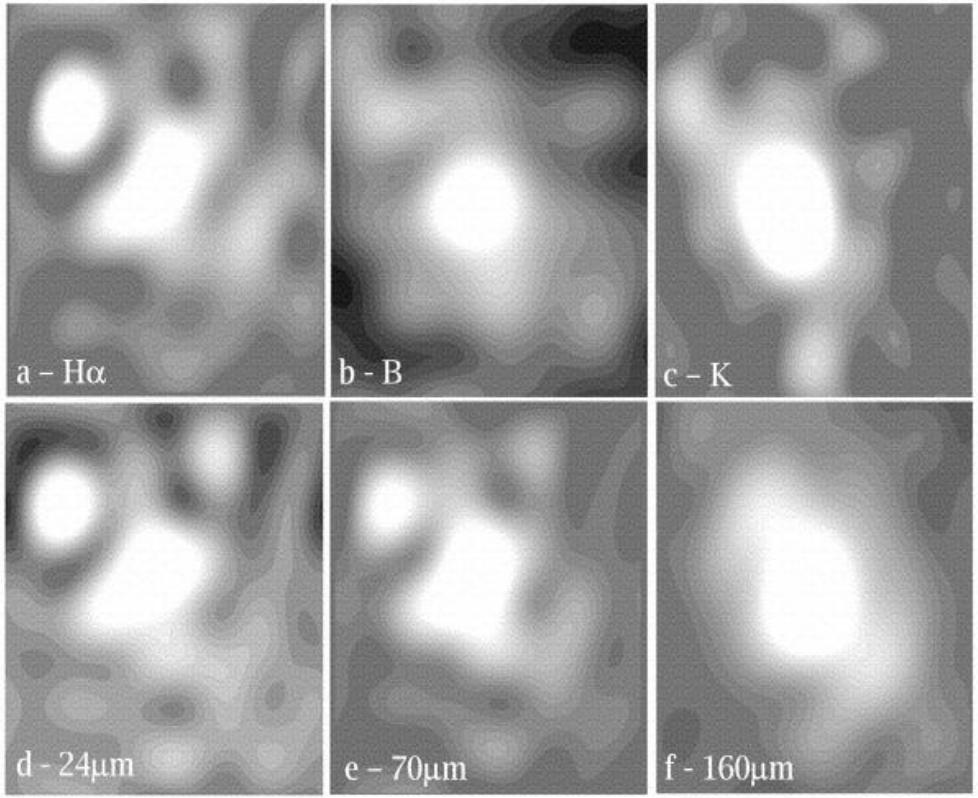

Hinz et al.
2004, ApJS, 154, 259

Radiative transfer models

- Some of the dust emission and radiative transfer models developed before Herschel had included a diffuse dust component

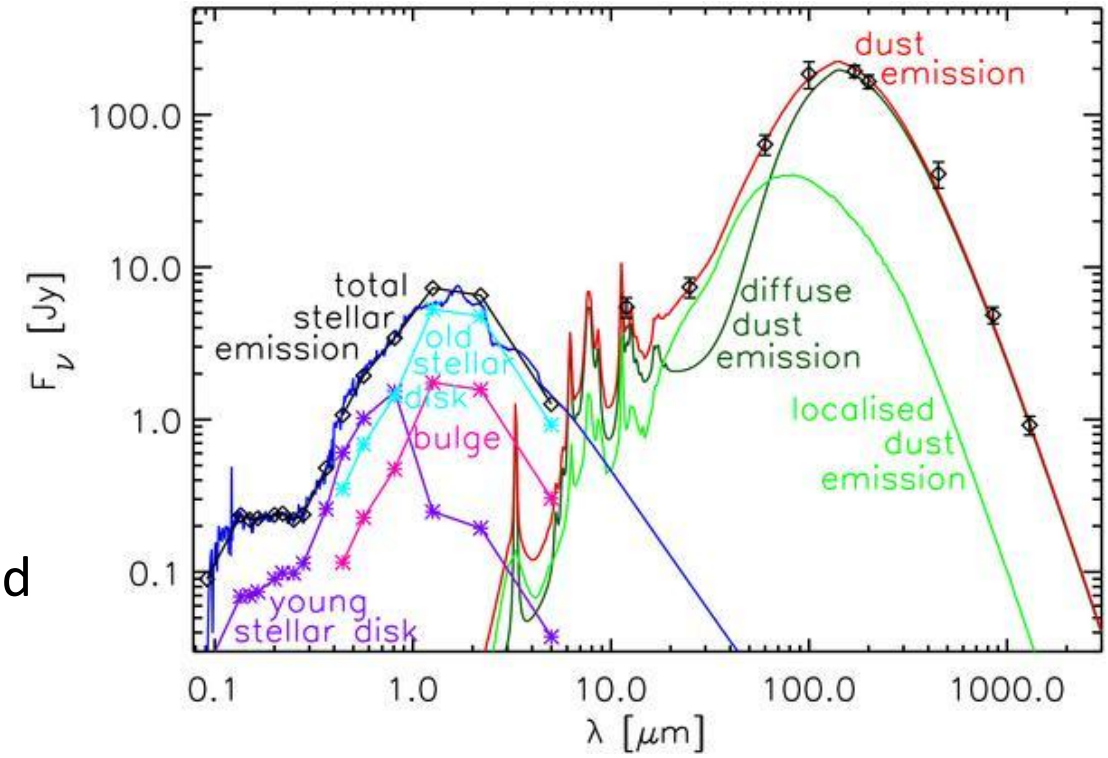

Popescu et al.
2011, A&A, 527, 109


M81, M83, and NGC 2403
analysis

Herschel analyses

The Herschel-based analyses of M81, M83, and NGC 2403 were based on comparing infrared colour variations to heating sources:

- Emission in a single band can be correlated to star formation as the result of either temperature or mass variations.

- The ratios of infrared surface brightnesses can only depend on temperature. If the star forming regions are heating the dust, the ratios will be enhanced in the regions.

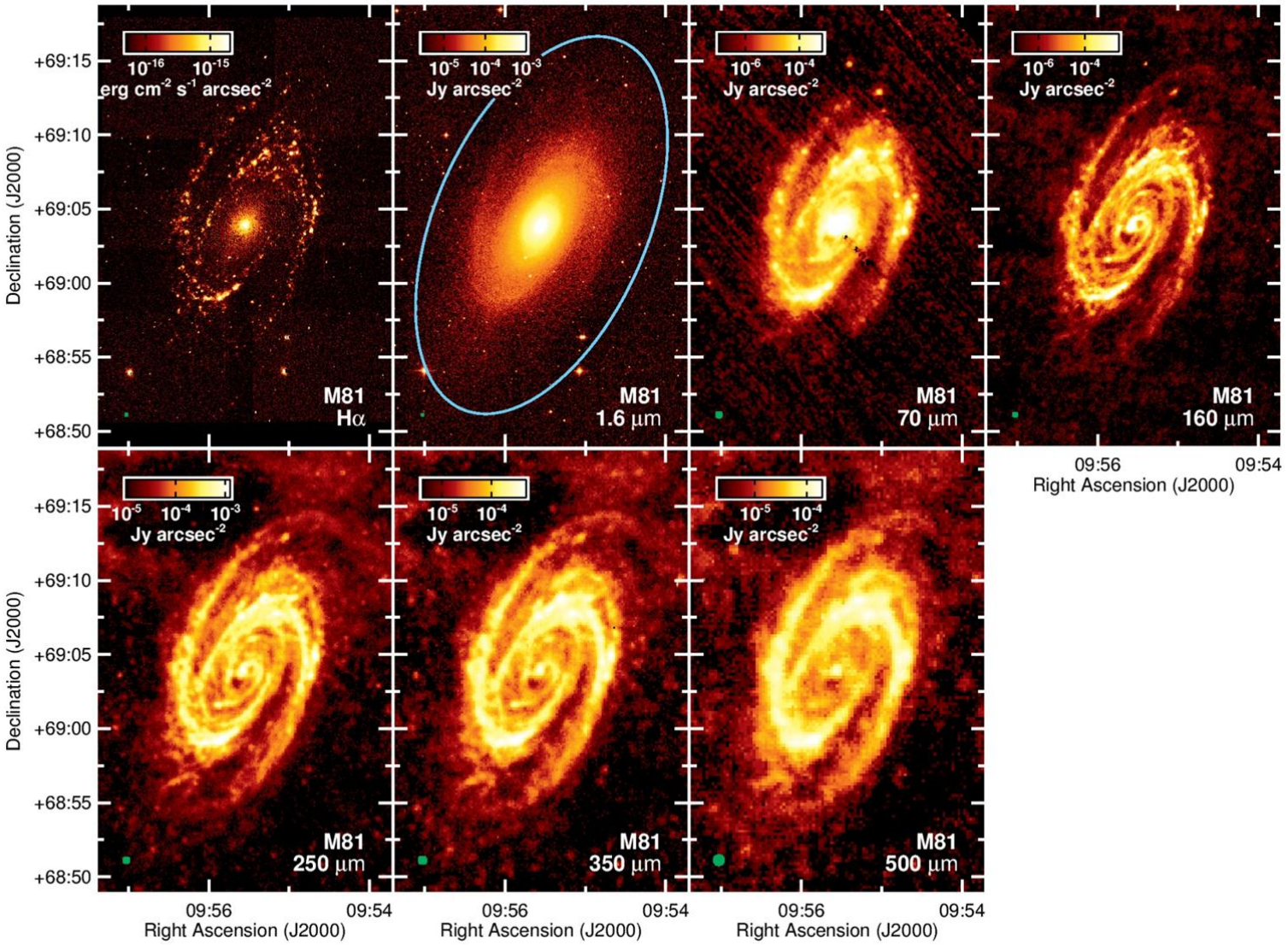
10^-16 10^-15
erg cm^-2 s^-1 arcsec^-2
M81
Hα
10^-5 10^-4 10^-3
Jy arcsec^-2
M81
1.6 μm
10^-6 10^-4
Jy arcsec^-2
M81
70 μm
10^-6 10^-4
Jy arcsec^-2
M81
160 μm
10^-5 10^-4 10^-3
Jy arcsec^-2
M81
250 μm
10^-5 10^-4
Jy arcsec^-2
M81
350 μm
10^-5 10^-4
Jy arcsec^-2
M81
500 μm
Declination (J2000)
+69:15
+69:10
+69:05
+69:00
+68:55
+68:50
09:56
09:54
Right Ascension (J2000)

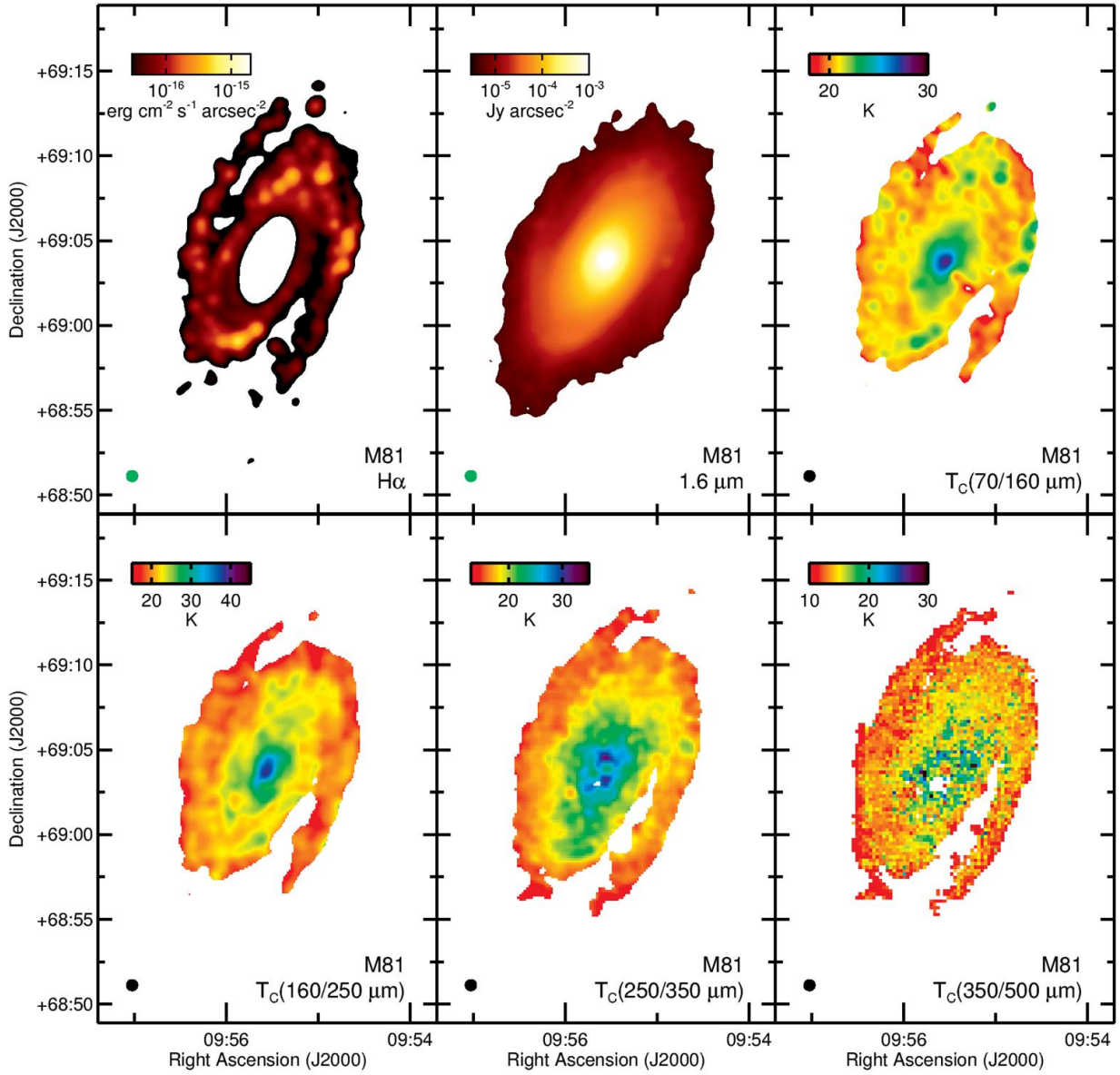
Declination (J2000)
+69:15
+69:10
+69:05
+69:00
+68:55
+68:50
10^-16 10^-15
erg cm^-2 s^-1 arcsec^-2
M81
Hα
10^-5 10^-4 10^-3
Jy arcsec^-2
M81
1.6 μm
20 30
K
M81
T_C(70/160 μm)
20 30 40
K
M81
T_C(160/250 μm)
20 30
K
M81
T_C(250/350 μm)
10 20 30
K
M81
T_C(350/500 μm)
09:56
09:54
Right Ascension (J2000)

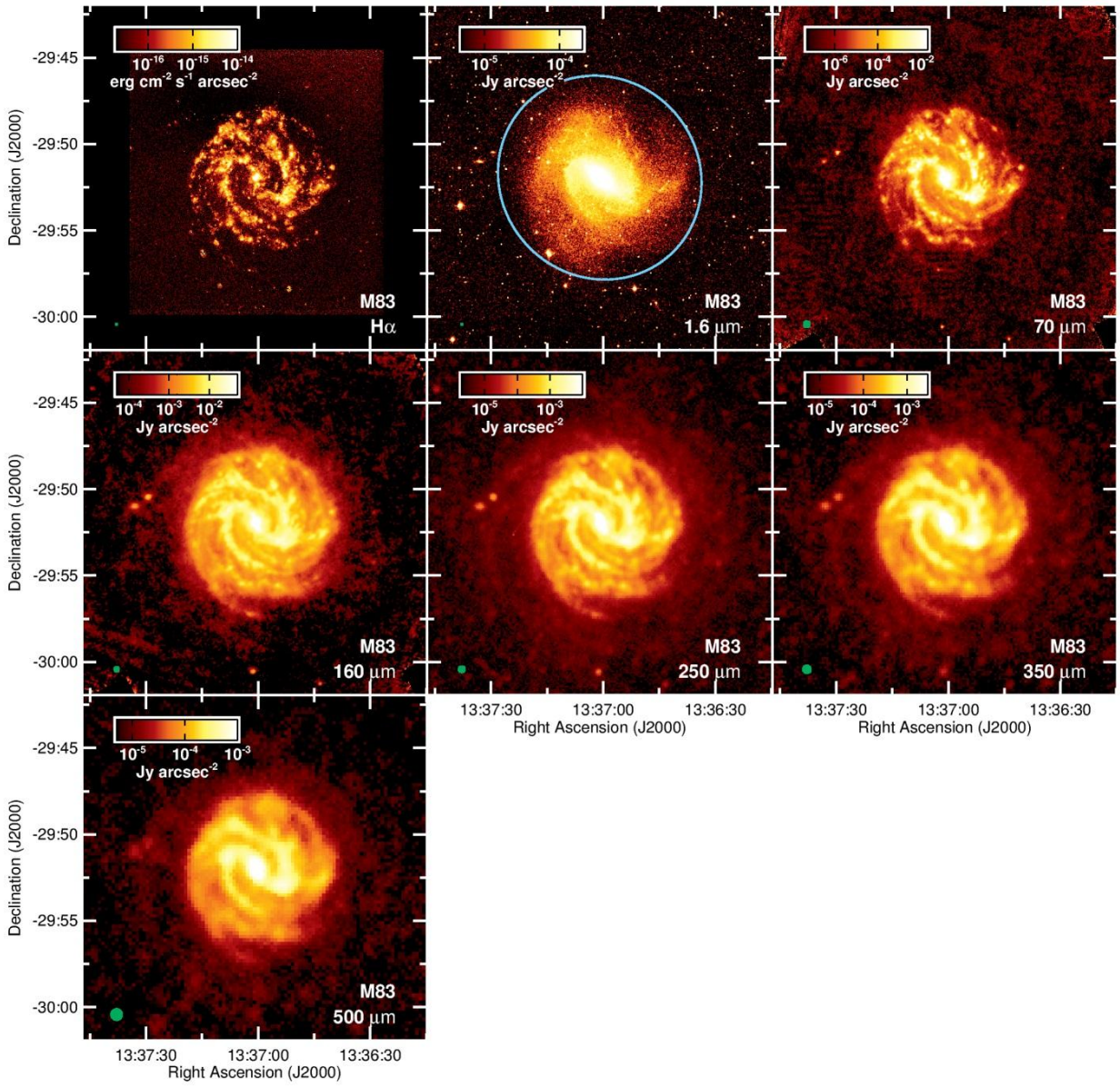
10^-16 10^-15 10^-14
erg cm^-2 s^-1 arcsec^-2
M83
Hα
10^-5 10^-4
Jy arcsec^-2
M83
1.6 μm
10^-6 10^-4 10^-2
Jy arcsec^-2
M83
70 μm
10^-4 10^-3 10^-2
Jy arcsec^-2
M83
160 μm
10^-5 10^-3
Jy arcsec^-2
M83
250 μm
10^-5 10^-4 10^-3
Jy arcsec^-2
M83
350 μm
10^-5 10^-4 10^-3
Jy arcsec^-2
M83
500 μm
Declination (J2000)
-29:45
-29:50
-29:55
-30:00
13:37:30
13:37:00
13:36:30
Right Ascension (J2000)

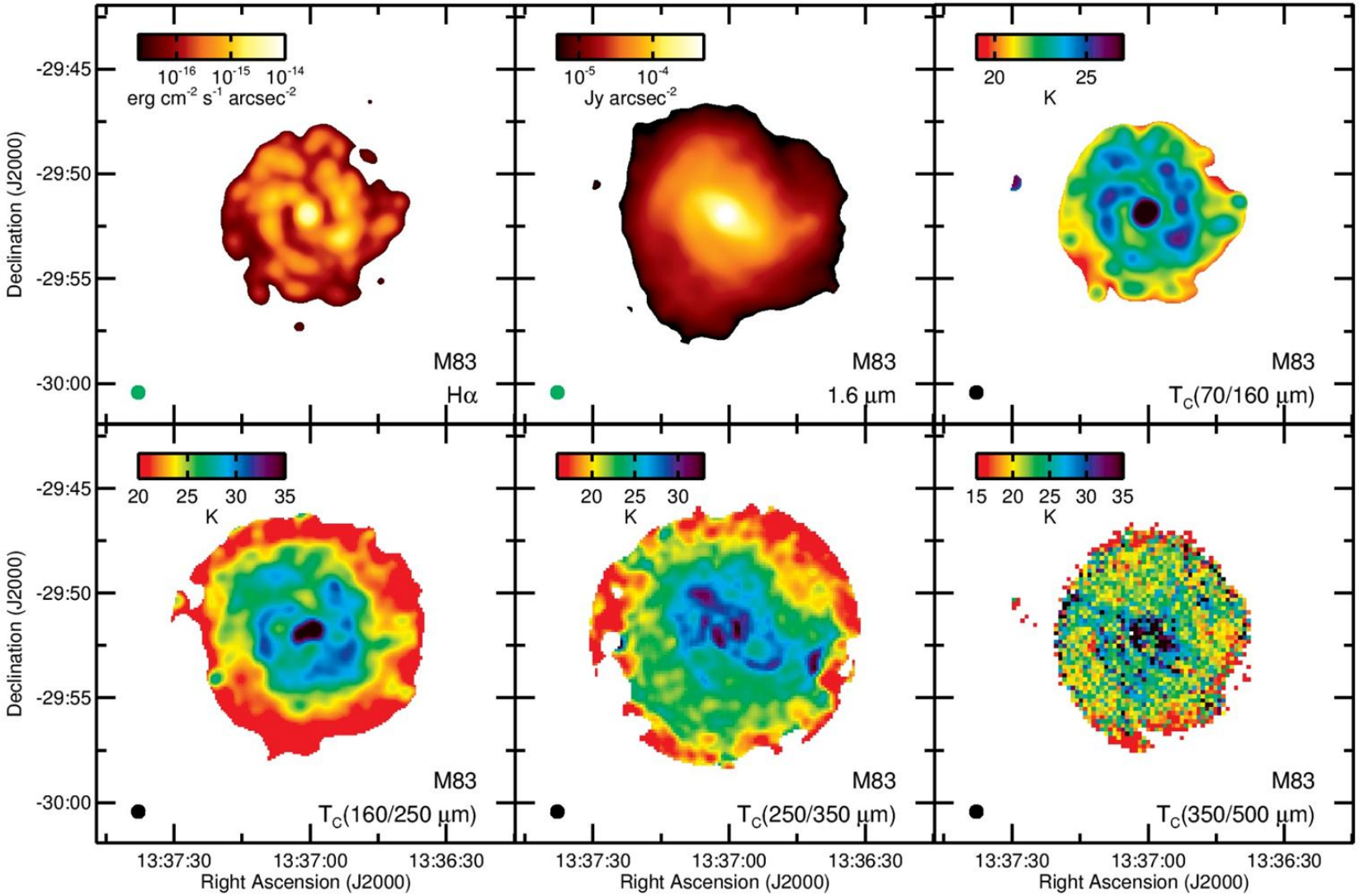
10^-16 10^-15 10^-14
erg cm^-2 s^-1 arcsec^-2
M83
Hα
10^-5 10^-4
Jy arcsec^-2
M83
1.6 μm
20 25
K
M83
T_C(70/160 μm)
20 25 30 35
K
M83
T_C(160/250 μm)
20 25 30
K
M83
T_C(250/350 μm)
15 20 25 30 35
K
M83
T_C(350/500 μm)
Declination (J2000)
-29:45
-29:50
-29:55
-30:00
13:37:30
13:37:00
13:36:30
Right Ascension (J2000)

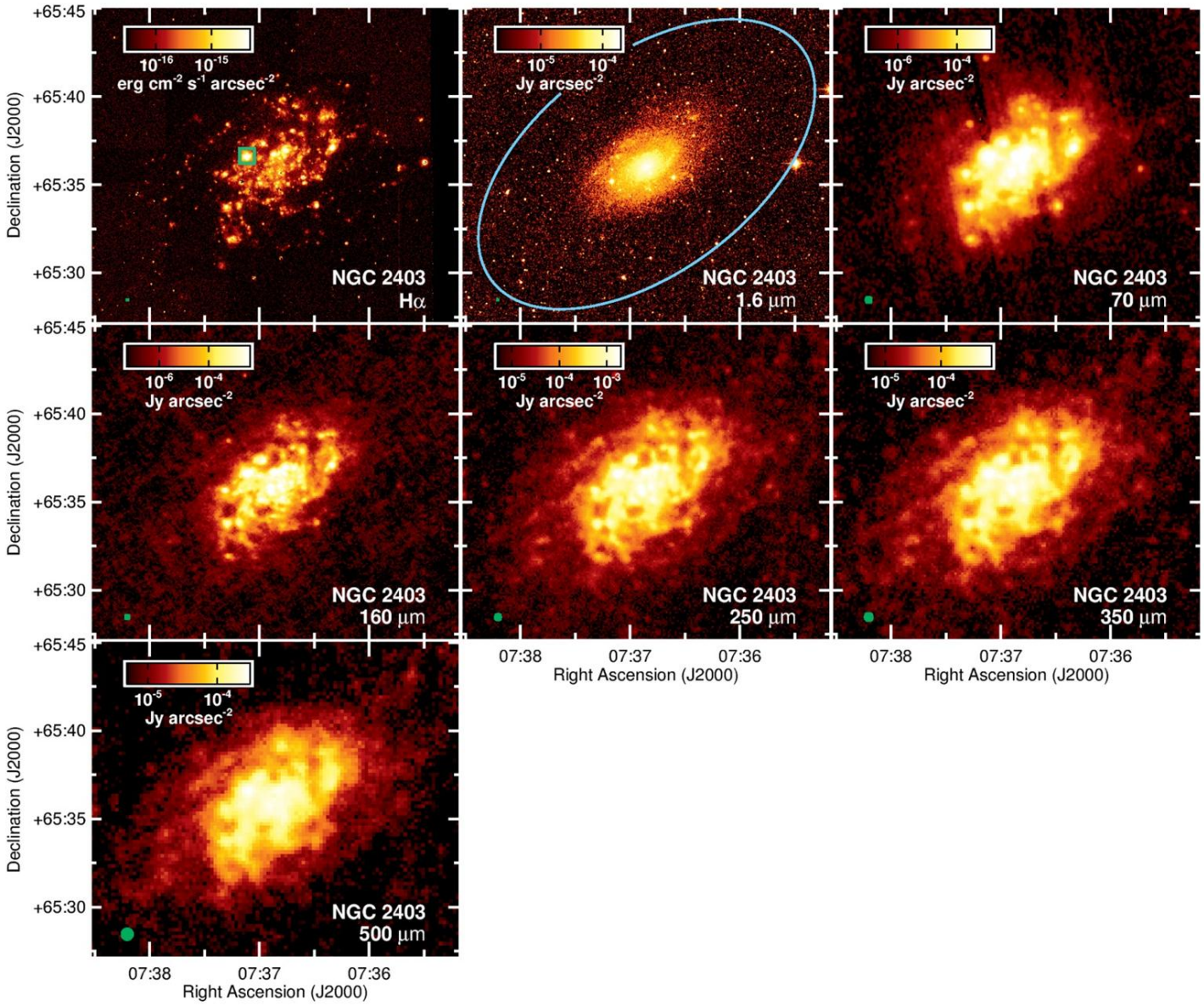
NGC 2403
Hα
NGC 2403
1.6 μm
NGC 2403
70 μm
NGC 2403
160 μm
NGC 2403
250 μm
NGC 2403
350 μm
NGC 2403
500 μm
Declination (J2000)
Right Ascension (J2000)
+65:45
+65:40
+65:35
+65:30
07:38
07:37
07:36
erg cm-2 s-1 arcsec-2
Jy arcsec-2

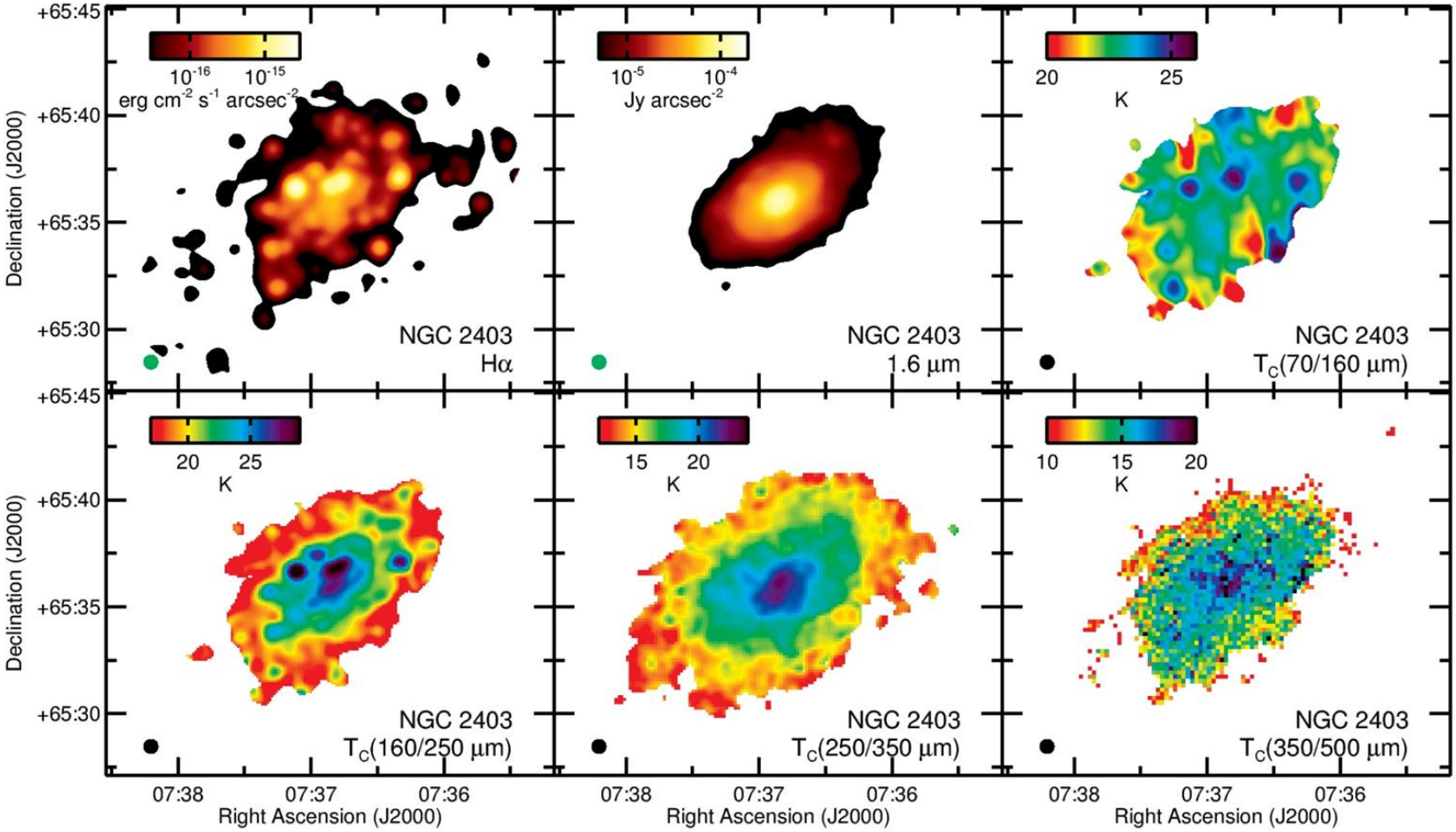
+65:45
+65:40
+65:35
+65:30
Declination (J2000)
10^{-16} 10^{-15}
erg cm^{-2} s^{-1} arcsec^{-2}
NGC 2403
Hα
10^{-5} 10^{-4}
Jy arcsec^{-2}
NGC 2403
1.6 μm
20 25
K
NGC 2403
T_C(70/160 μm)
20 25
K
NGC 2403
T_C(160/250 μm)
15 20
K
NGC 2403
T_C(250/350 μm)
10 15 20
K
NGC 2403
T_C(350/500 μm)
07:38
07:37
07:36
Right Ascension (J2000)

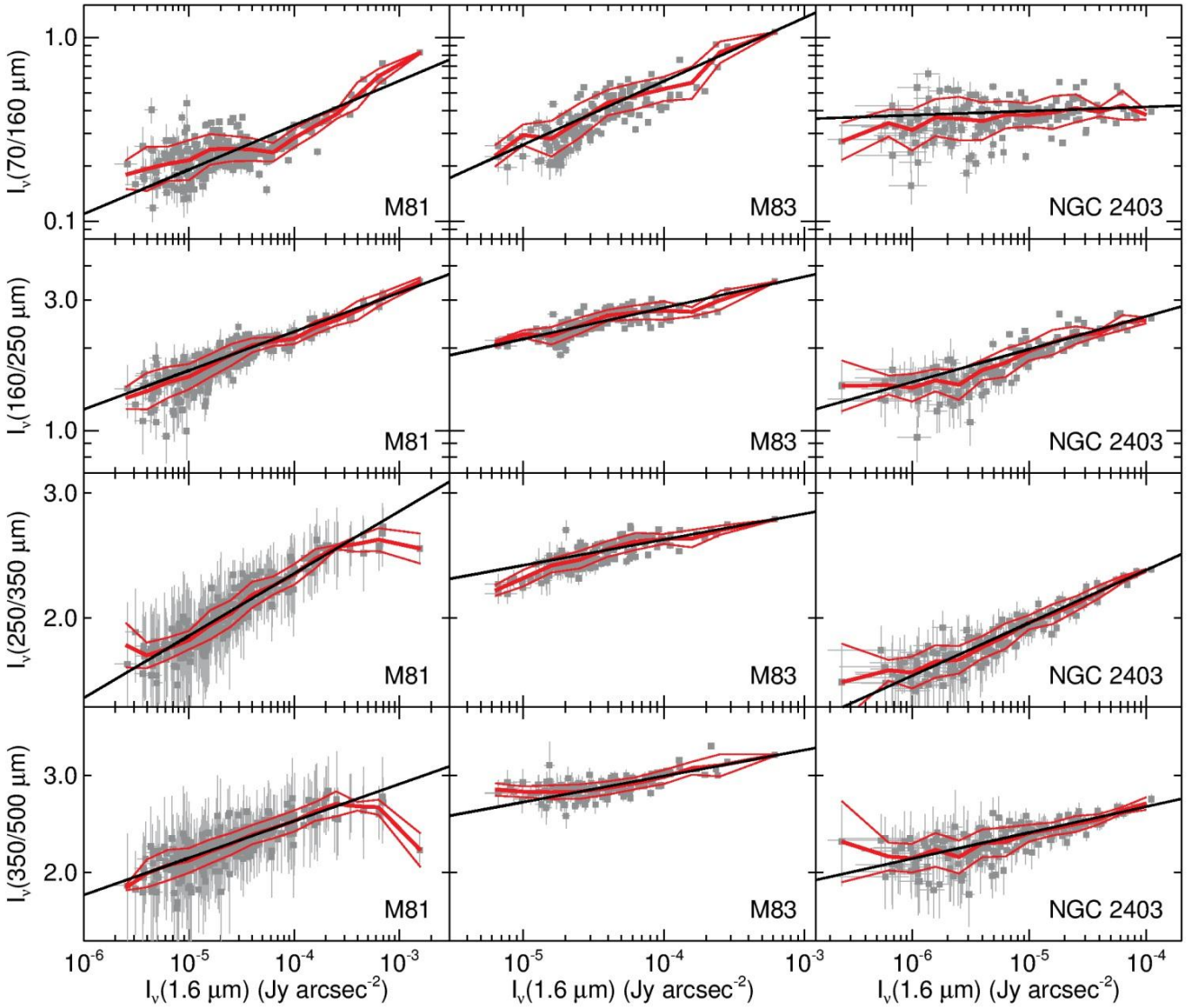
M81
M83
NGC 2403
I_ν(70/160 μm)
I_ν(160/250 μm)
I_ν(250/350 μm)
I_ν(350/500 μm)
I_ν(1.6 μm) (Jy arcsec^{-2})

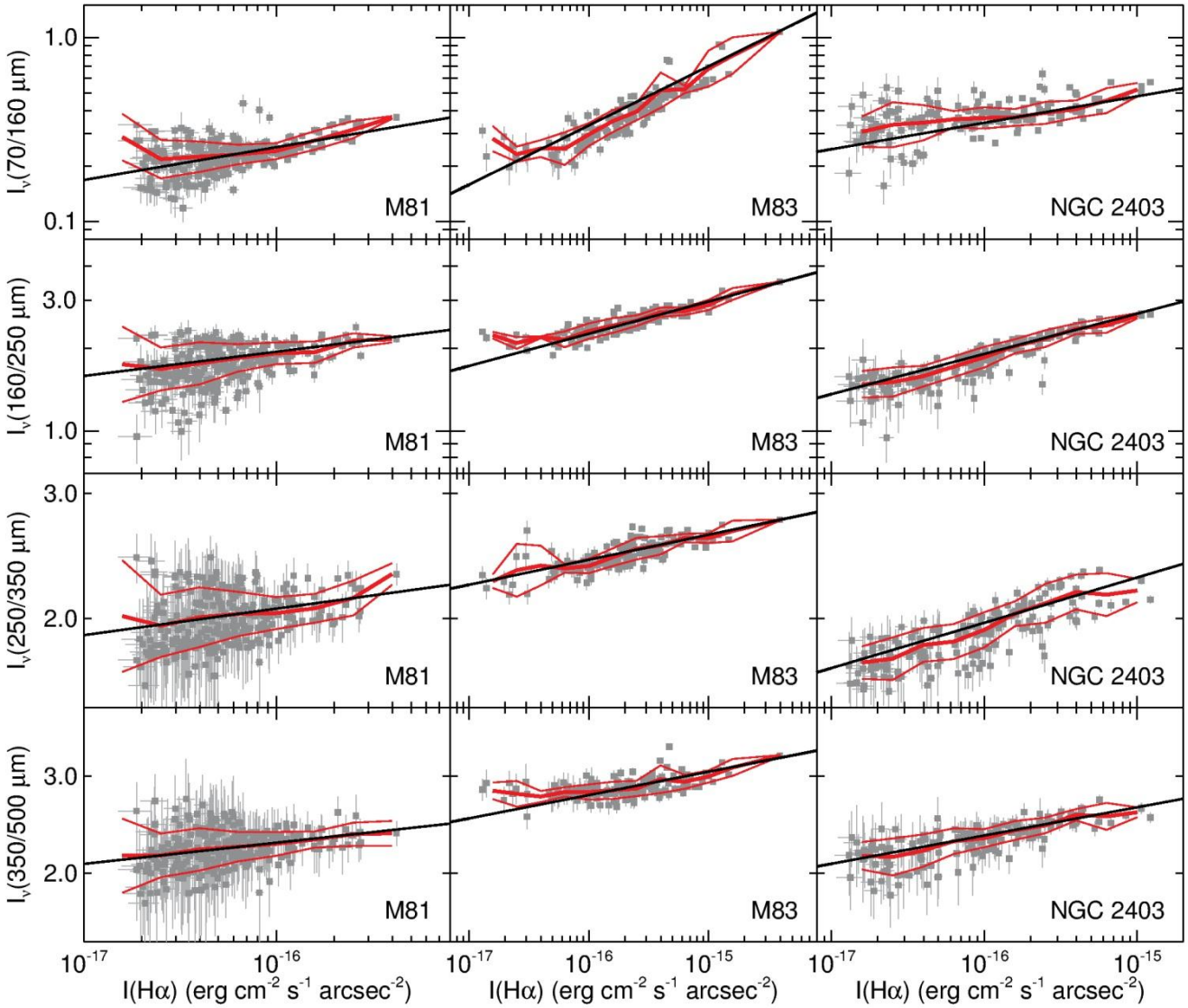
1.0
0.1
I_ν(70/160 μm)
M81
M83
NGC 2403
3.0
1.0
I_ν(160/250 μm)
M81
M83
NGC 2403
3.0
2.0
I_ν(250/350 μm)
M81
M83
NGC 2403
3.0
2.0
I_ν(350/500 μm)
M81
M83
NGC 2403
10^{-17}
10^{-16}
10^{-15}
I(Hα) (erg cm^{-2} s^{-1} arcsec^{-2})

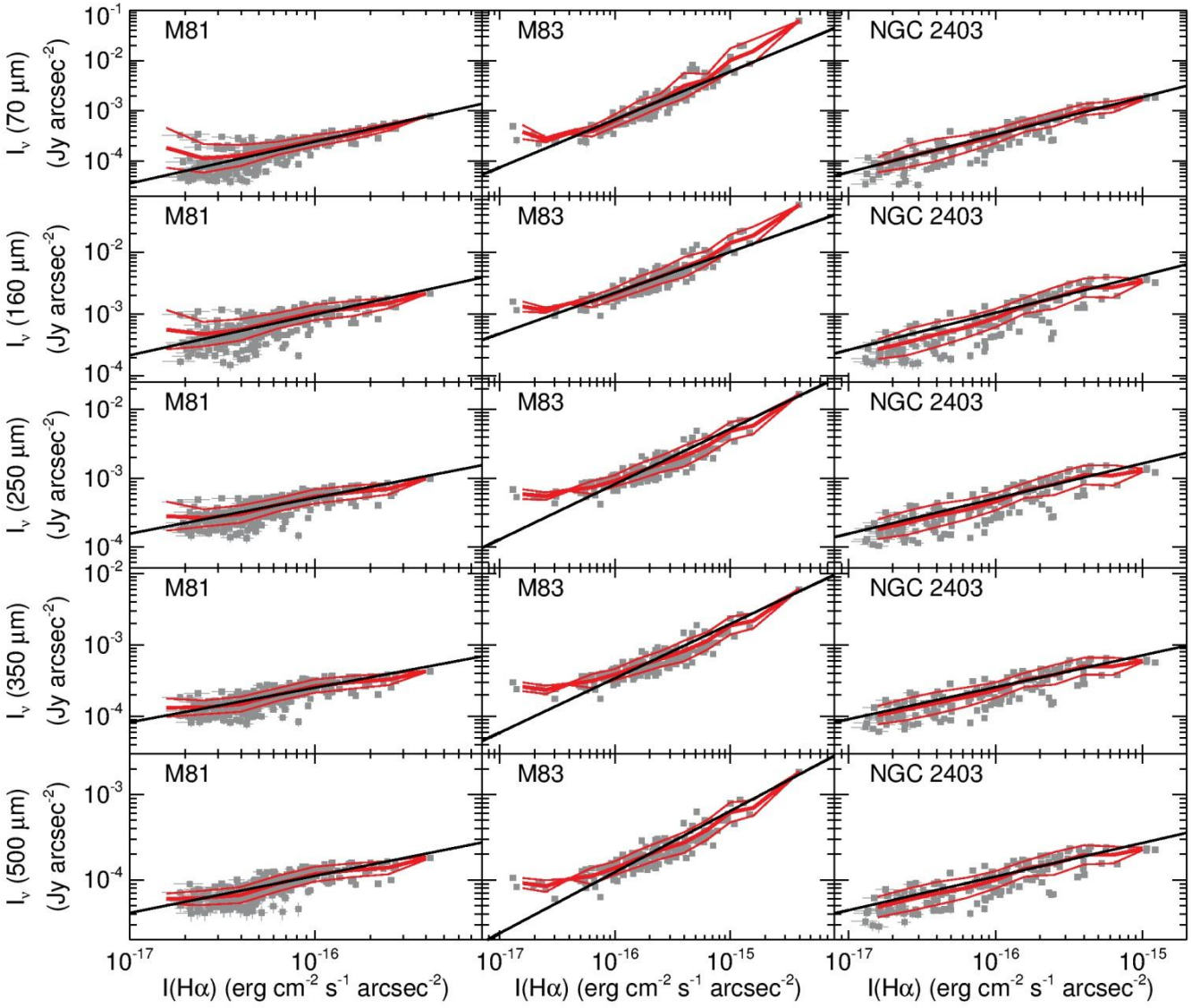
M81
M83
NGC 2403
I$_\nu$ (70 μm) (Jy arcsec^{-2})
I$_\nu$ (160 μm) (Jy arcsec^{-2})
I$_\nu$ (250 μm) (Jy arcsec^{-2})
I$_\nu$ (350 μm) (Jy arcsec^{-2})
I$_\nu$ (500 μm) (Jy arcsec^{-2})
I(Hα) (erg cm^{-2} s^{-1} arcsec^{-2})

To measure the relative contributions of star forming regions and the total stellar populations to dust heating, we fit the following equation to the data:

$$\ln(f_{\nu 1}/f_{\nu 2}) = \alpha \ln(I(H\alpha) + A_1 I_\nu(1.6\ \mu m)) + A_2$$

$$\ln(\ \boxed{}\ ) = \alpha \ln(\ \boxed{}\ ) + A_1 \boxed{}\ ) + A_2$$

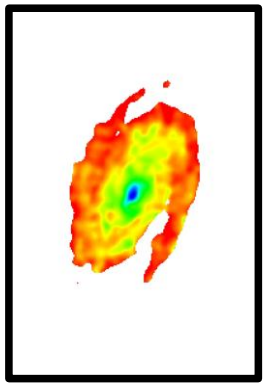

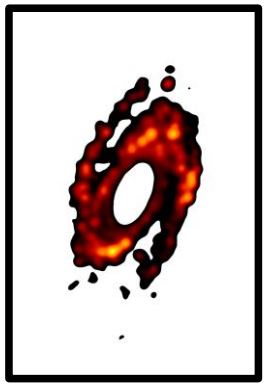

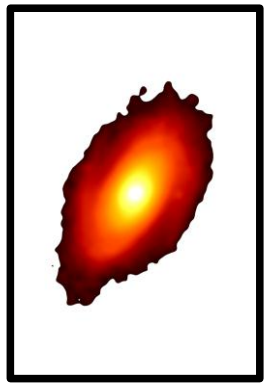

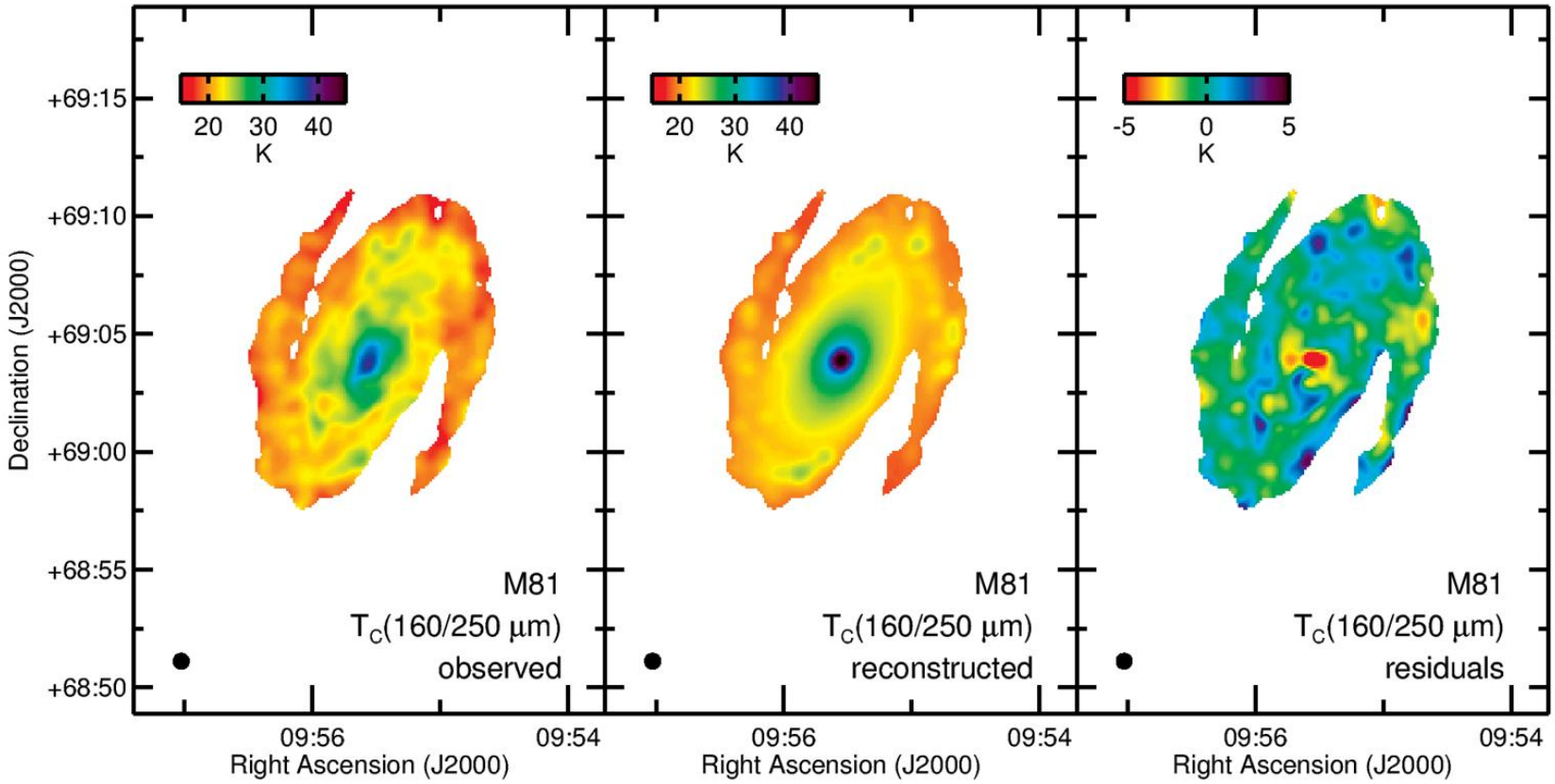
+69:15
+69:10
+69:05
+69:00
+68:55
+68:50
Declination (J2000)
20 30 40
K
M81
T_C(160/250 μm)
observed
09:56
09:54
Right Ascension (J2000)
20 30 40
K
M81
T_C(160/250 μm)
reconstructed
09:56
09:54
Right Ascension (J2000)
-5 0 5
K
M81
T_C(160/250 μm)
residuals
09:56
09:54
Right Ascension (J2000)

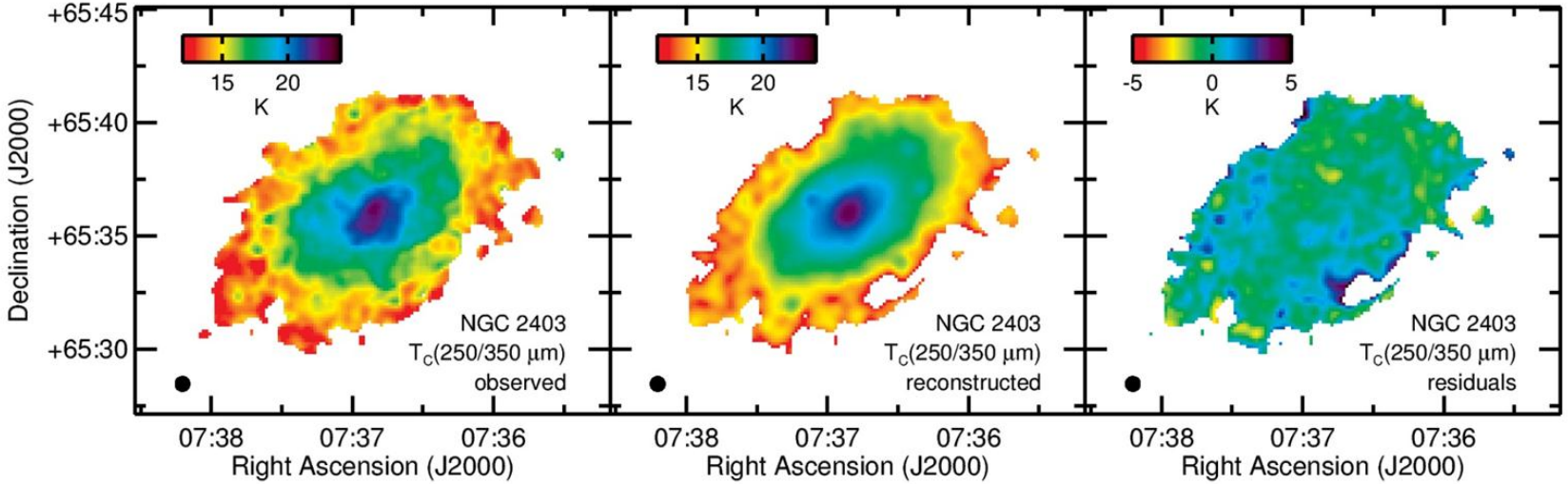
+65:45
+65:40
+65:35
+65:30
Declination (J2000)
15 20
K
NGC 2403
T_C(250/350 μm)
observed
07:38 07:37 07:36
Right Ascension (J2000)
15 20
K
NGC 2403
T_C(250/350 μm)
reconstructed
07:38 07:37 07:36
Right Ascension (J2000)
-5 0 5
K
NGC 2403
T_C(250/350 μm)
residuals
07:38 07:37 07:36
Right Ascension (J2000)

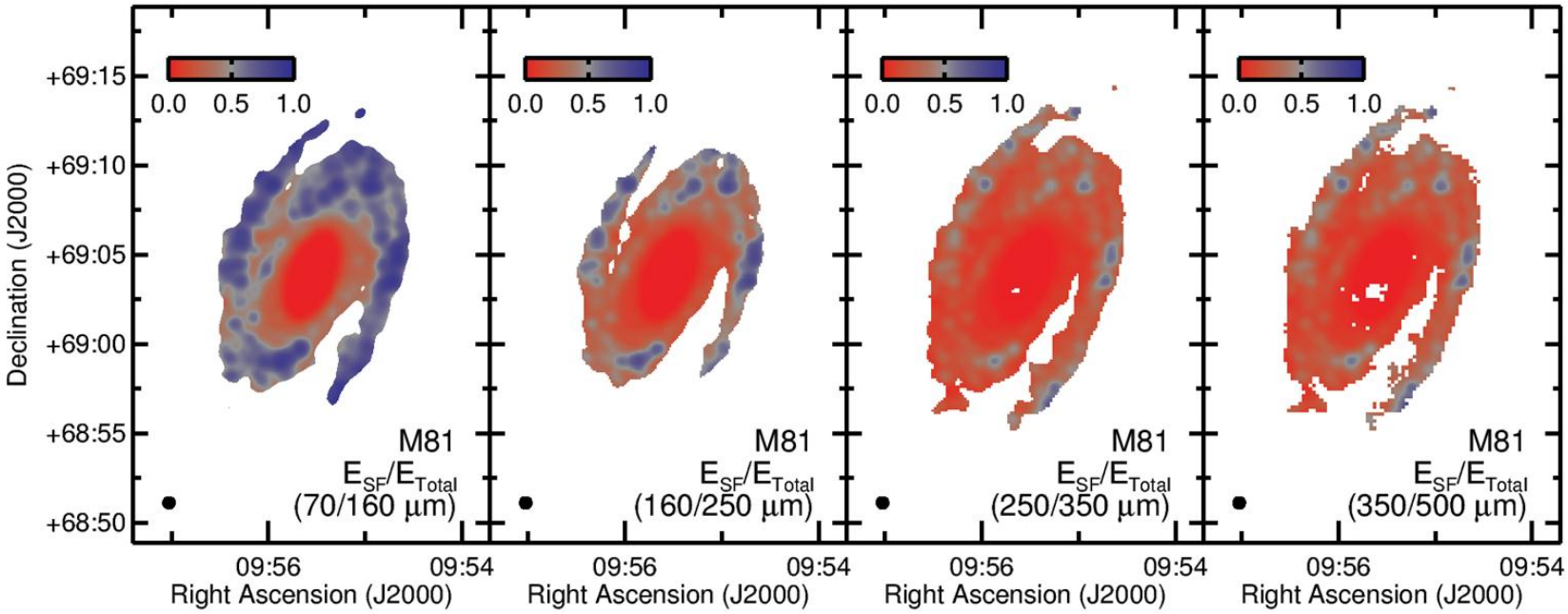
Declination (J2000)
+69:15
+69:10
+69:05
+69:00
+68:55
+68:50
0.0 0.5 1.0
M81
E_{SF}/E_{Total}
(70/160 μm)
(160/250 μm)
(250/350 μm)
(350/500 μm)
09:56
09:54
Right Ascension (J2000)

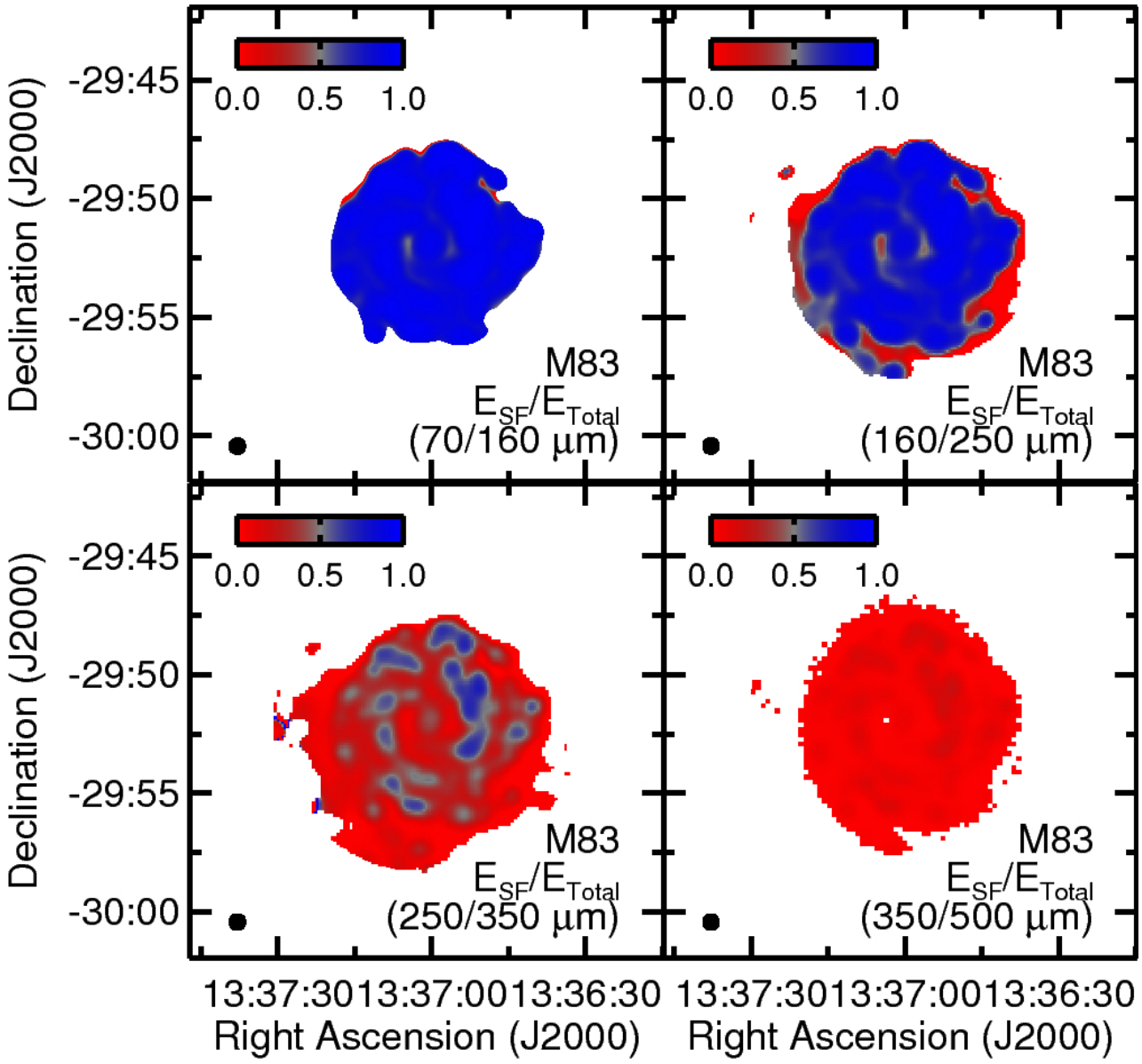
0.0 0.5 1.0
M83
E_{SF}/E_{Total}
(70/160 μm)
0.0 0.5 1.0
M83
E_{SF}/E_{Total}
(160/250 μm)
0.0 0.5 1.0
M83
E_{SF}/E_{Total}
(250/350 μm)
0.0 0.5 1.0
M83
E_{SF}/E_{Total}
(350/500 μm)
Declination (J2000)
-29:45
-29:50
-29:55
-30:00
13:37:30 13:37:00 13:36:30
Right Ascension (J2000)

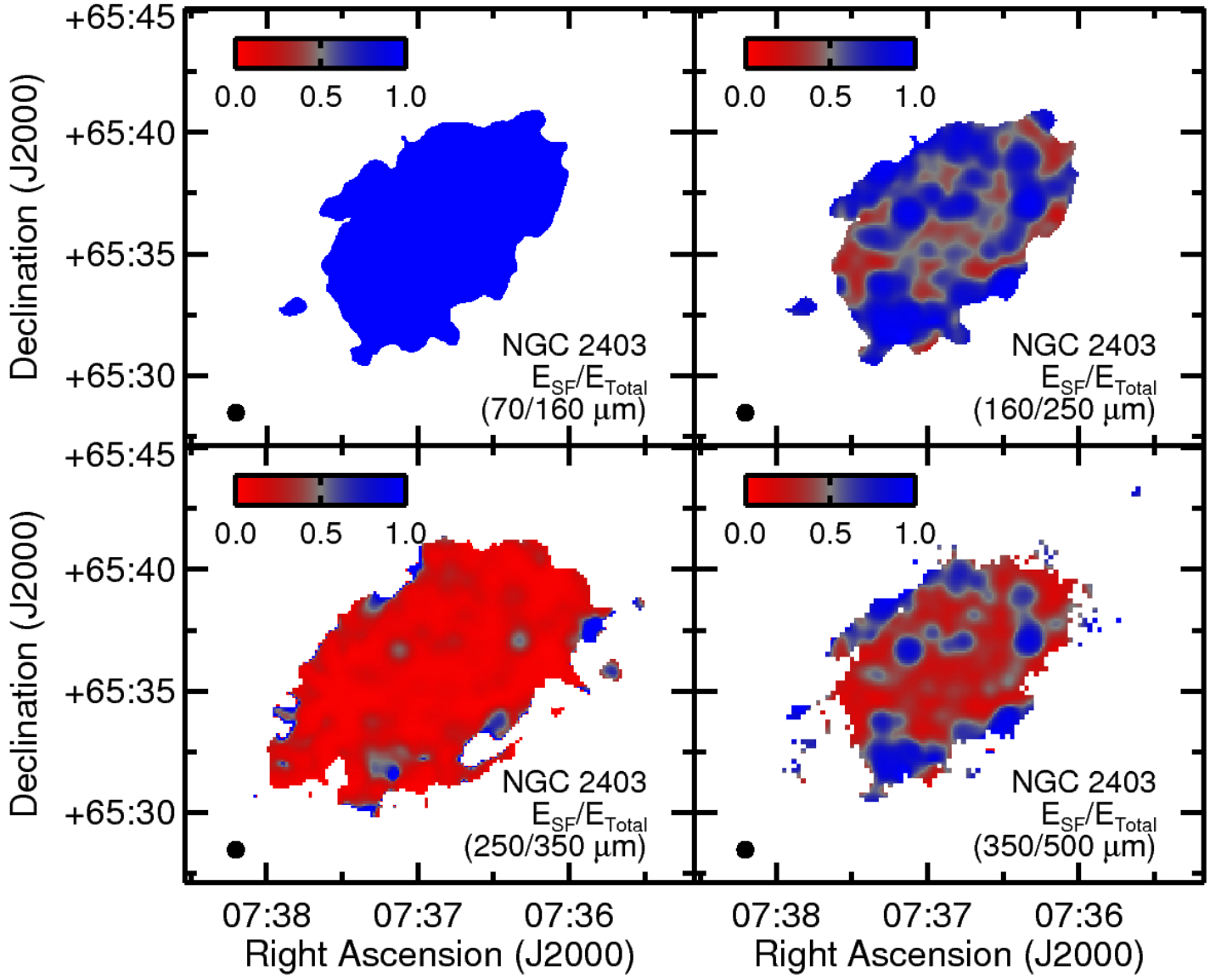
+65:45
+65:40
+65:35
+65:30
Declination (J2000)
0.0 0.5 1.0
NGC 2403
E_{SF}/E_{Total}
(70/160 μm)
NGC 2403
E_{SF}/E_{Total}
(160/250 μm)
NGC 2403
E_{SF}/E_{Total}
(250/350 μm)
NGC 2403
E_{SF}/E_{Total}
(350/500 μm)
07:38
07:37
07:36
Right Ascension (J2000)

Handling diffusion of photons through galaxies

These analyses are based on assuming that the photons from heating sources do not propagate outside the ~1 kpc bins used for the analysis.

- Mean free path of photons is expected to be ~1 kpc.
- Diffuse Hα emission accounts for photons diffusing from star forming regions.

Nonetheless, we performed some additional tests with NGC 2403 where we separated the Hα emission into compact and diffuse components.

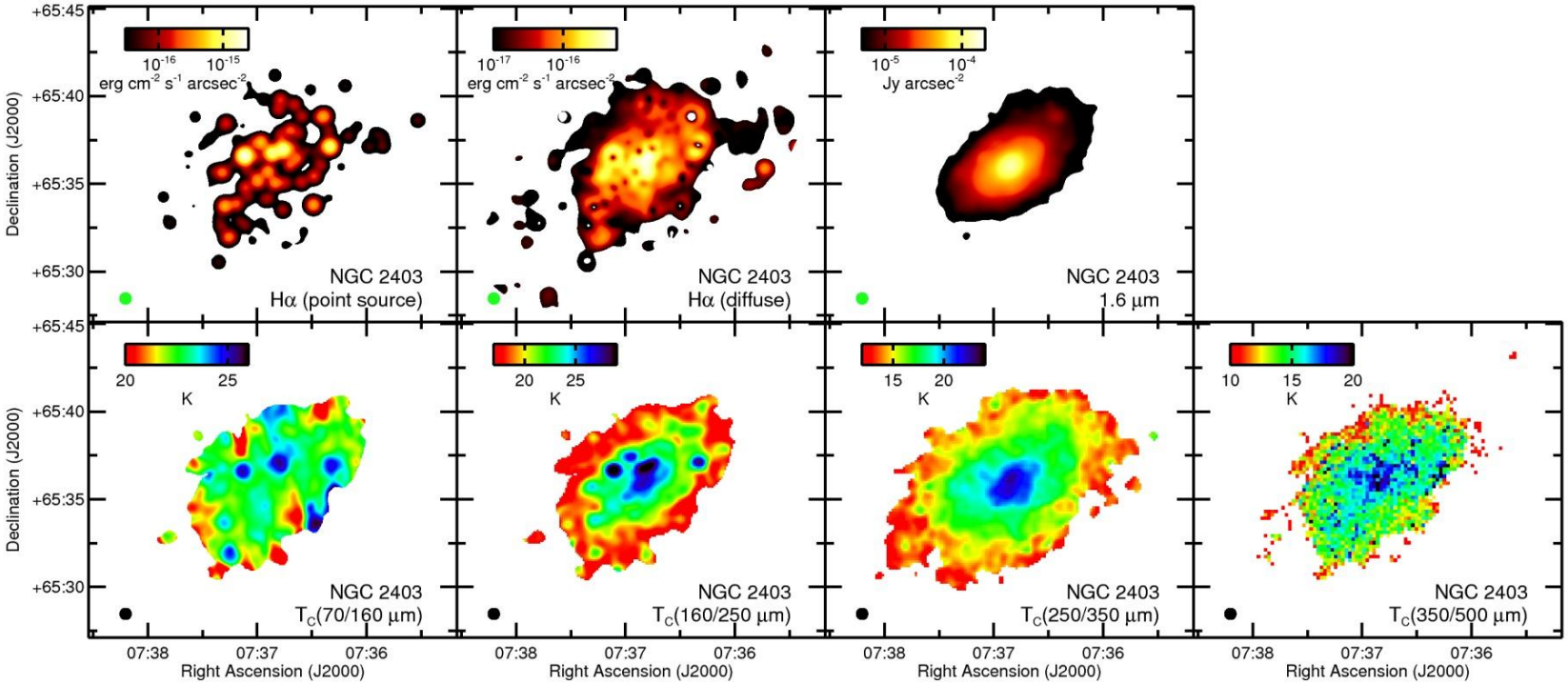
10^-16 10^-15
erg cm^-2 s^-1 arcsec^-2
NGC 2403
Hα (point source)
10^-17 10^-16
erg cm^-2 s^-1 arcsec^-2
NGC 2403
Hα (diffuse)
10^-5 10^-4
Jy arcsec^-2
NGC 2403
1.6 μm
20 25
K
NGC 2403
T_C(70/160 μm)
20 25
K
NGC 2403
T_C(160/250 μm)
15 20
K
NGC 2403
T_C(250/350 μm)
10 15 20
K
NGC 2403
T_C(350/500 μm)
Declination (J2000)
+65:45
+65:40
+65:35
+65:30
07:38
07:37
07:36
Right Ascension (J2000)

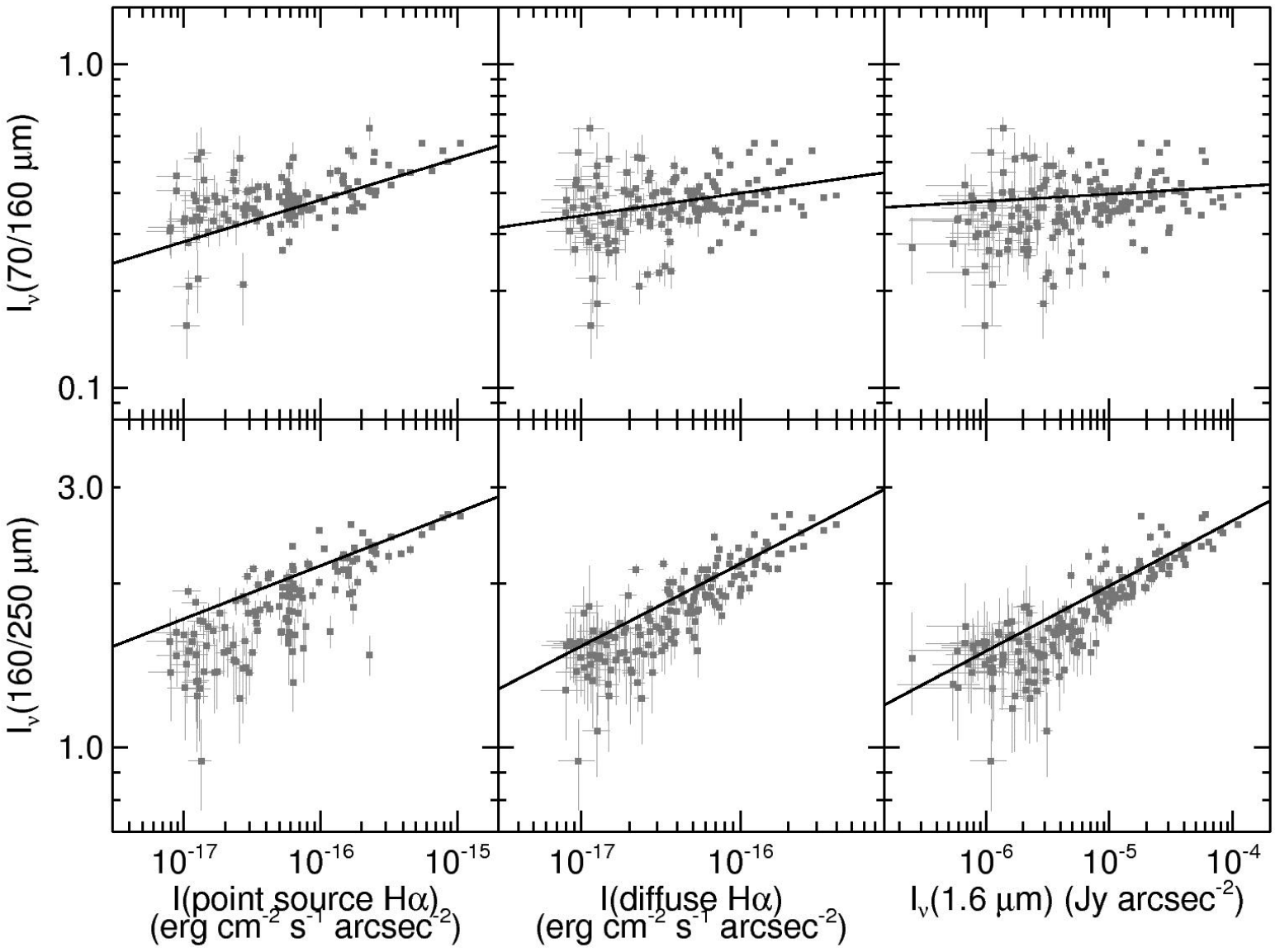
1.0
0.1
3.0
1.0
I_ν(70/160 μm)
I_ν(160/250 μm)
10^{-17}
10^{-16}
10^{-15}
I(point source Hα)
(erg cm^{-2} s^{-1} arcsec^{-2})
10^{-17}
10^{-16}
I(diffuse Hα)
(erg cm^{-2} s^{-1} arcsec^{-2})
10^{-6}
10^{-5}
10^{-4}
I_ν(1.6 μm) (Jy arcsec^{-2})

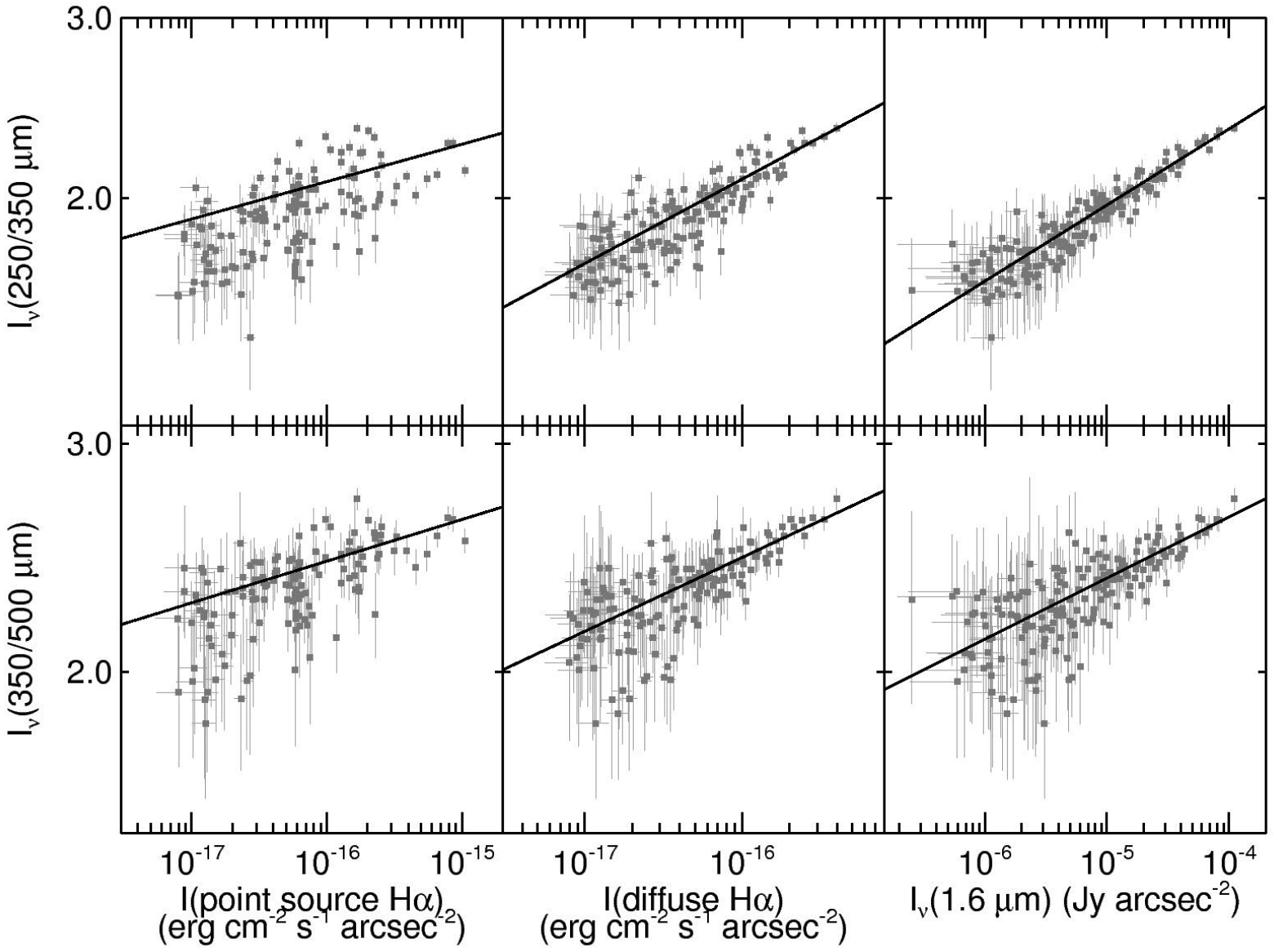
3.0
2.0
I_ν(250/350 μm)
3.0
2.0
I_ν(350/500 μm)
10^{-17}
10^{-16}
10^{-15}
I(point source Hα)
(erg cm^{-2} s^{-1} arcsec^{-2})
10^{-17}
10^{-16}
I(diffuse Hα)
(erg cm^{-2} s^{-1} arcsec^{-2})
10^{-6}
10^{-5}
10^{-4}
I_ν(1.6 μm) (Jy arcsec^{-2})

Dust heating scenario

- Dust found primarily around star forming regions.
- Inner regions of dust clouds heated by young stars.
- Outer regions heated by older stars in the vicinity of the dust clouds.

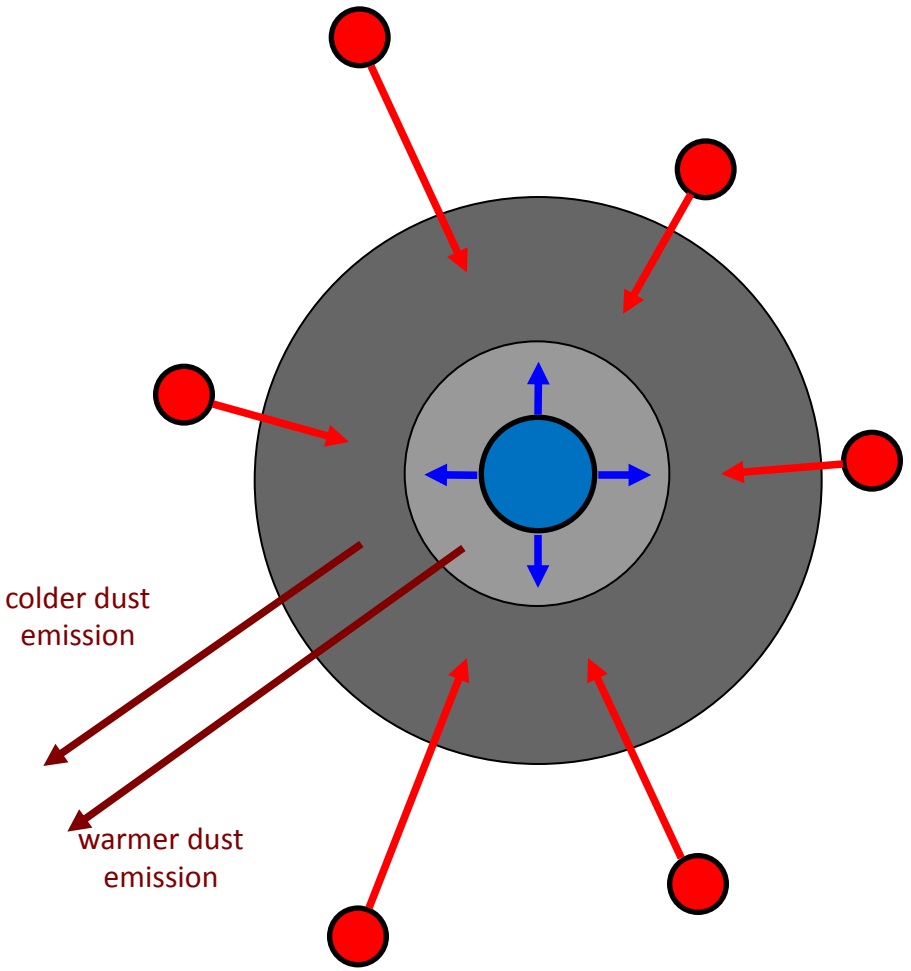


Other Herschel analyses

M33

- Early analyses showed that 100-250 µm emission was correlated with other star formation tracers.
- Boquien et al. (2011), using a colour analysis similar to what was shown above, demonstrated that the >250 µm emission was from dust heated by the total stellar population.

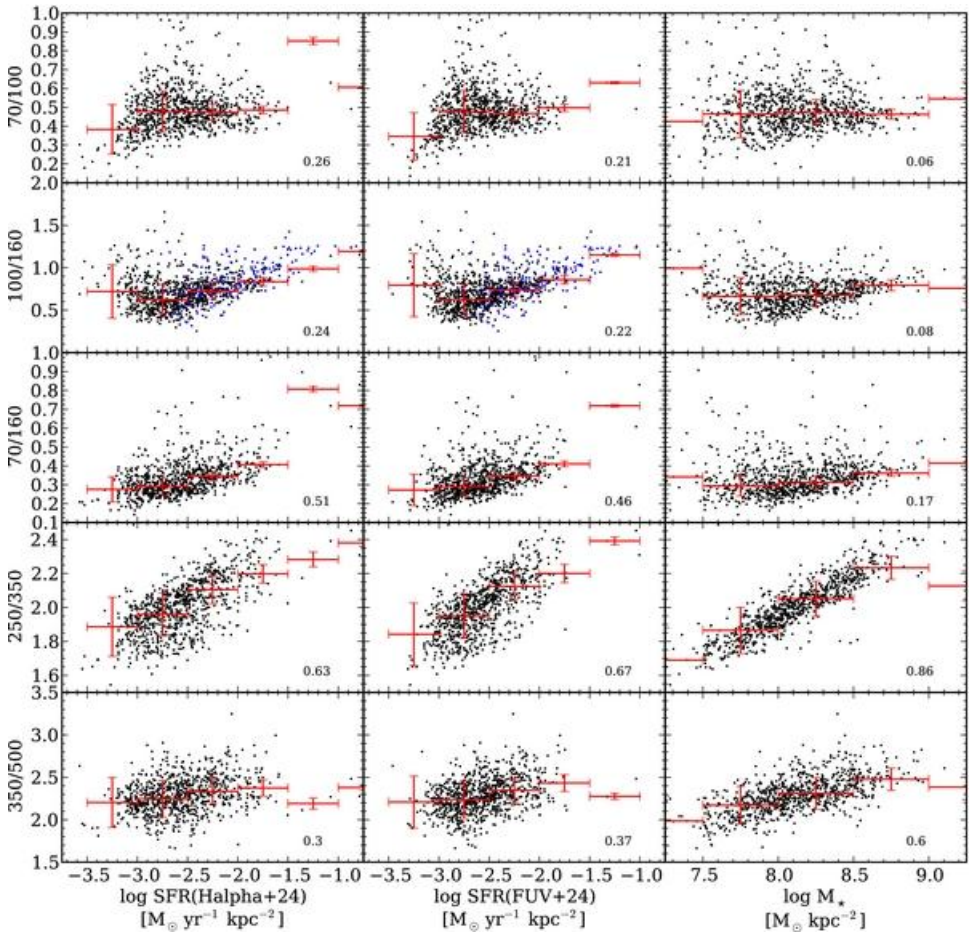

Boquien et al., 2011, AJ, 142, 111

M31

- Smith et al. (2012) and Groves et al. (2012) found that the dust temperature in the centre of M31 was well-correlated with the de Vaucouleurs light profile.

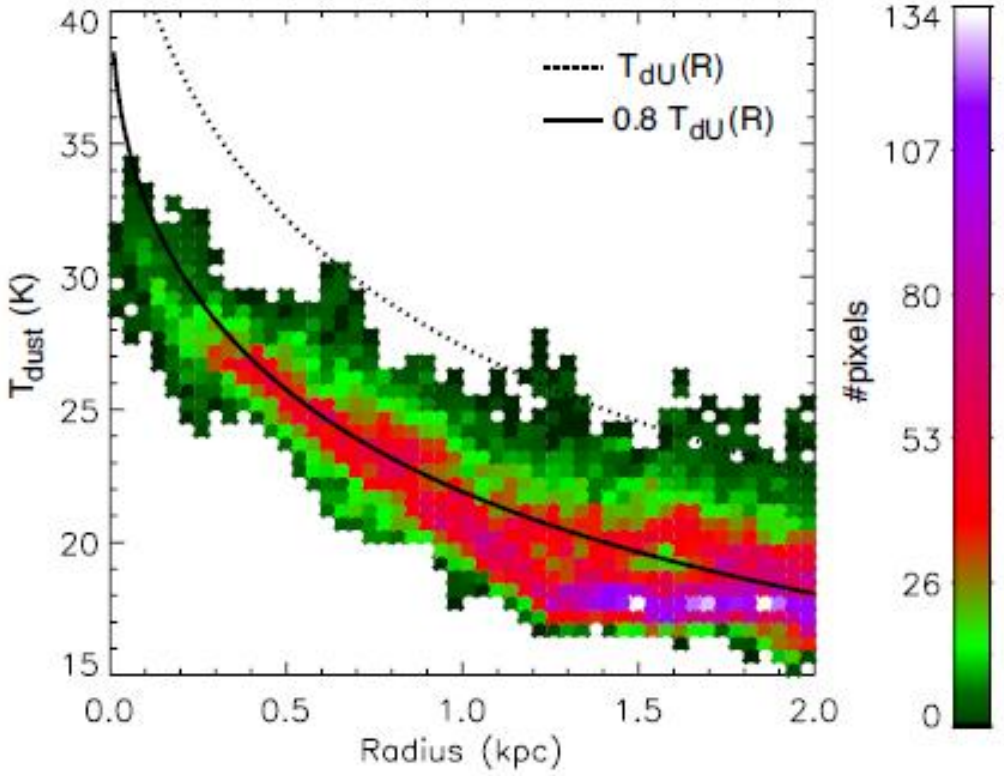

Groves et al.
2012, preprint (astro-ph/1206.2925)

M31

- Smith et al. (2012) and Groves et al. (2012) found that the dust temperature in the centre of M31 was well-correlated with the de Vaucouleurs light profile.

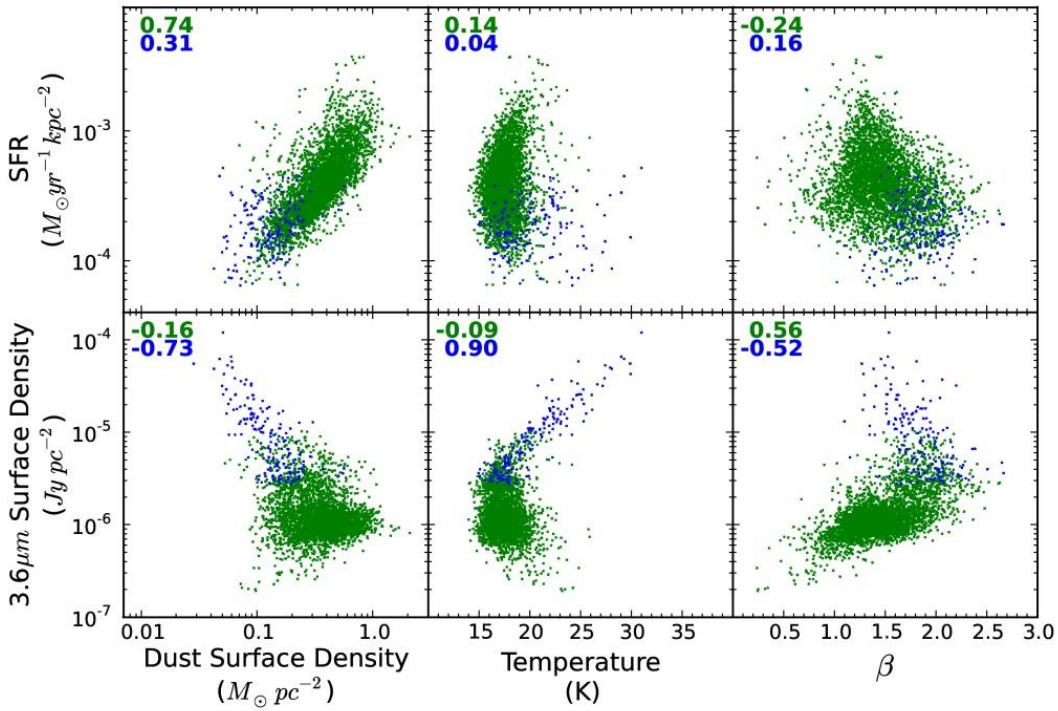

Smith et al.
2012, ApJ, 756, 40

NGC 6822

- Galametz et al. (2010) found that the 250/500 µm ratio was correlated with 24 µm emission (and hence with star formation).

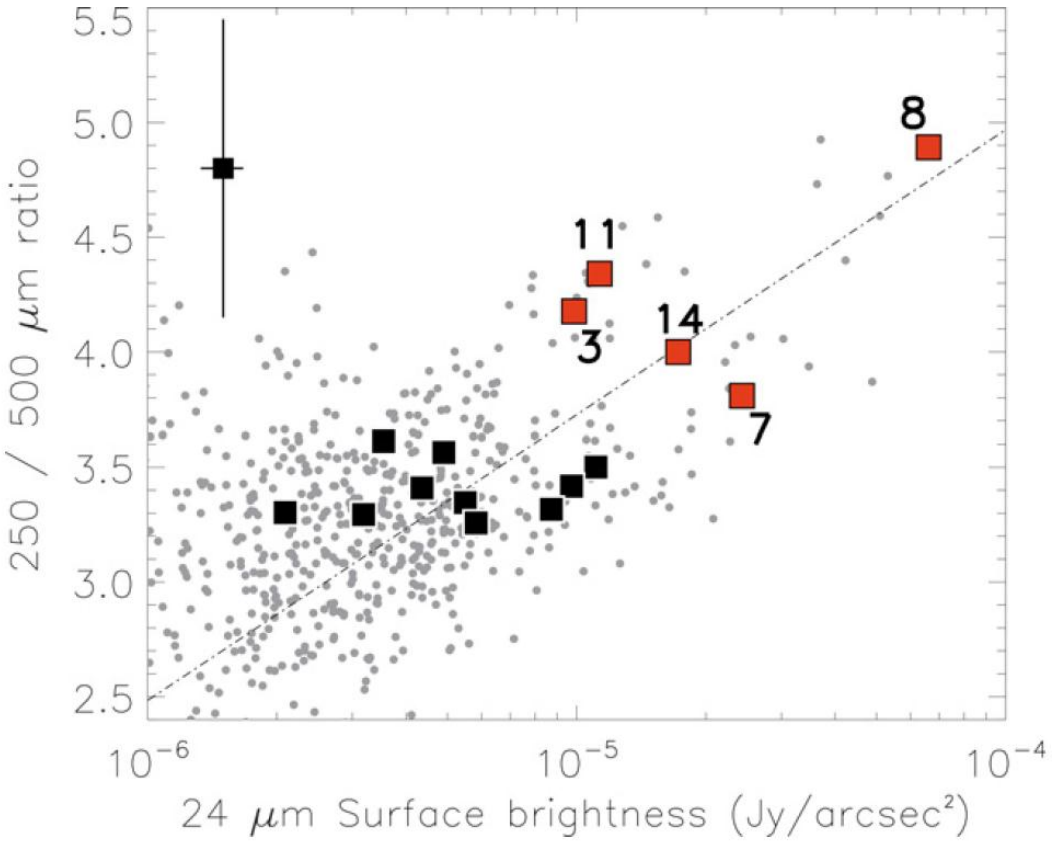

Galametz et al., 2010, A&A, 518, L55

KINGFISH

- Engelbracht et al. (2010) found that dust temperatures increased as bulge size increased.

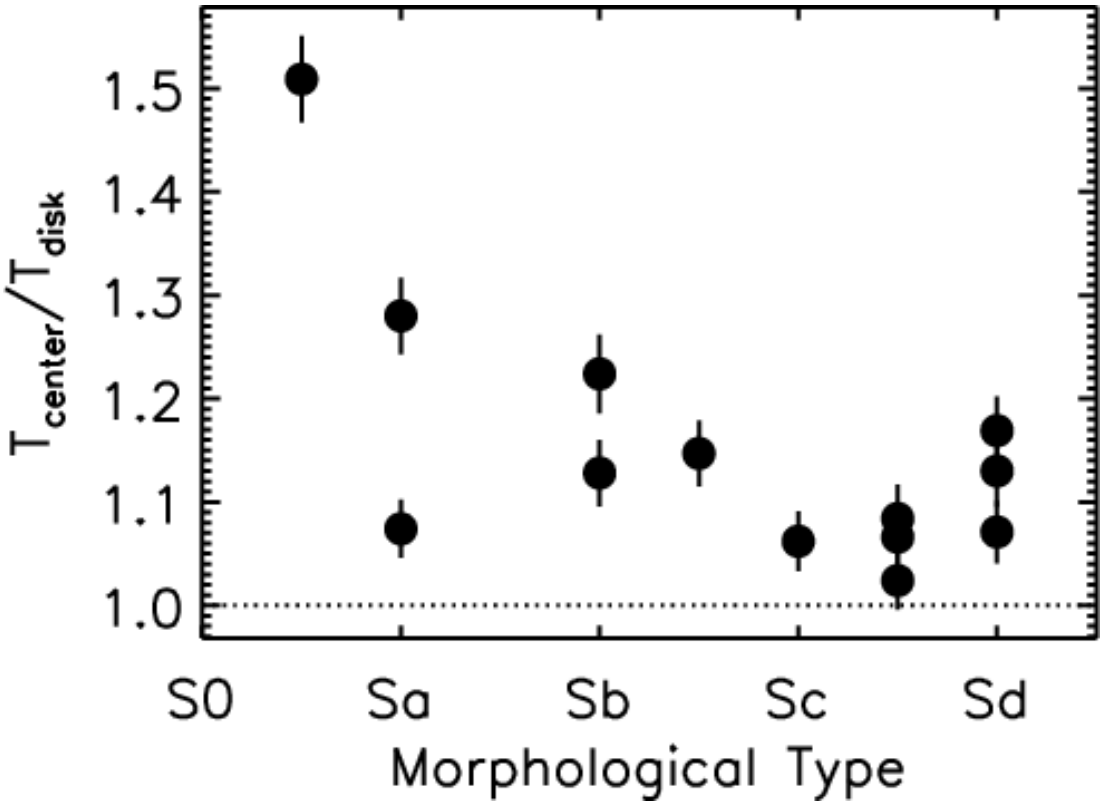

Engelbracht et al., 2010, A&A, 518, L56

HerMES

- Rowan-Robinson et al. (2010) found evidence through SED template fitting that diffuse dust heated by evolved stellar populations may be present in HerMES sources.

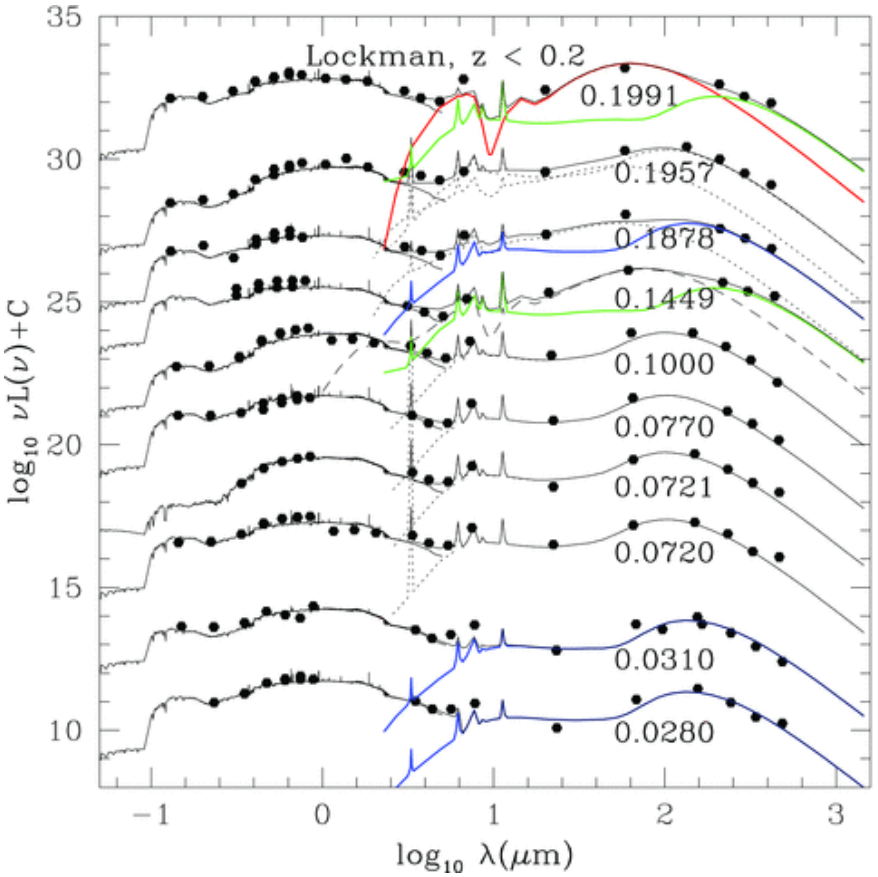

Rowan-Robinson et al., 2010, MNRAS, 409, 2


New Herschel analyses

New Data

Subsample of galaxies selected from Herschel Reference Survey with following characteristics (some are intrinsic to HRS, some intrinsic to subsample):

- Distance 15-25 Mpc
- K-band flux-limited
- Field and Virgo Cluster galaxies included
- Hubble type Sa-Sc
- Angular size >5’
- Minor/major axis ratio: >1/2

Worked with only 250/350 μm ratios

- SPIRE data available for all galaxies in subsample
- 250, 350 μm data have better resolution than 500 μm data
- 250/350 μm ratio still sensitive to temperature variations

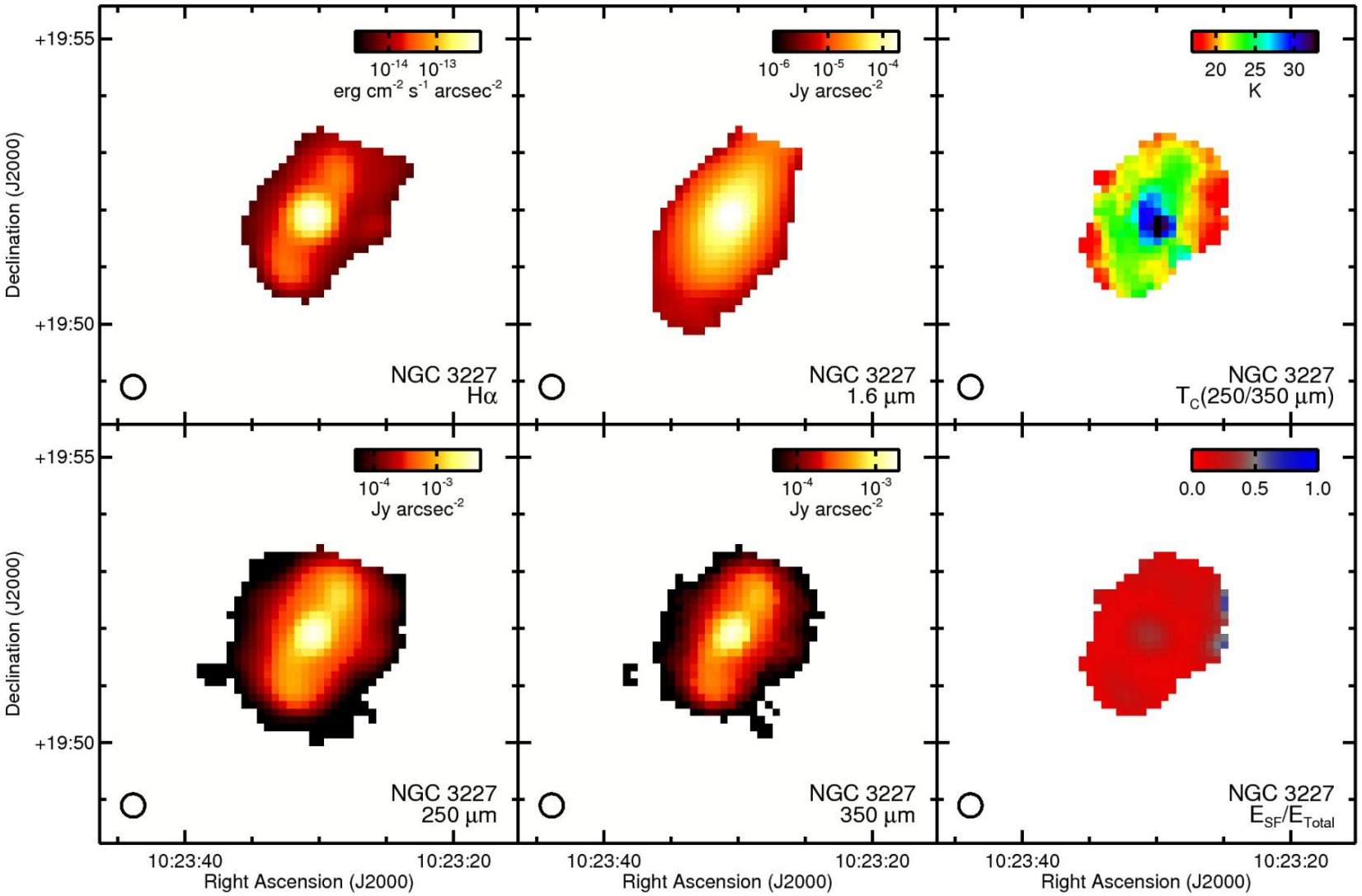
+19:55
+19:50
Declination (J2000)
10^{-14} 10^{-13}
erg cm^{-2} s^{-1} arcsec^{-2}
NGC 3227
Hα
10^{-6} 10^{-5} 10^{-4}
Jy arcsec^{-2}
NGC 3227
1.6 μm
20 25 30
K
NGC 3227
T_C(250/350 μm)
10^{-4} 10^{-3}
Jy arcsec^{-2}
NGC 3227
250 μm
10^{-4} 10^{-3}
Jy arcsec^{-2}
NGC 3227
350 μm
0.0 0.5 1.0
NGC 3227
E_{SF}/E_{Total}
10:23:40
10:23:20
Right Ascension (J2000)

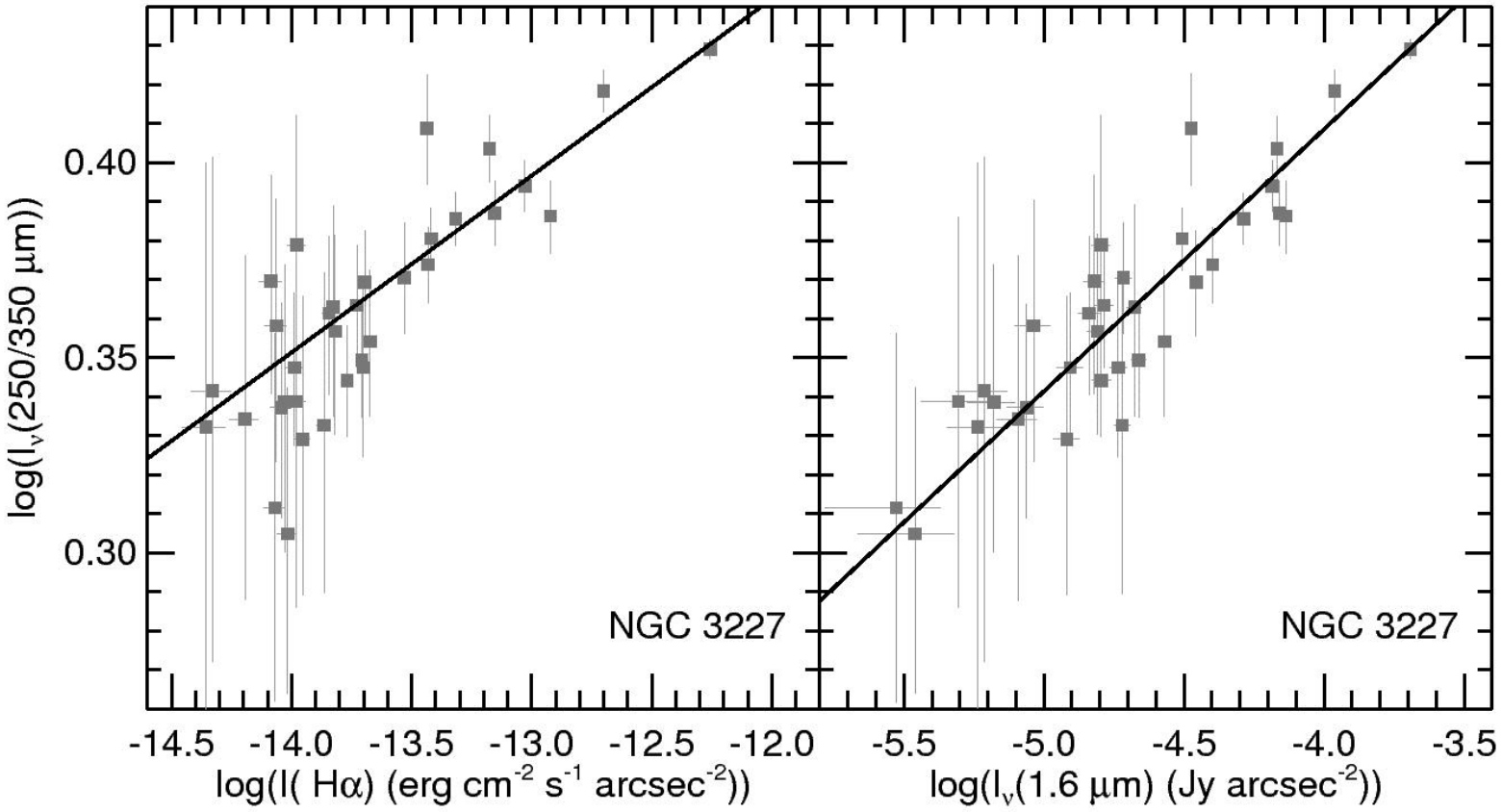
0.40
0.35
0.30
log(I$_\nu$(250/350 μm))
NGC 3227
-14.5 -14.0 -13.5 -13.0 -12.5 -12.0
log(I(Hα) (erg cm^{-2} s^{-1} arcsec^{-2}))
NGC 3227
-5.5 -5.0 -4.5 -4.0 -3.5
log(I$_\nu$(1.6 μm) (Jy arcsec^{-2}))

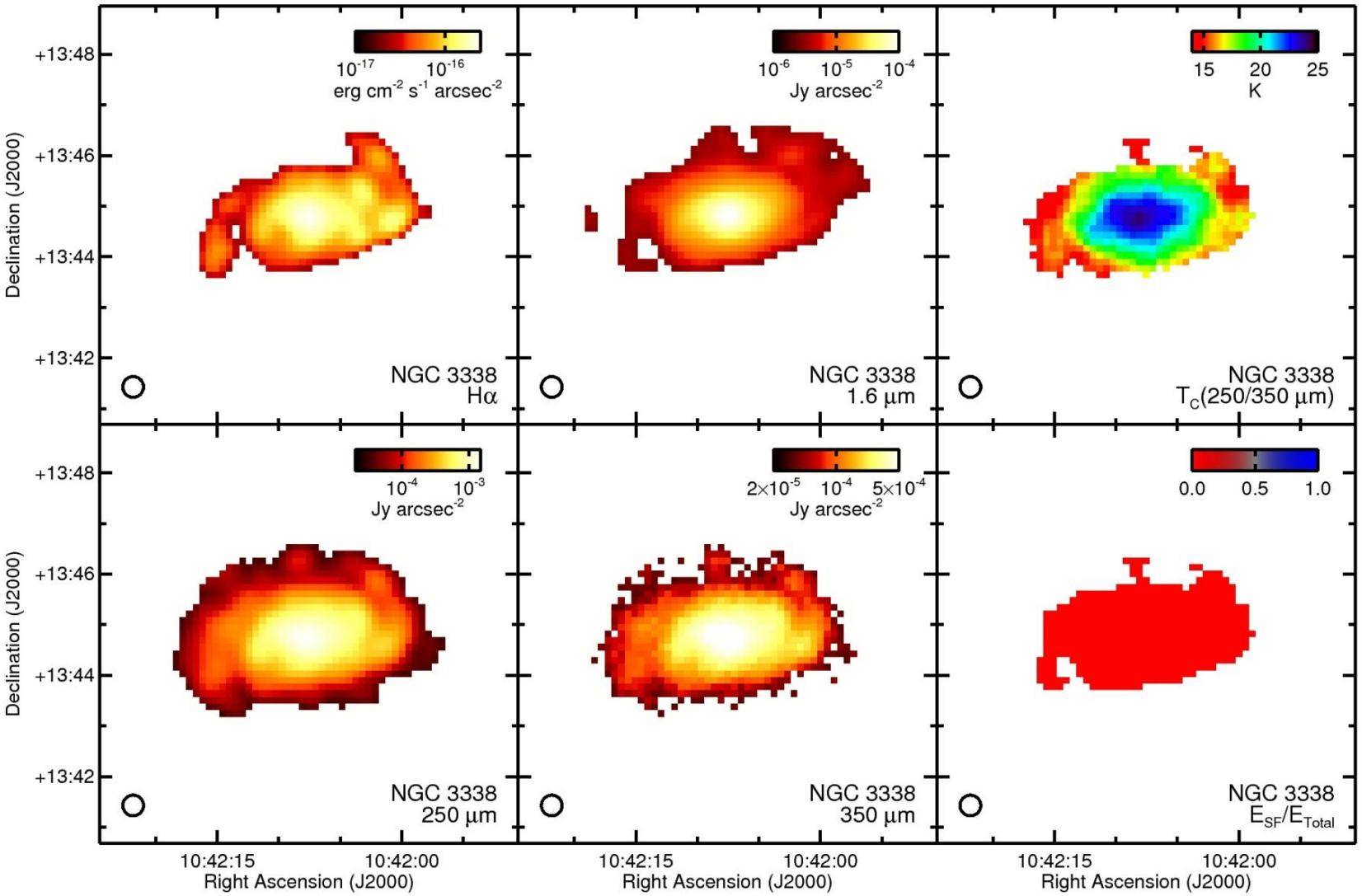
10^-17 10^-16
erg cm^-2 s^-1 arcsec^-2
NGC 3338
Hα
10^-6 10^-5 10^-4
Jy arcsec^-2
NGC 3338
1.6 μm
15 20 25
K
NGC 3338
T_C(250/350 μm)
10^-4 10^-3
Jy arcsec^-2
NGC 3338
250 μm
2×10^-5 10^-4 5×10^-4
Jy arcsec^-2
NGC 3338
350 μm
0.0 0.5 1.0
NGC 3338
E_SF/E_Total
Declination (J2000)
+13:48
+13:46
+13:44
+13:42
10:42:15
10:42:00
Right Ascension (J2000)

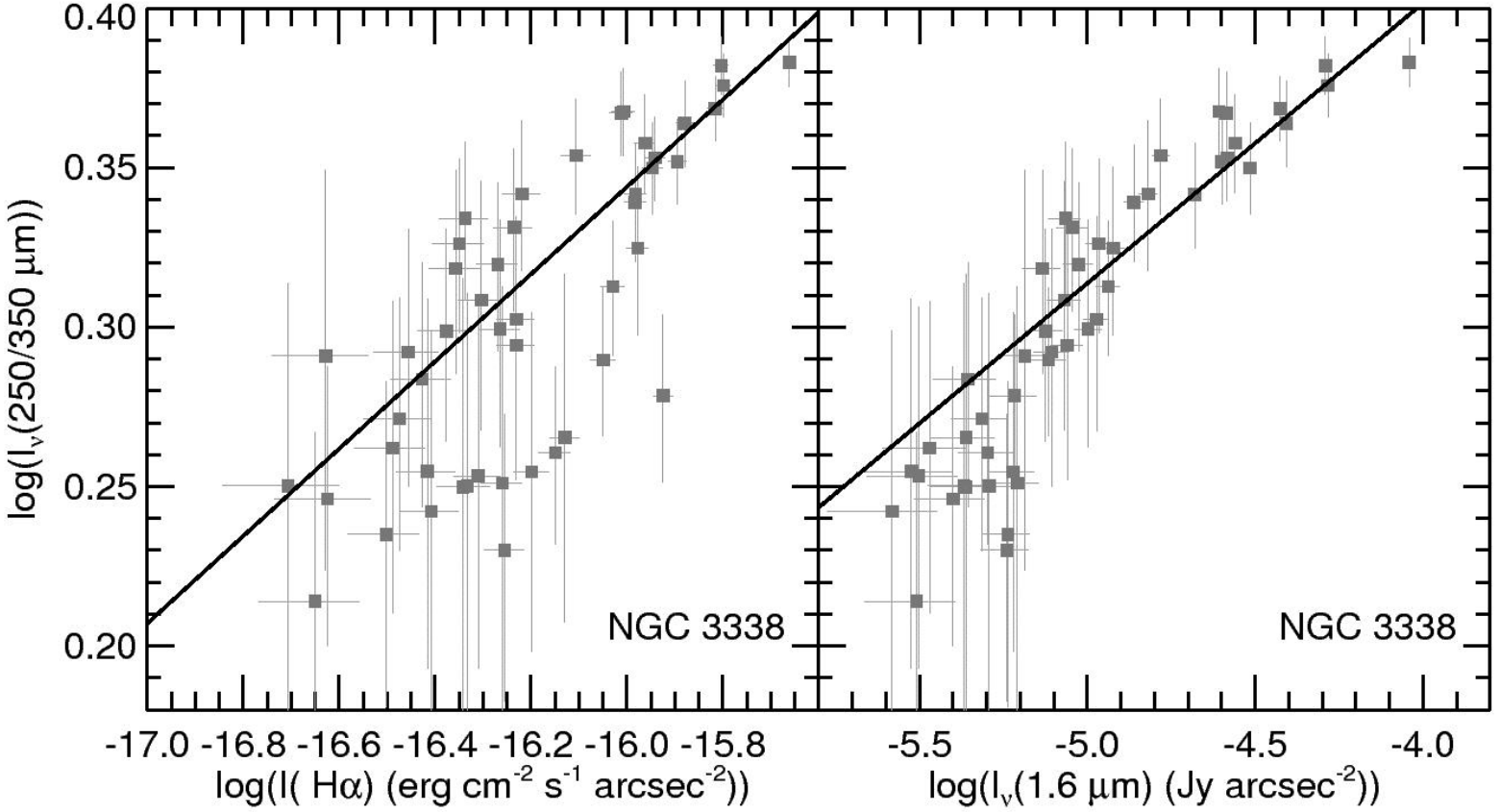
0.40
0.35
0.30
0.25
0.20
log(I$_\nu$(250/350 μm))
NGC 3338
-17.0 -16.8 -16.6 -16.4 -16.2 -16.0 -15.8
log(I(Hα) (erg cm^{-2} s^{-1} arcsec^{-2}))
NGC 3338
-5.5 -5.0 -4.5 -4.0
log(I$_\nu$(1.6 μm) (Jy arcsec^{-2}))

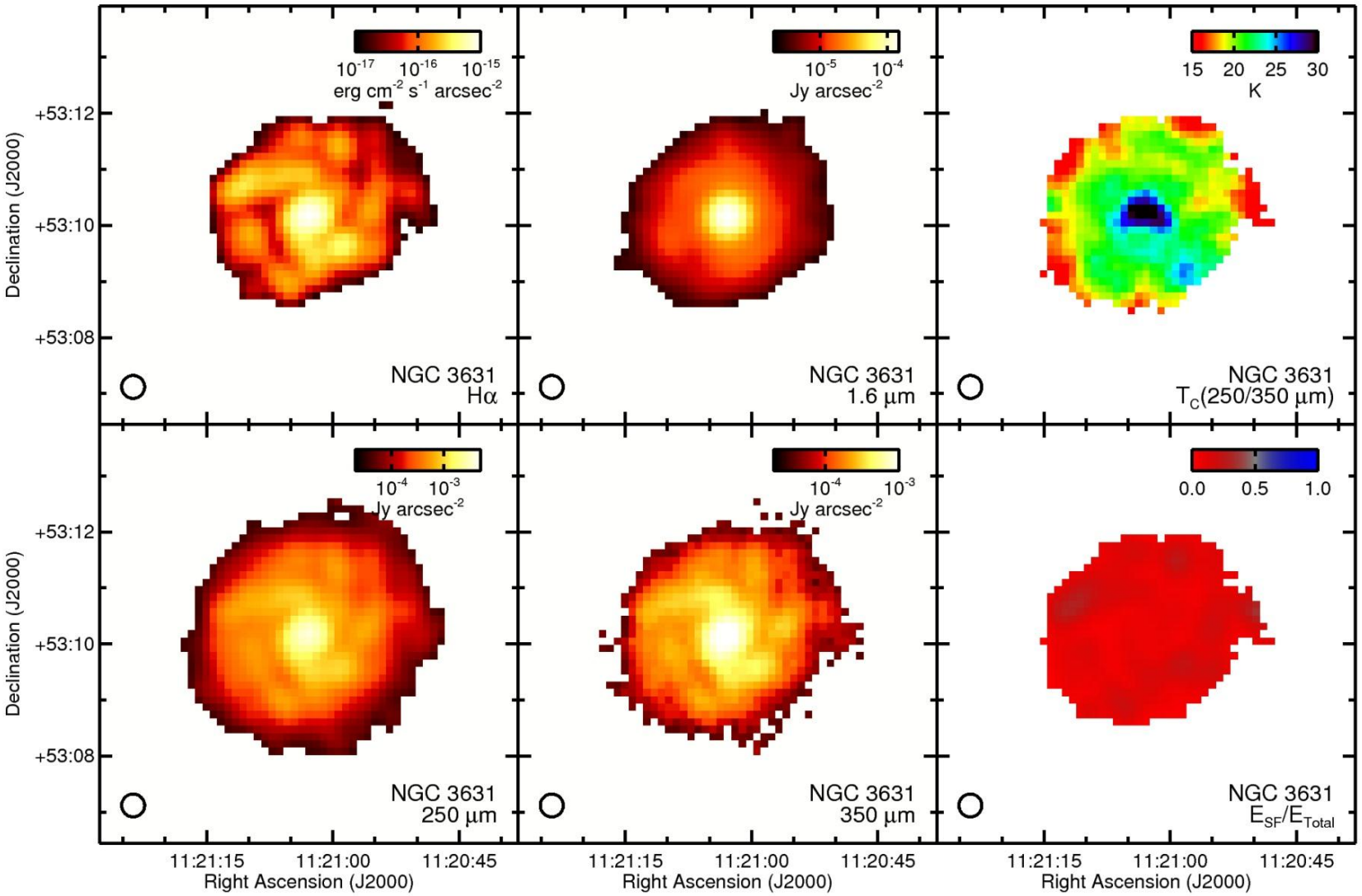
10^-17 10^-16 10^-15
erg cm^-2 s^-1 arcsec^-2
NGC 3631
Hα
10^-5 10^-4
Jy arcsec^-2
NGC 3631
1.6 μm
15 20 25 30
K
NGC 3631
T_C(250/350 μm)
10^-4 10^-3
Jy arcsec^-2
NGC 3631
250 μm
10^-4 10^-3
Jy arcsec^-2
NGC 3631
350 μm
0.0 0.5 1.0
NGC 3631
E_SF/E_Total
Declination (J2000)
+53:12
+53:10
+53:08
11:21:15 11:21:00 11:20:45
Right Ascension (J2000)

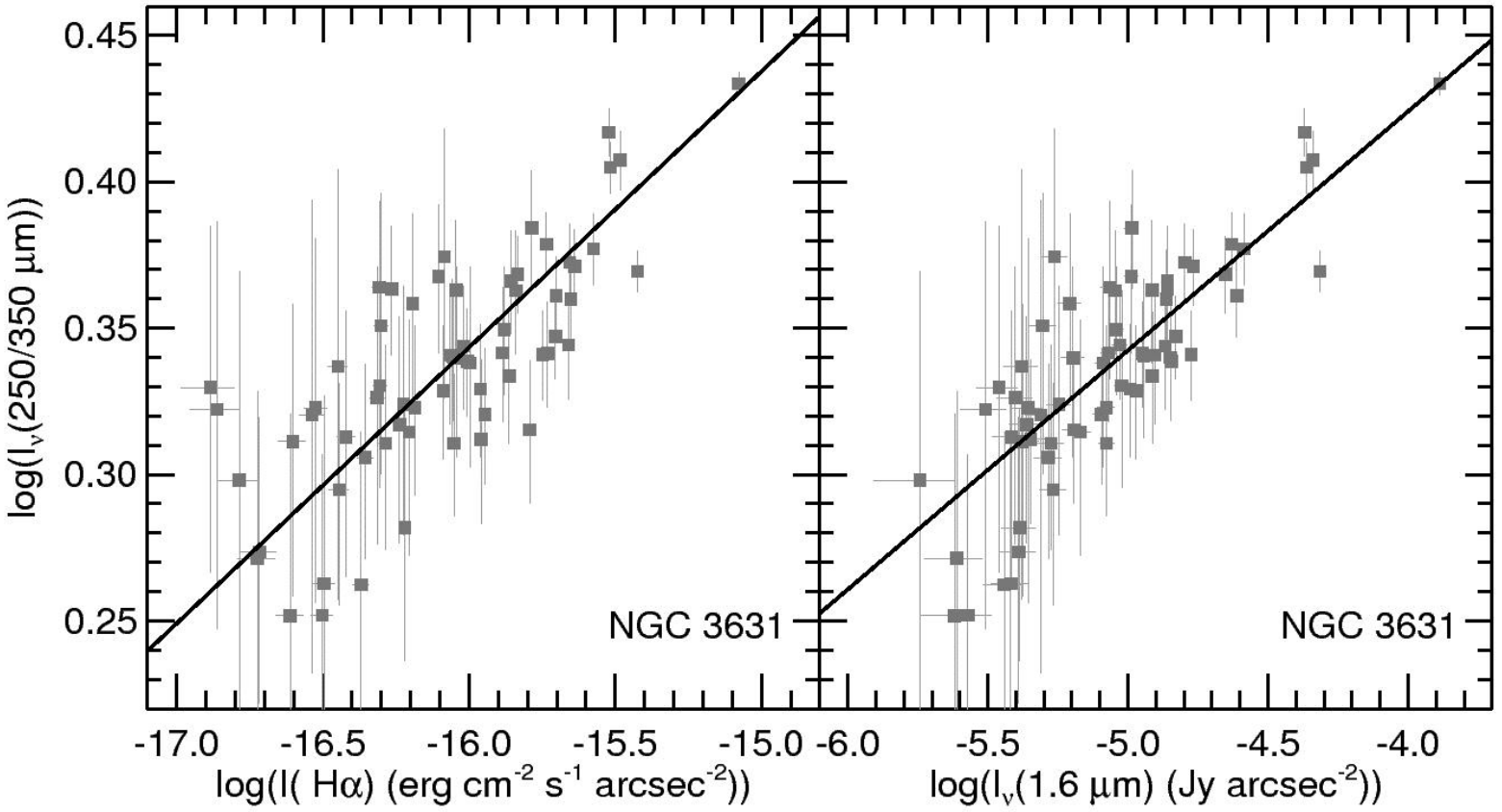
0.45
0.40
0.35
0.30
0.25
log(I$_\nu$(250/350 μm))
NGC 3631
-17.0
-16.5
-16.0
-15.5
-15.0
log(I(Hα) (erg cm^{-2} s^{-1} arcsec^{-2}))
-6.0
-5.5
-5.0
-4.5
-4.0
log(I$_\nu$(1.6 μm) (Jy arcsec^{-2}))
NGC 3631

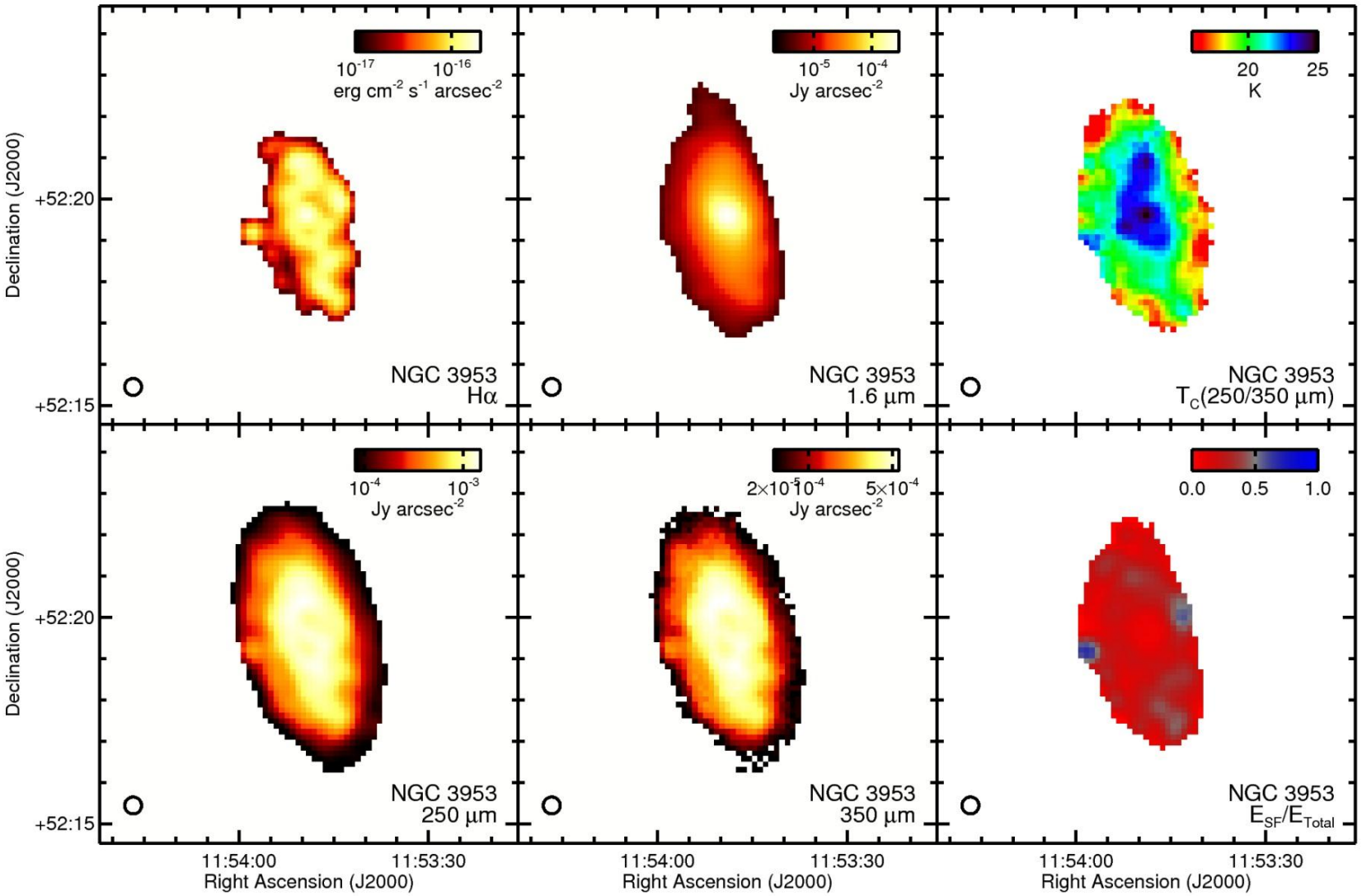
10^-17 10^-16
erg cm^-2 s^-1 arcsec^-2
NGC 3953
Hα
10^-5 10^-4
Jy arcsec^-2
NGC 3953
1.6 μm
20 25
K
NGC 3953
T_C(250/350 μm)
10^-4 10^-3
Jy arcsec^-2
NGC 3953
250 μm
2×10^-5 10^-4 5×10^-4
Jy arcsec^-2
NGC 3953
350 μm
0.0 0.5 1.0
NGC 3953
E_SF/E_Total
Declination (J2000)
+52:20
+52:15
11:54:00
11:53:30
Right Ascension (J2000)

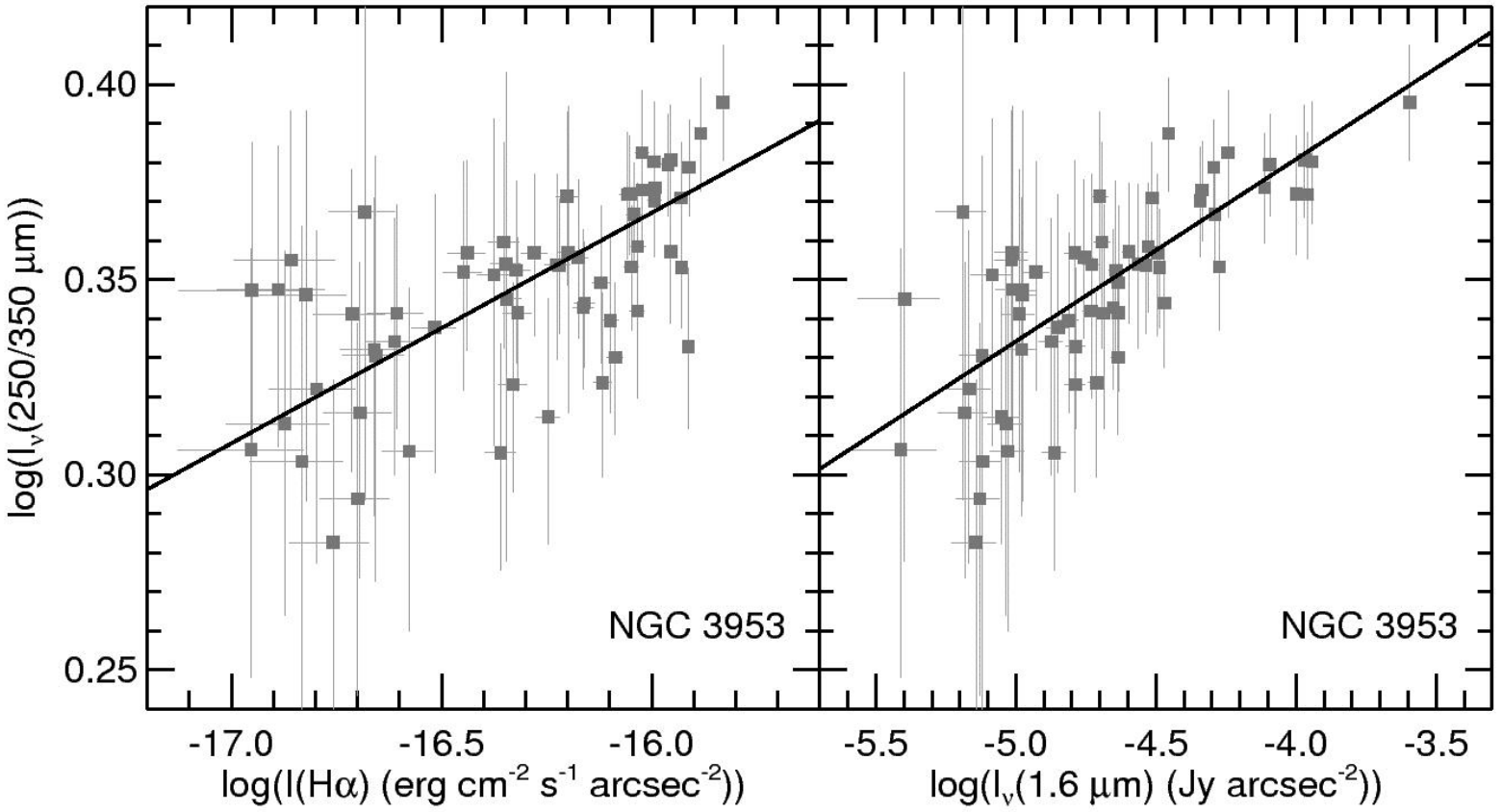
0.40
0.35
0.30
0.25
log(I$_\nu$(250/350 μm))
NGC 3953
-17.0
-16.5
-16.0
log(I(Hα) (erg cm^{-2} s^{-1} arcsec^{-2}))
NGC 3953
-5.5
-5.0
-4.5
-4.0
-3.5
log(I$_\nu$(1.6 μm) (Jy arcsec^{-2}))

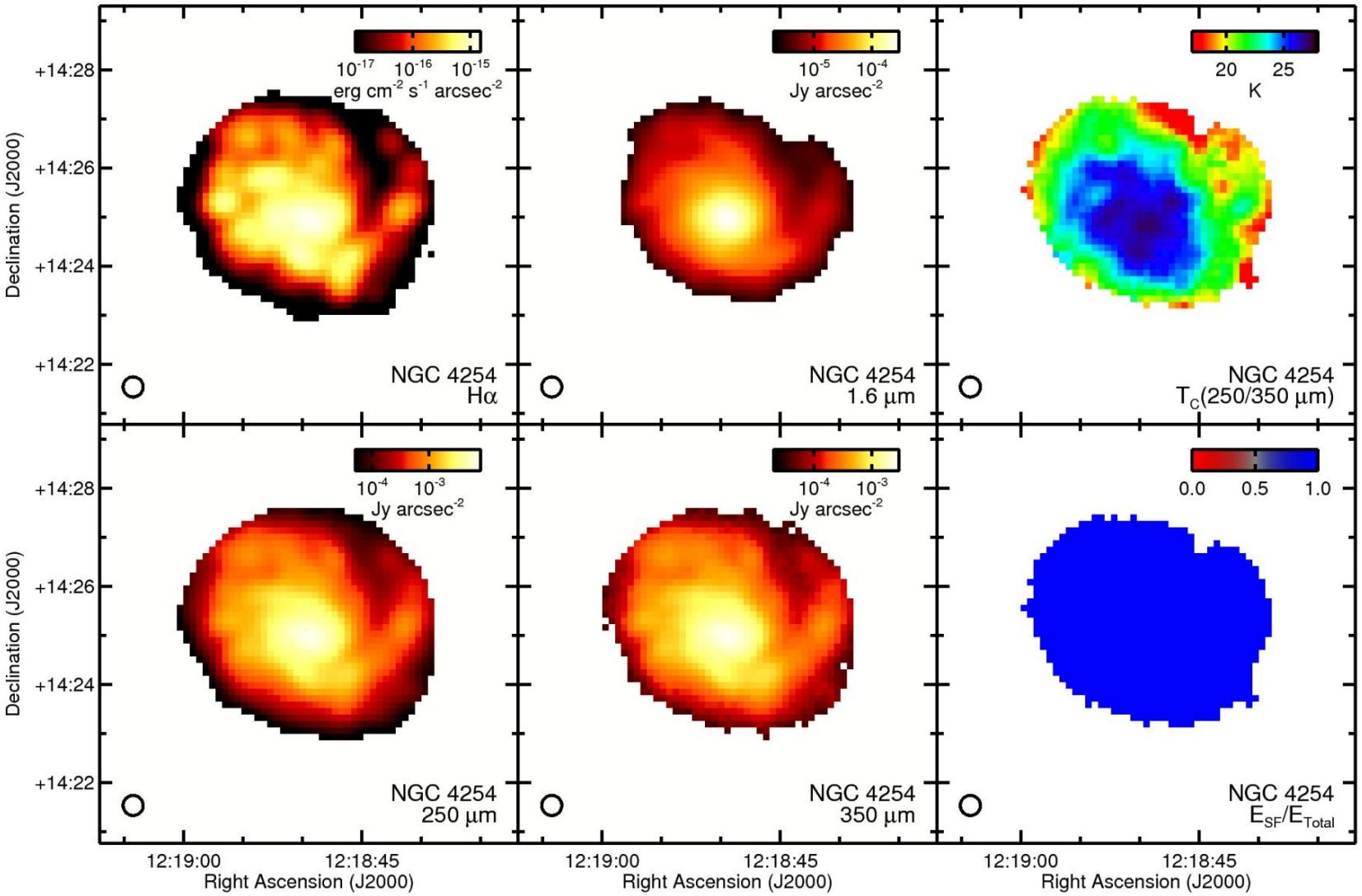
10^-17 10^-16 10^-15
erg cm^-2 s^-1 arcsec^-2
NGC 4254
Hα
10^-5 10^-4
Jy arcsec^-2
NGC 4254
1.6 μm
20 25
K
NGC 4254
T_C(250/350 μm)
10^-4 10^-3
Jy arcsec^-2
NGC 4254
250 μm
10^-4 10^-3
Jy arcsec^-2
NGC 4254
350 μm
0.0 0.5 1.0
NGC 4254
E_SF/E_Total
Declination (J2000)
+14:28
+14:26
+14:24
+14:22
12:19:00
12:18:45
Right Ascension (J2000)

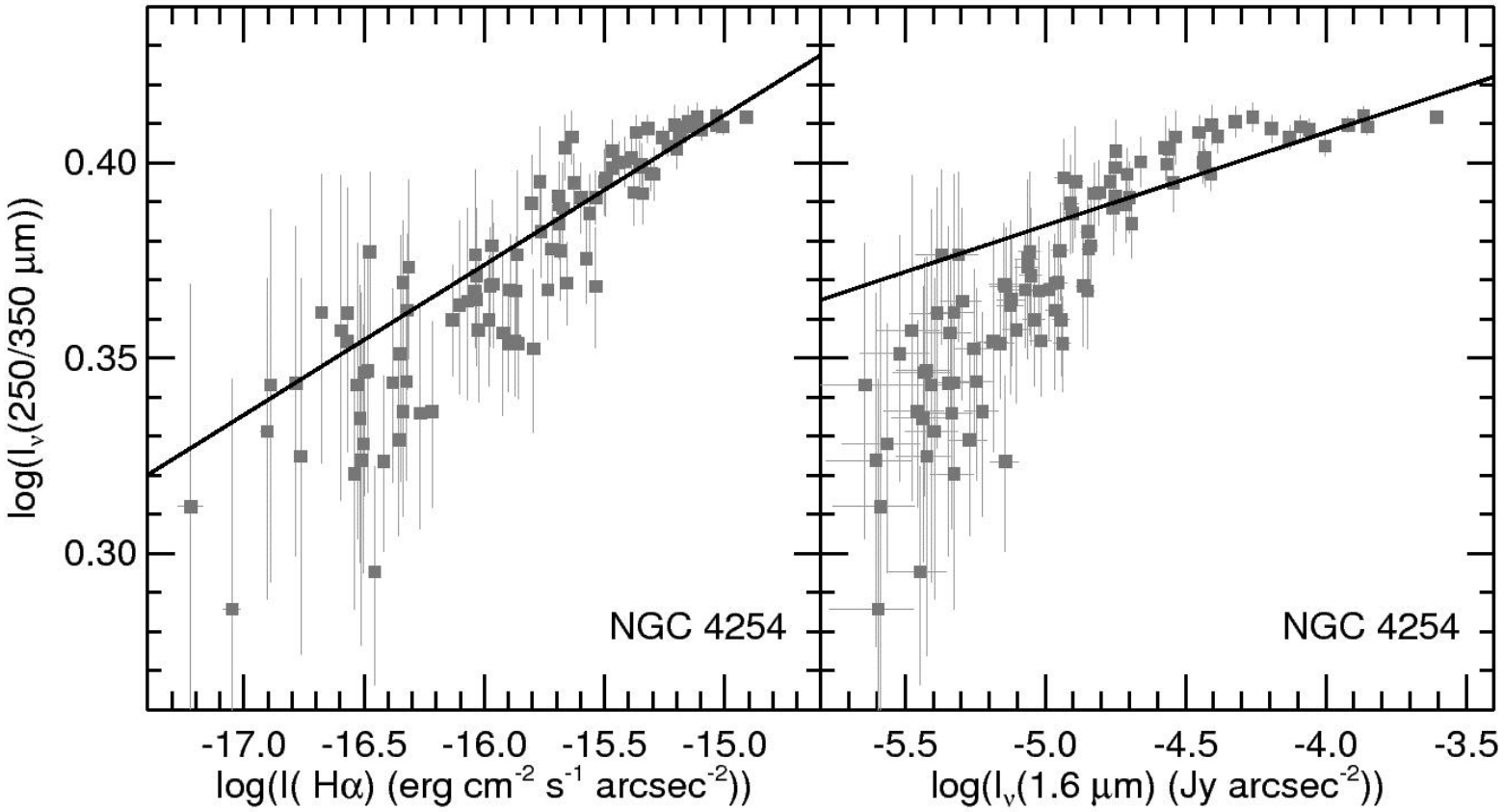
0.40
0.35
0.30
log(I$_\nu$(250/350 μm))
NGC 4254
-17.0
-16.5
-16.0
-15.5
-15.0
log(I(Hα) (erg cm^{-2} s^{-1} arcsec^{-2}))
NGC 4254
-5.5
-5.0
-4.5
-4.0
-3.5
log(I$_\nu$(1.6 μm) (Jy arcsec^{-2}))

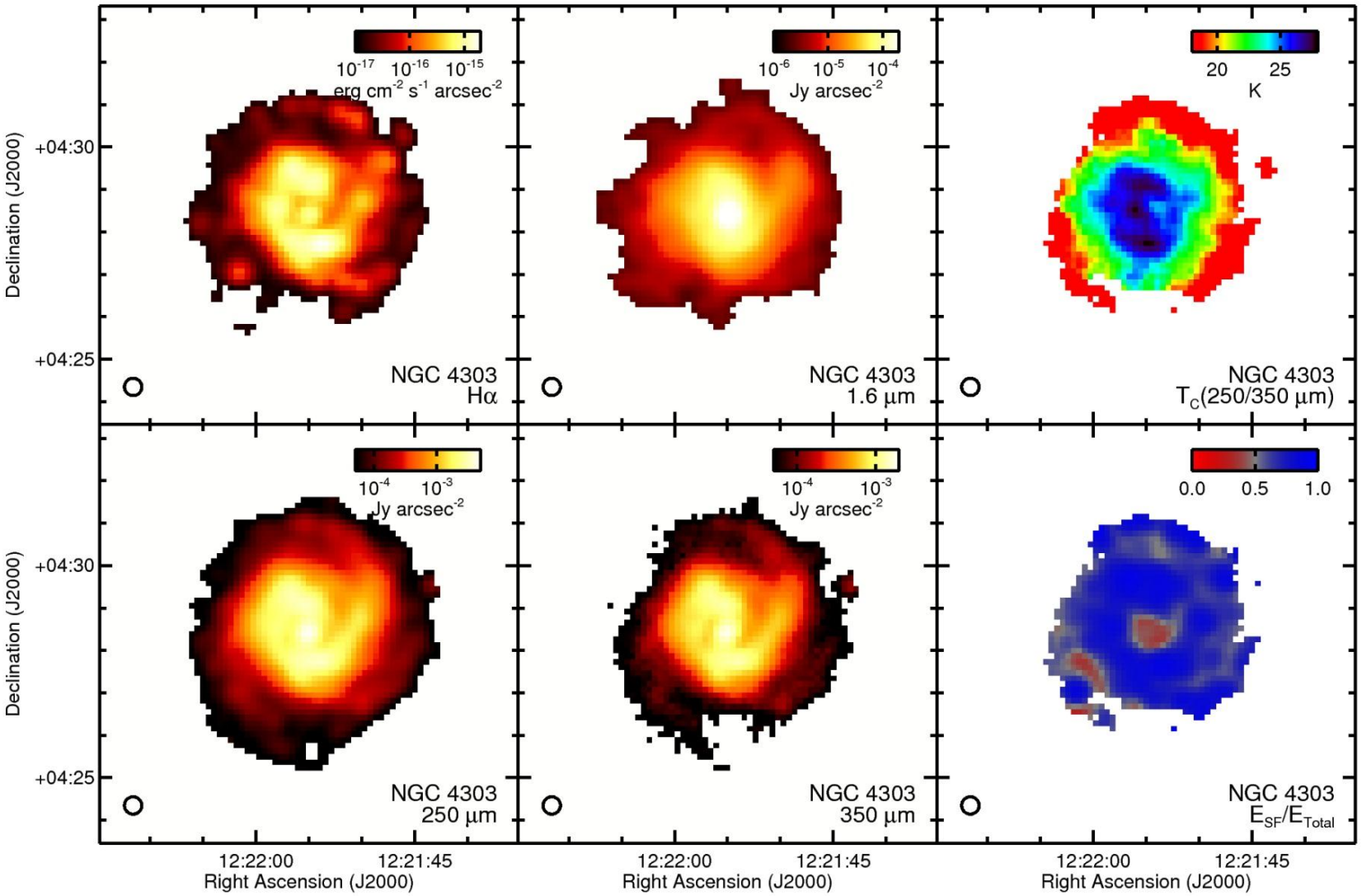
10^-17 10^-16 10^-15
erg cm^-2 s^-1 arcsec^-2
NGC 4303
Hα
10^-6 10^-5 10^-4
Jy arcsec^-2
NGC 4303
1.6 μm
20 25
K
NGC 4303
T_C(250/350 μm)
10^-4 10^-3
Jy arcsec^-2
NGC 4303
250 μm
10^-4 10^-3
Jy arcsec^-2
NGC 4303
350 μm
0.0 0.5 1.0
NGC 4303
E_SF/E_Total
Declination (J2000)
+04:30
+04:25
12:22:00
12:21:45
Right Ascension (J2000)

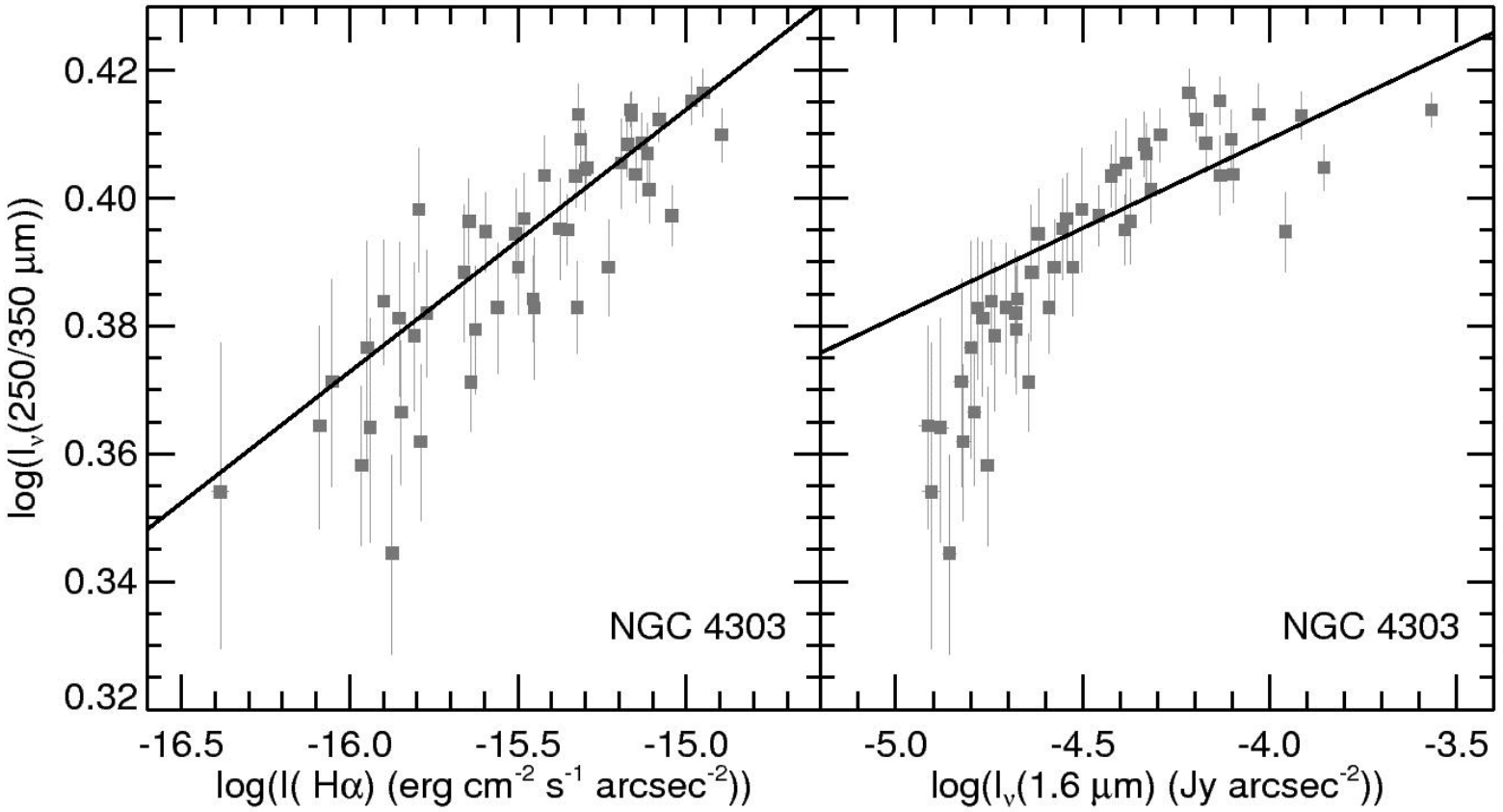
0.42
0.40
0.38
0.36
0.34
0.32
log(I$_\nu$(250/350 μm))
NGC 4303
-16.5
-16.0
-15.5
-15.0
log(I(Hα) (erg cm^{-2} s^{-1} arcsec^{-2}))
NGC 4303
-5.0
-4.5
-4.0
-3.5
log(I$_\nu$(1.6 μm) (Jy arcsec^{-2}))

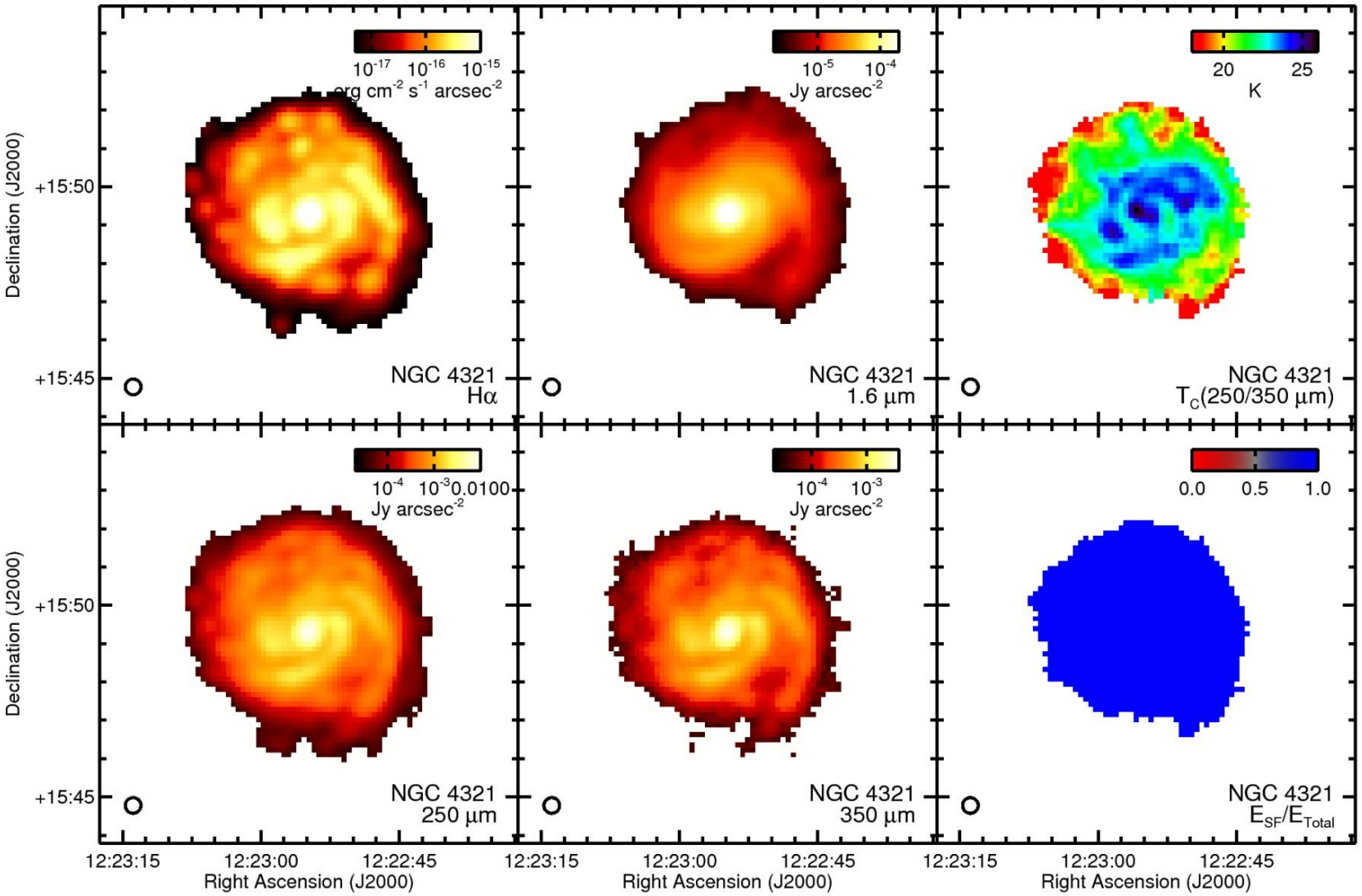
10^-17 10^-16 10^-15
erg cm^-2 s^-1 arcsec^-2
NGC 4321
Hα
10^-5 10^-4
Jy arcsec^-2
NGC 4321
1.6 μm
20 25
K
NGC 4321
T_C(250/350 μm)
10^-4 10^-3 0.0100
Jy arcsec^-2
NGC 4321
250 μm
10^-4 10^-3
Jy arcsec^-2
NGC 4321
350 μm
0.0 0.5 1.0
NGC 4321
E_SF/E_Total
Declination (J2000)
+15:50
+15:45
12:23:15
12:23:00
12:22:45
Right Ascension (J2000)

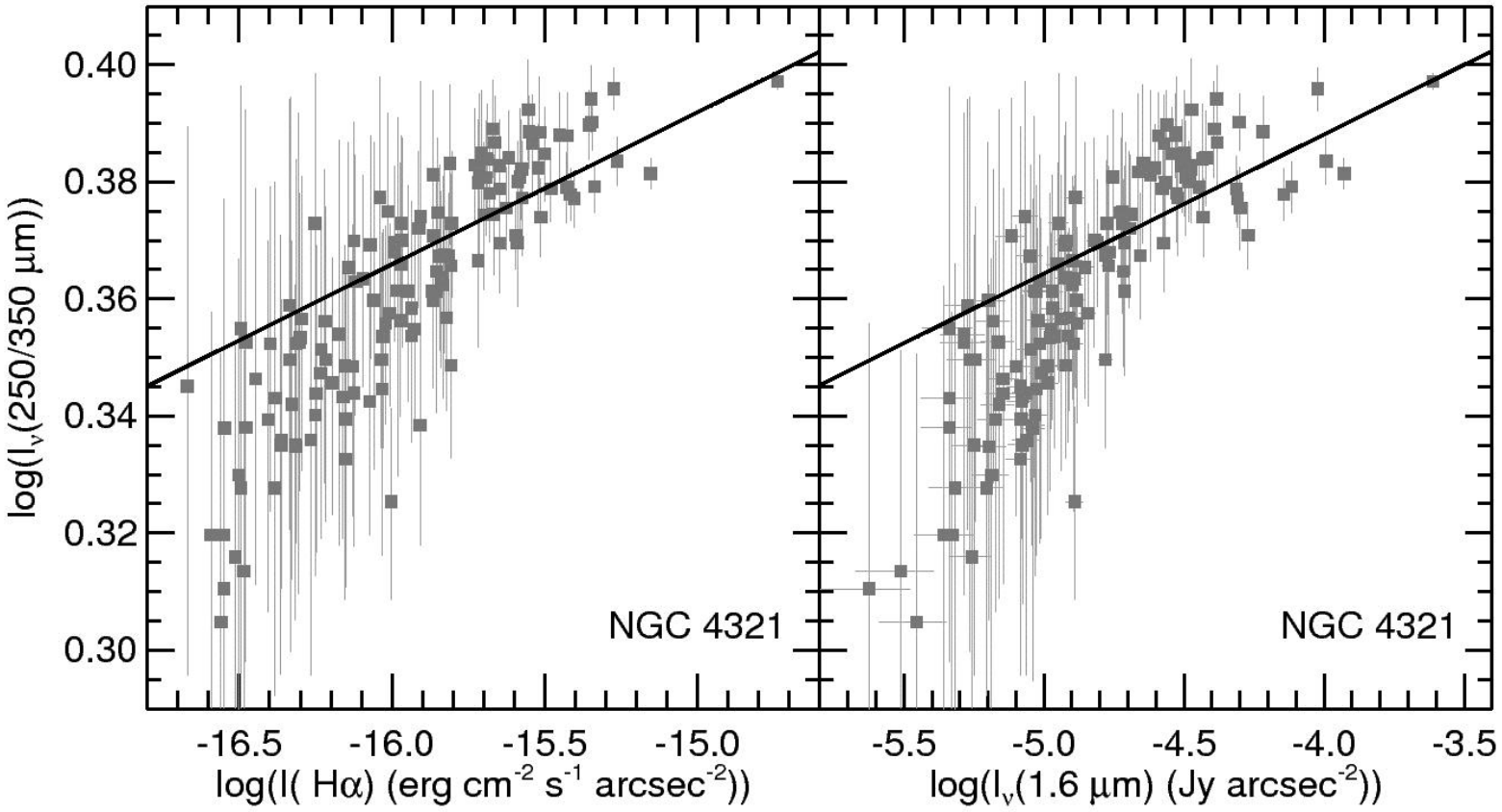
0.40
0.38
0.36
0.34
0.32
0.30
log(I$_\nu$(250/350 μm))
NGC 4321
-16.5
-16.0
-15.5
-15.0
log(I(Hα) (erg cm^{-2} s^{-1} arcsec^{-2}))
NGC 4321
-5.5
-5.0
-4.5
-4.0
-3.5
log(I$_\nu$(1.6 μm) (Jy arcsec^{-2}))

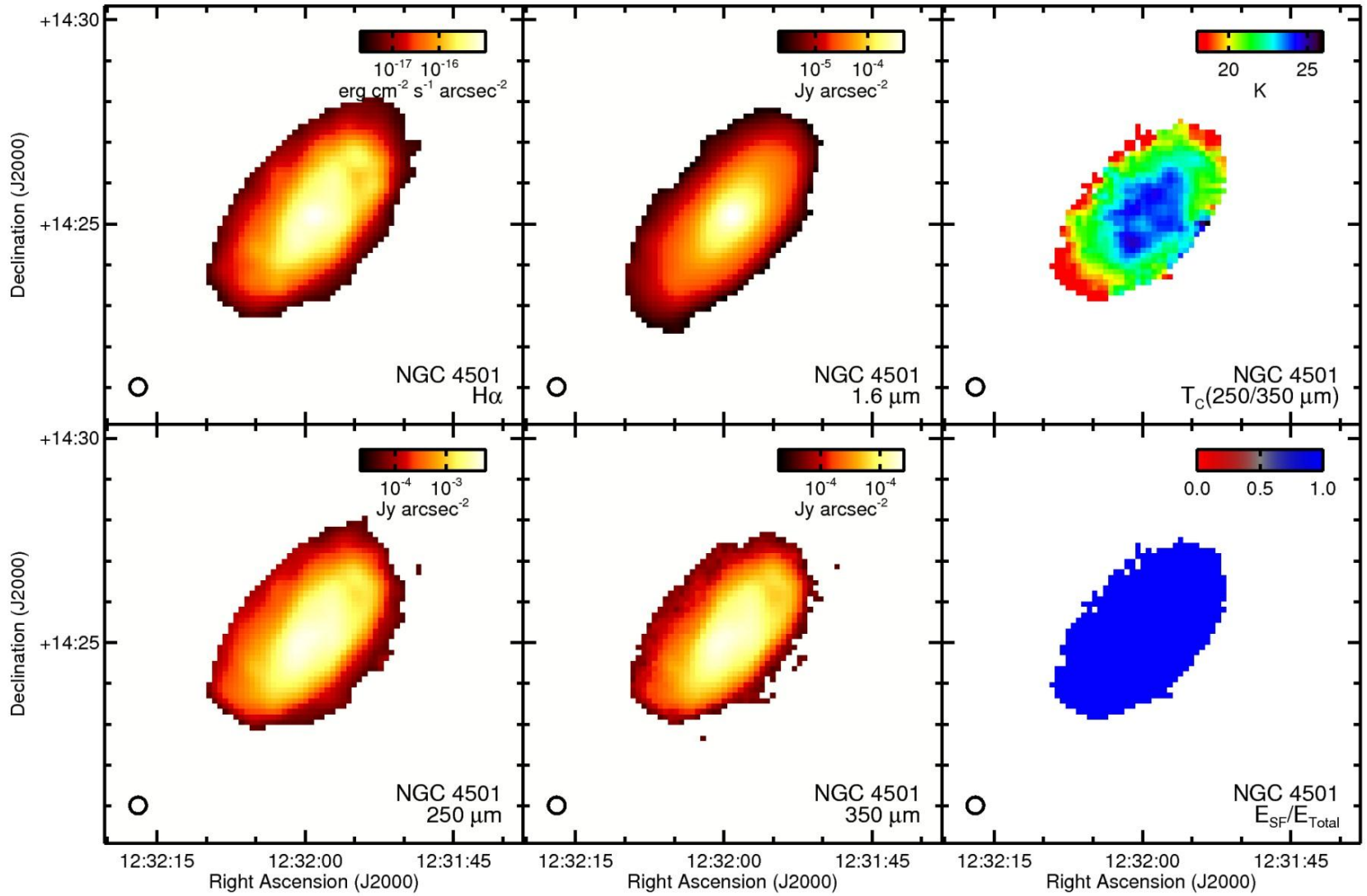
+14:30
+14:25
Declination (J2000)
10^{-17} 10^{-16}
erg cm^{-2} s^{-1} arcsec^{-2}
NGC 4501
Hα
10^{-5} 10^{-4}
Jy arcsec^{-2}
NGC 4501
1.6 μm
20 25
K
NGC 4501
T_C(250/350 μm)
10^{-4} 10^{-3}
Jy arcsec^{-2}
NGC 4501
250 μm
10^{-4} 10^{-4}
Jy arcsec^{-2}
NGC 4501
350 μm
0.0 0.5 1.0
NGC 4501
E_{SF}/E_{Total}
12:32:15
12:32:00
12:31:45
Right Ascension (J2000)

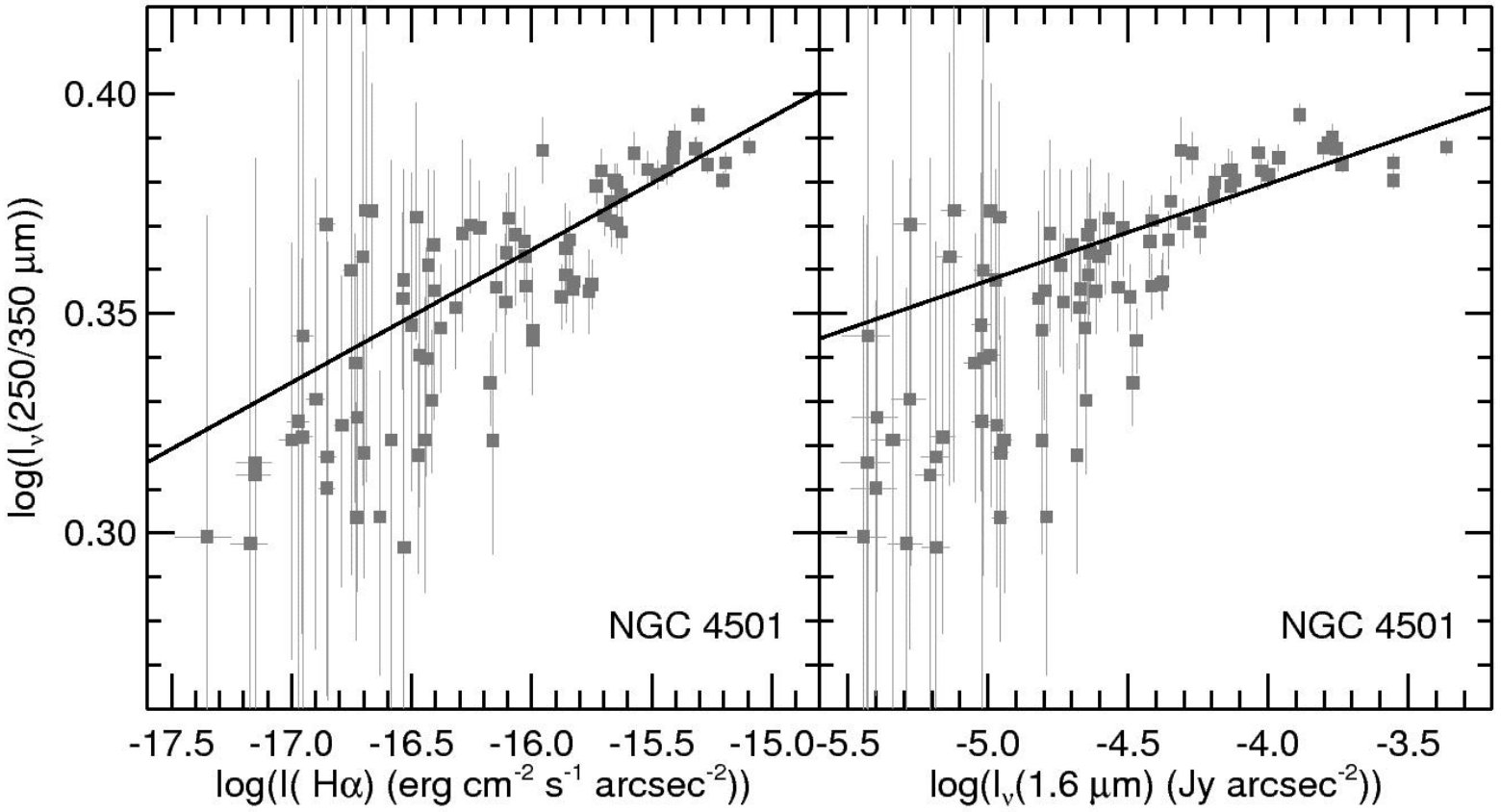
0.40
0.35
0.30
log(I$_\nu$(250/350 μm))
NGC 4501
NGC 4501
-17.5
-17.0
-16.5
-16.0
-15.5
-15.0
-5.5
-5.0
-4.5
-4.0
-3.5
log(I(Hα) (erg cm^{-2} s^{-1} arcsec^{-2}))
log(I$_\nu$(1.6 μm) (Jy arcsec^{-2}))

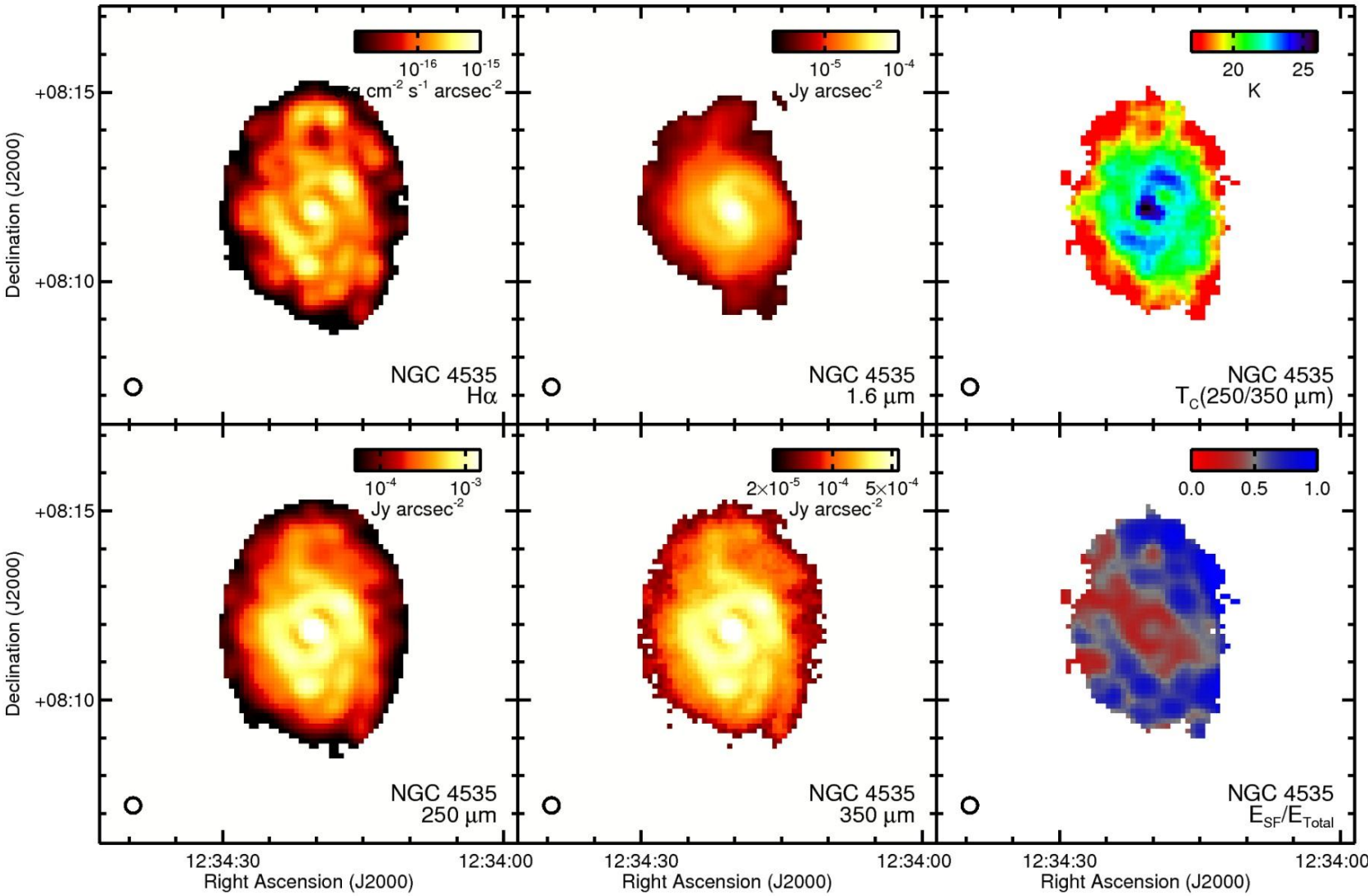
10^-16 10^-15
cm^-2 s^-1 arcsec^-2
NGC 4535
Hα
10^-5 10^-4
Jy arcsec^-2
NGC 4535
1.6 μm
20 25
K
NGC 4535
T_C(250/350 μm)
10^-4 10^-3
Jy arcsec^-2
NGC 4535
250 μm
2×10^-5 10^-4 5×10^-4
Jy arcsec^-2
NGC 4535
350 μm
0.0 0.5 1.0
NGC 4535
E_SF/E_Total
Declination (J2000)
+08:15
+08:10
12:34:30
12:34:00
Right Ascension (J2000)

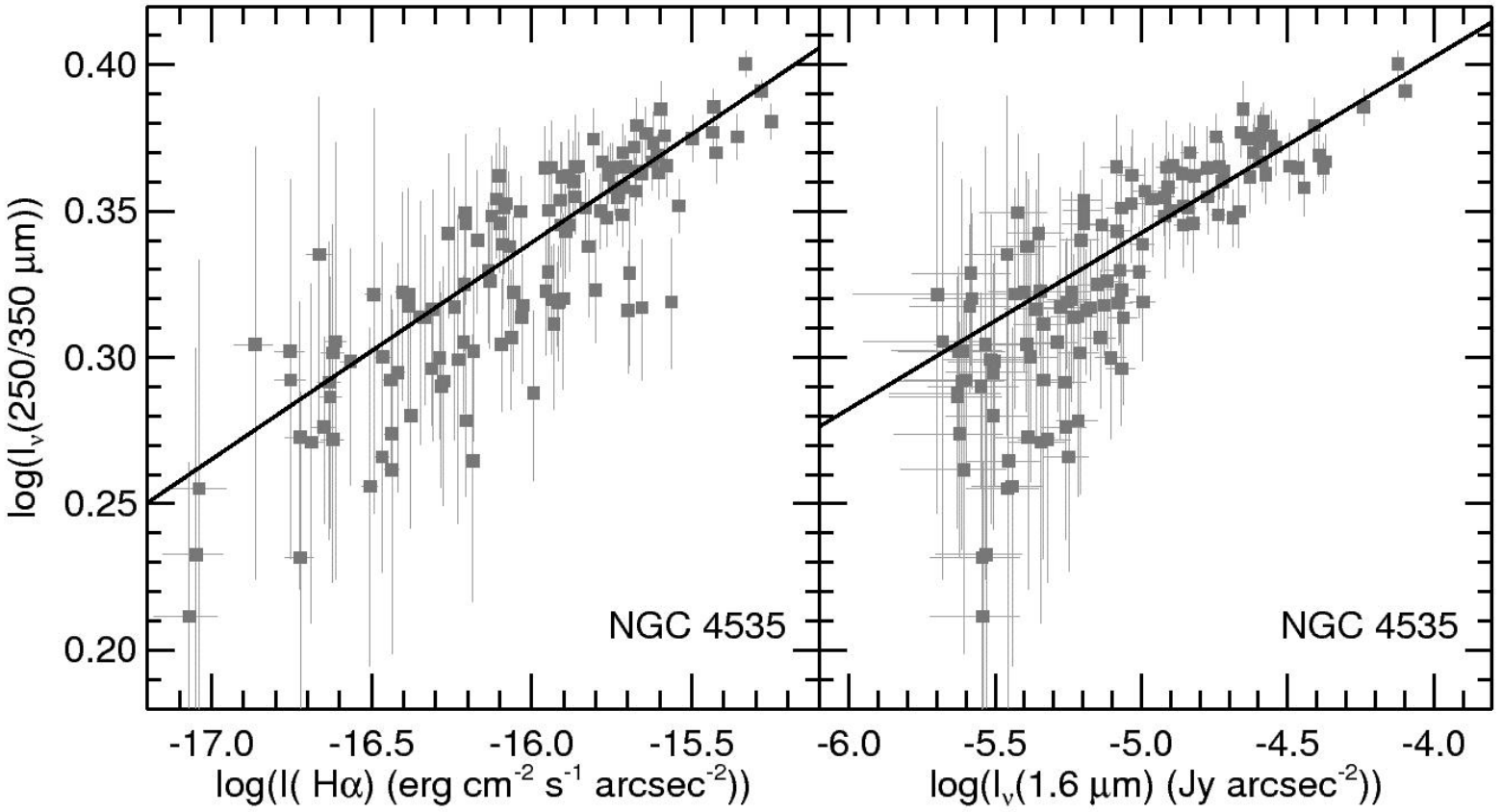
0.40
0.35
0.30
0.25
0.20
log(I$_\nu$(250/350 μm))
NGC 4535
-17.0
-16.5
-16.0
-15.5
log(I(Hα) (erg cm^{-2} s^{-1} arcsec^{-2}))
-6.0
-5.5
-5.0
-4.5
-4.0
log(I$_\nu$(1.6 μm) (Jy arcsec^{-2}))
NGC 4535

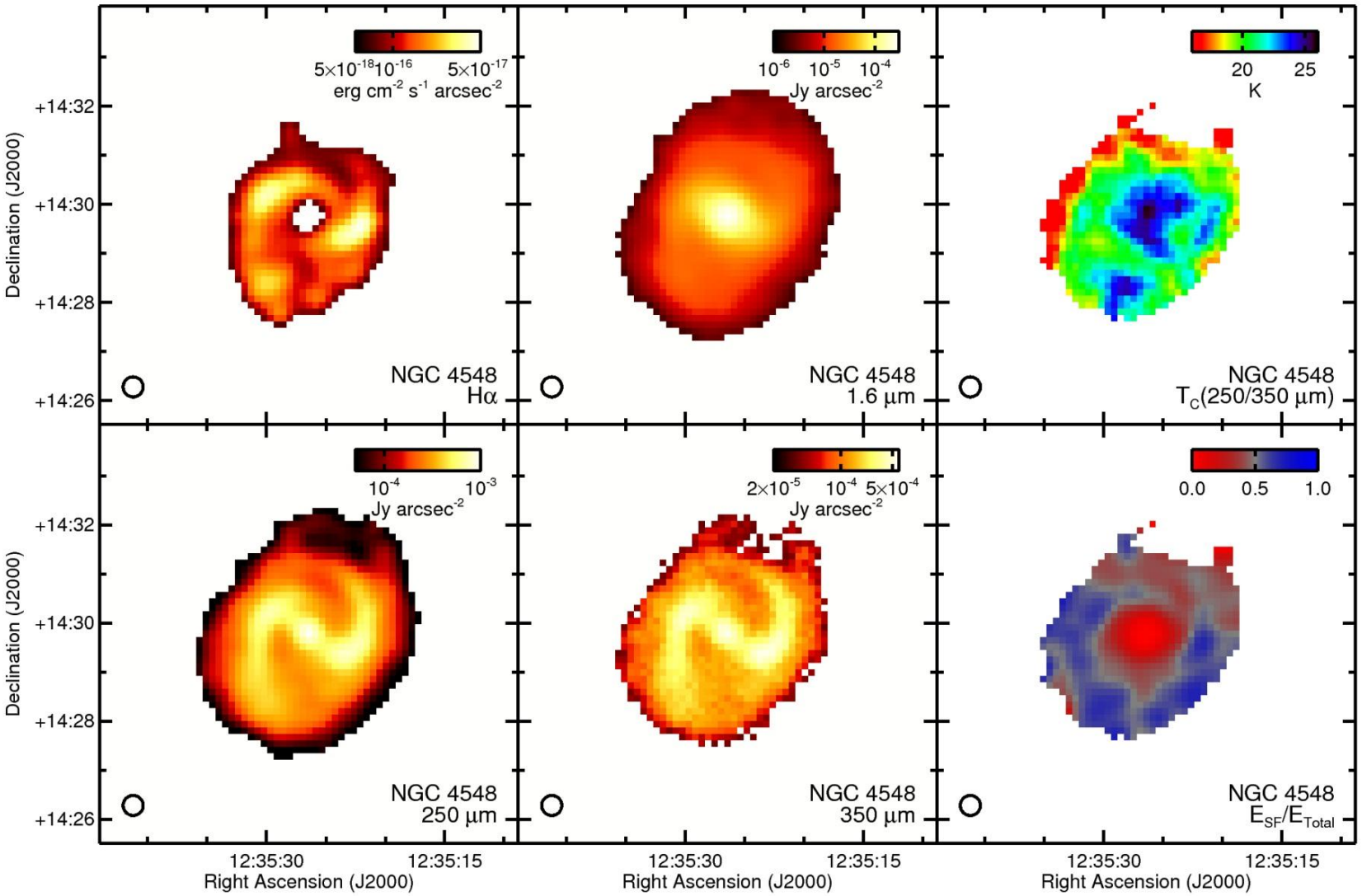
5×10-18 10-16 5×10-17
erg cm-2 s-1 arcsec-2
NGC 4548
Hα
10-6 10-5 10-4
Jy arcsec-2
NGC 4548
1.6 μm
20 25
K
NGC 4548
TC(250/350 μm)
10-4 10-3
Jy arcsec-2
NGC 4548
250 μm
2×10-5 10-4 5×10-4
Jy arcsec-2
NGC 4548
350 μm
0.0 0.5 1.0
NGC 4548
ESF/ETotal
Declination (J2000)
+14:32
+14:30
+14:28
+14:26
12:35:30
12:35:15
Right Ascension (J2000)

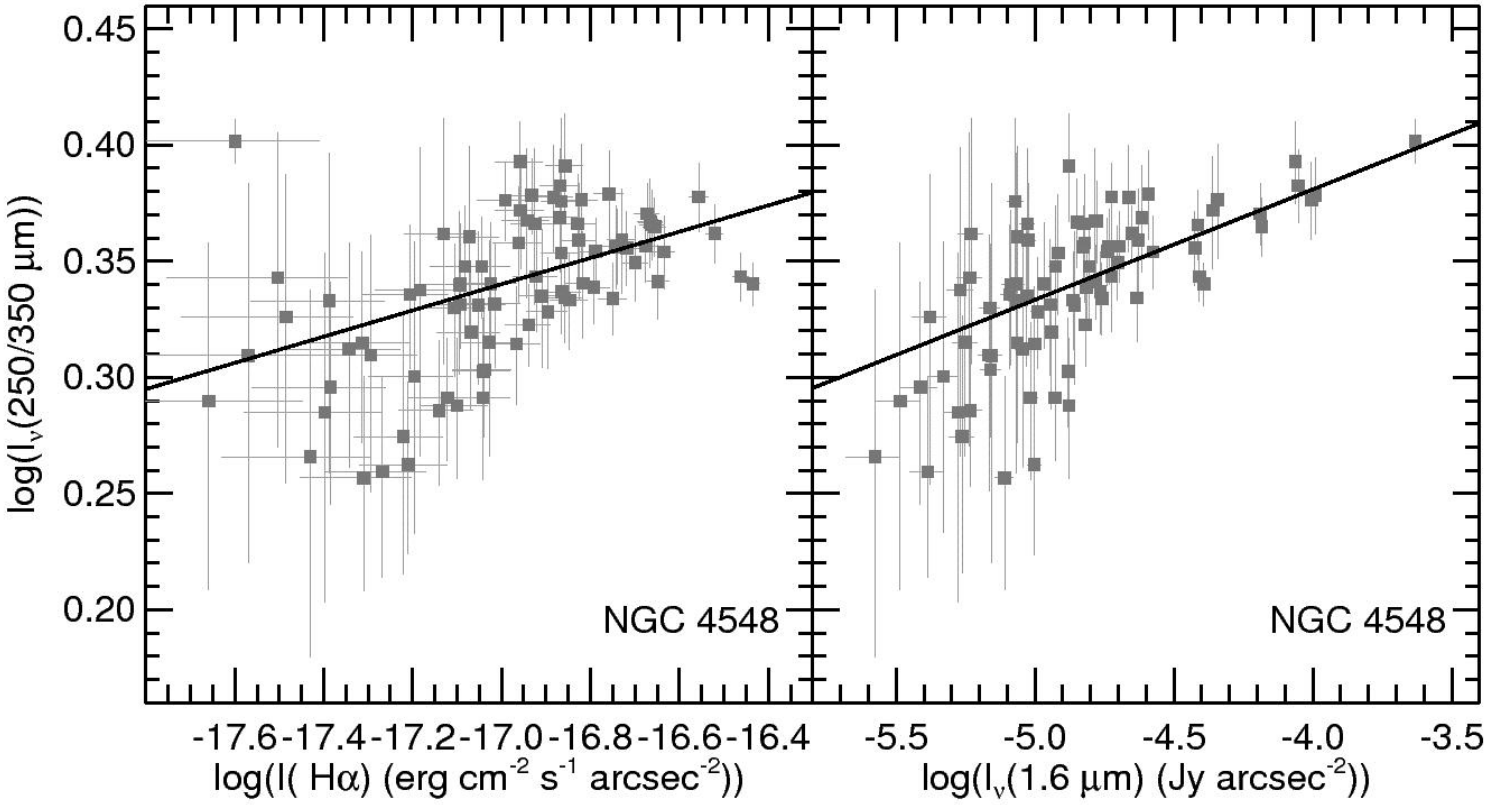
0.45
0.40
0.35
0.30
0.25
0.20
log(I$_\nu$(250/350 μm))
NGC 4548
NGC 4548
-17.6 -17.4 -17.2 -17.0 -16.8 -16.6 -16.4
log(I(Hα) (erg cm^{-2} s^{-1} arcsec^{-2}))
-5.5 -5.0 -4.5 -4.0 -3.5
log(I$_\nu$(1.6 μm) (Jy arcsec^{-2}))

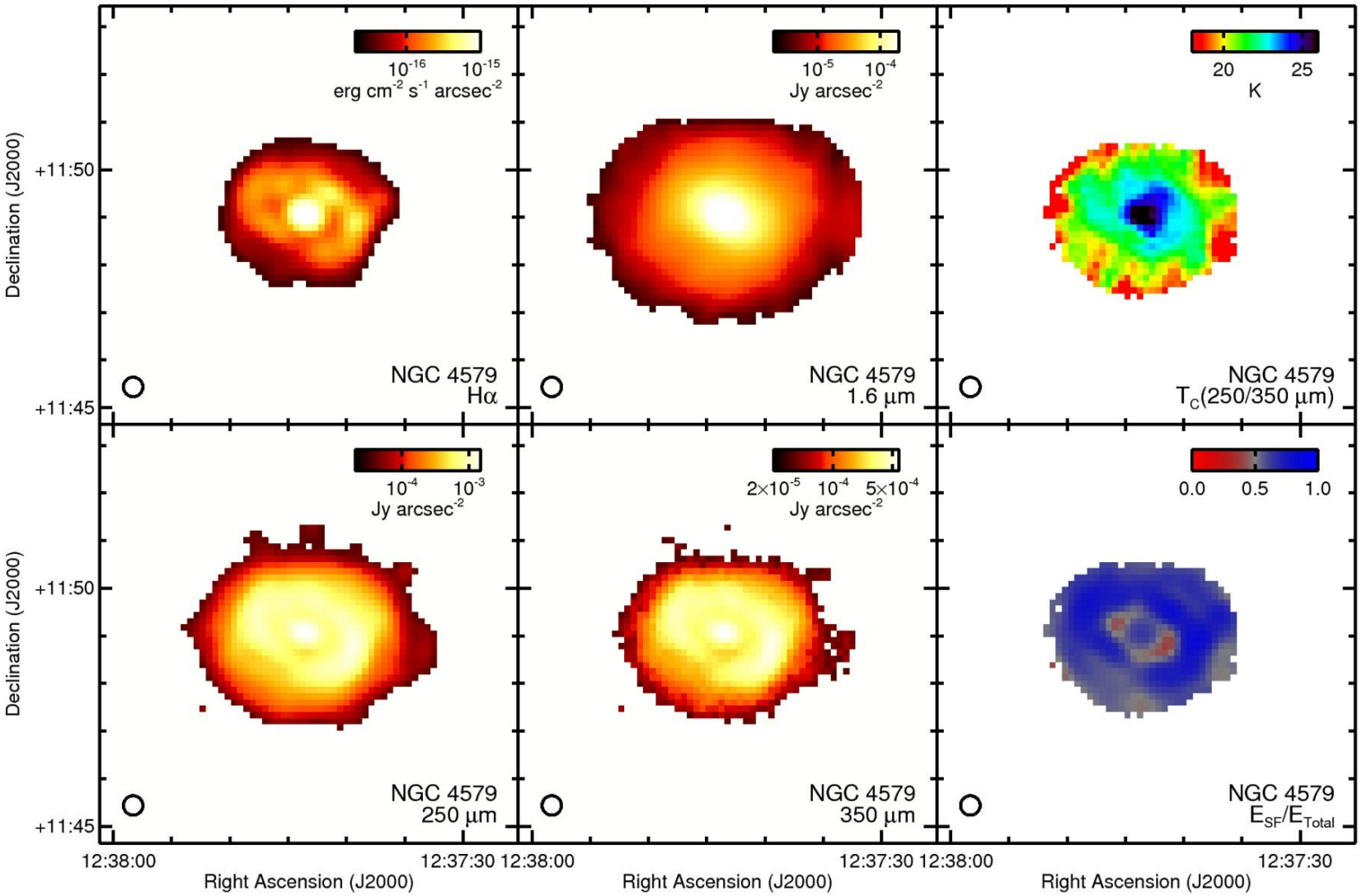
10^-16 10^-15
erg cm^-2 s^-1 arcsec^-2
NGC 4579
Hα
10^-5 10^-4
Jy arcsec^-2
NGC 4579
1.6 μm
20 25
K
NGC 4579
T_C(250/350 μm)
10^-4 10^-3
Jy arcsec^-2
NGC 4579
250 μm
2×10^-5 10^-4 5×10^-4
Jy arcsec^-2
NGC 4579
350 μm
0.0 0.5 1.0
NGC 4579
E_SF/E_Total
Declination (J2000)
+11:50
+11:45
12:38:00
12:37:30
Right Ascension (J2000)

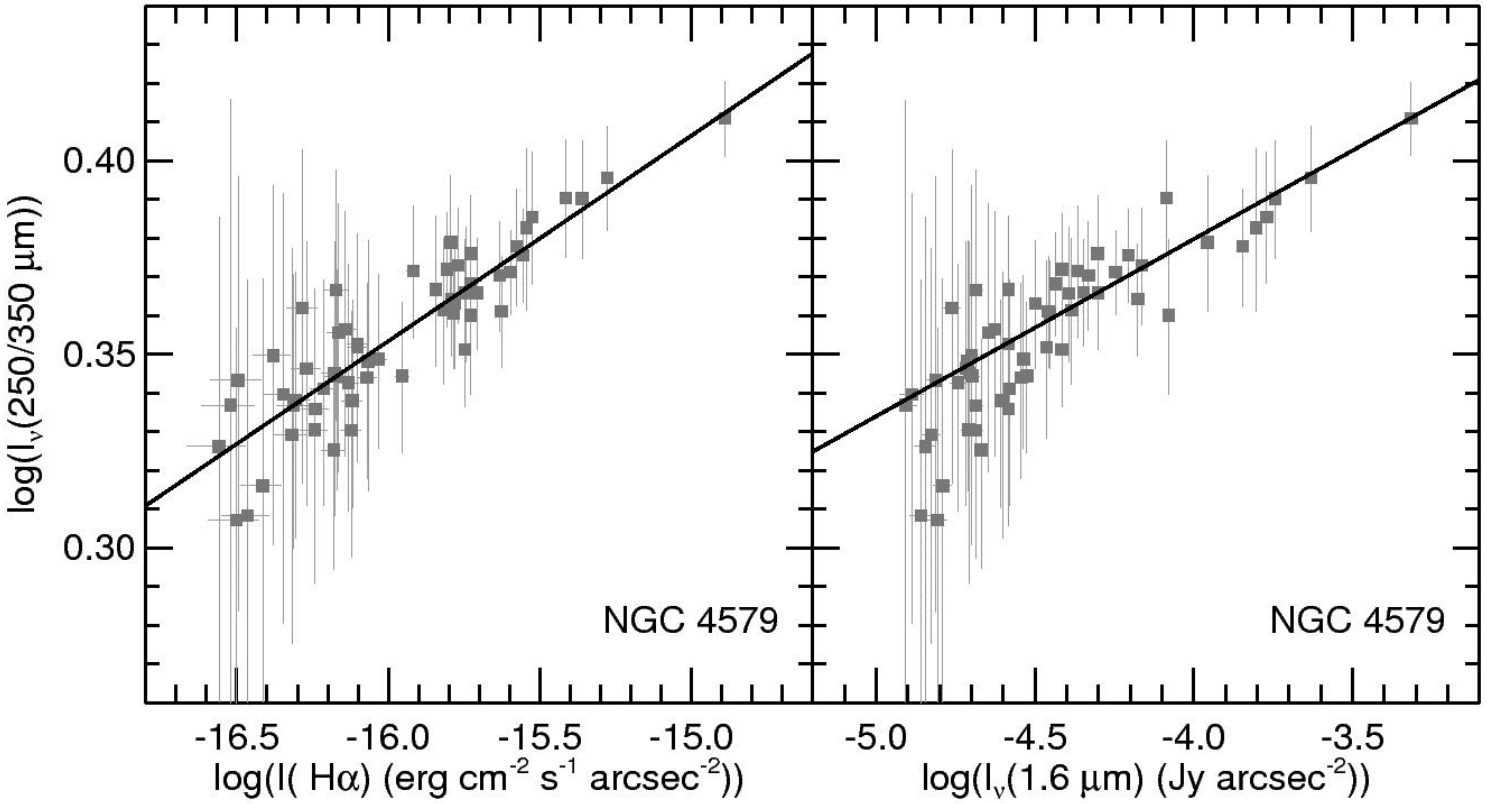
0.40
0.35
0.30
log(I$_\nu$(250/350 μm))
NGC 4579
-16.5
-16.0
-15.5
-15.0
log(I(Hα) (erg cm^{-2} s^{-1} arcsec^{-2}))
NGC 4579
-5.0
-4.5
-4.0
-3.5
log(I$_\nu$(1.6 μm) (Jy arcsec^{-2}))

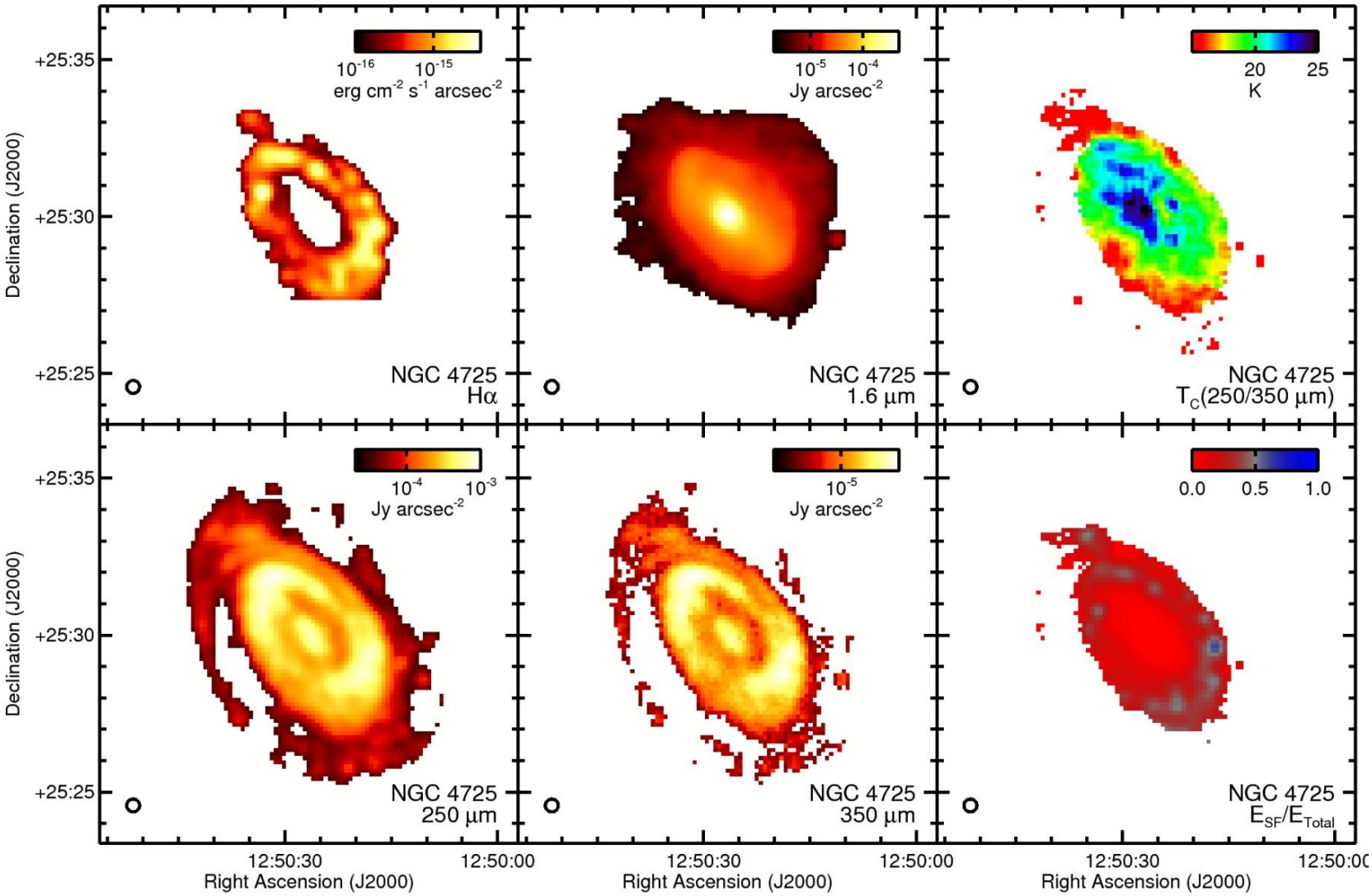
10^-16 10^-15
erg cm^-2 s^-1 arcsec^-2
NGC 4725
Hα
10^-5 10^-4
Jy arcsec^-2
NGC 4725
1.6 μm
20 25
K
NGC 4725
T_C(250/350 μm)
10^-4 10^-3
Jy arcsec^-2
NGC 4725
250 μm
10^-5
Jy arcsec^-2
NGC 4725
350 μm
0.0 0.5 1.0
NGC 4725
E_SF/E_Total
Declination (J2000)
+25:35
+25:30
+25:25
12:50:30
12:50:00
Right Ascension (J2000)

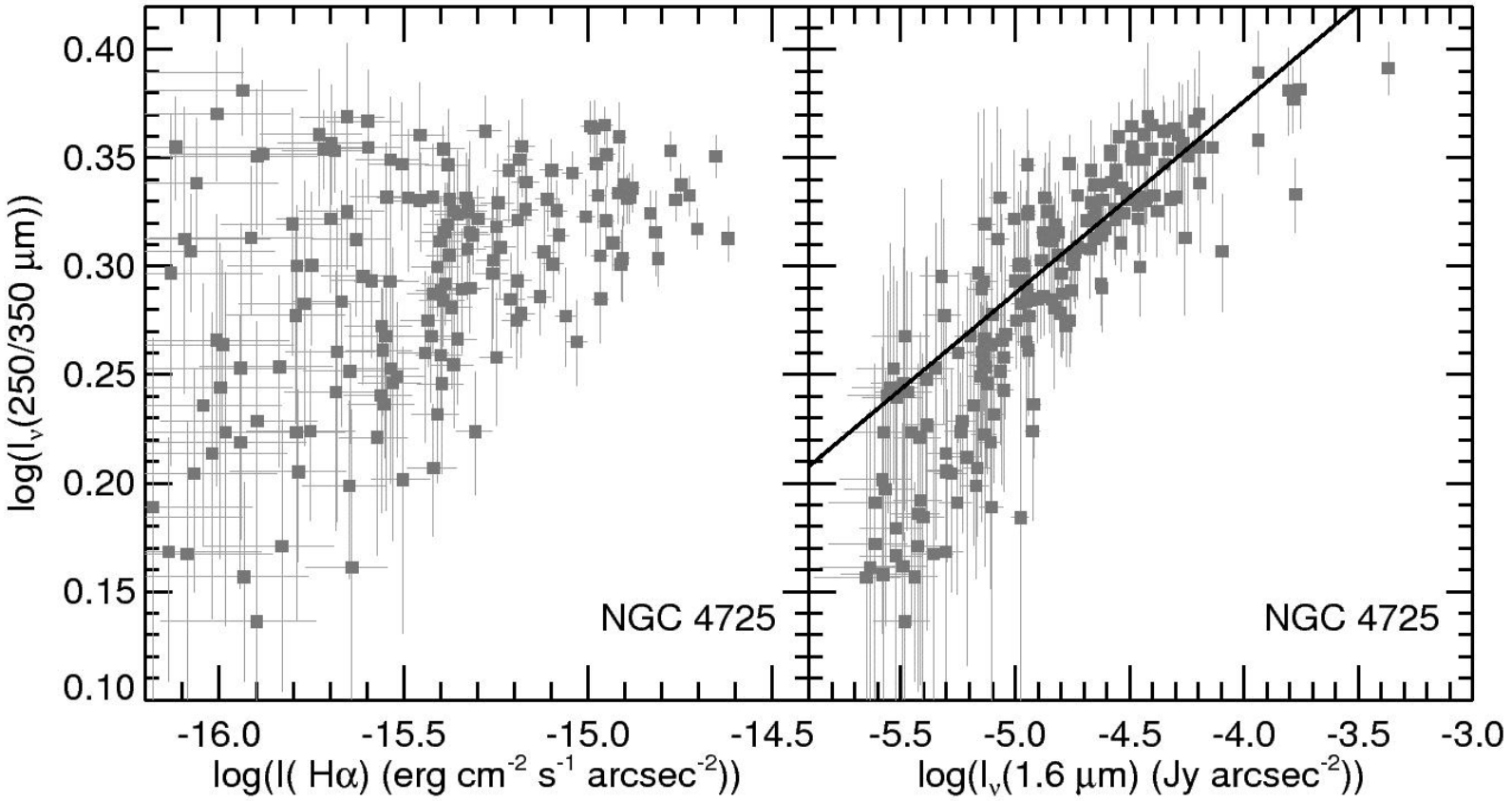
0.40
0.35
0.30
0.25
0.20
0.15
0.10
log(I$_\nu$(250/350 μm))
NGC 4725
NGC 4725
-16.0
-15.5
-15.0
-14.5
log(I(Hα) (erg cm^{-2} s^{-1} arcsec^{-2}))
-5.5
-5.0
-4.5
-4.0
-3.5
-3.0
log(I$_\nu$(1.6 μm) (Jy arcsec^{-2}))

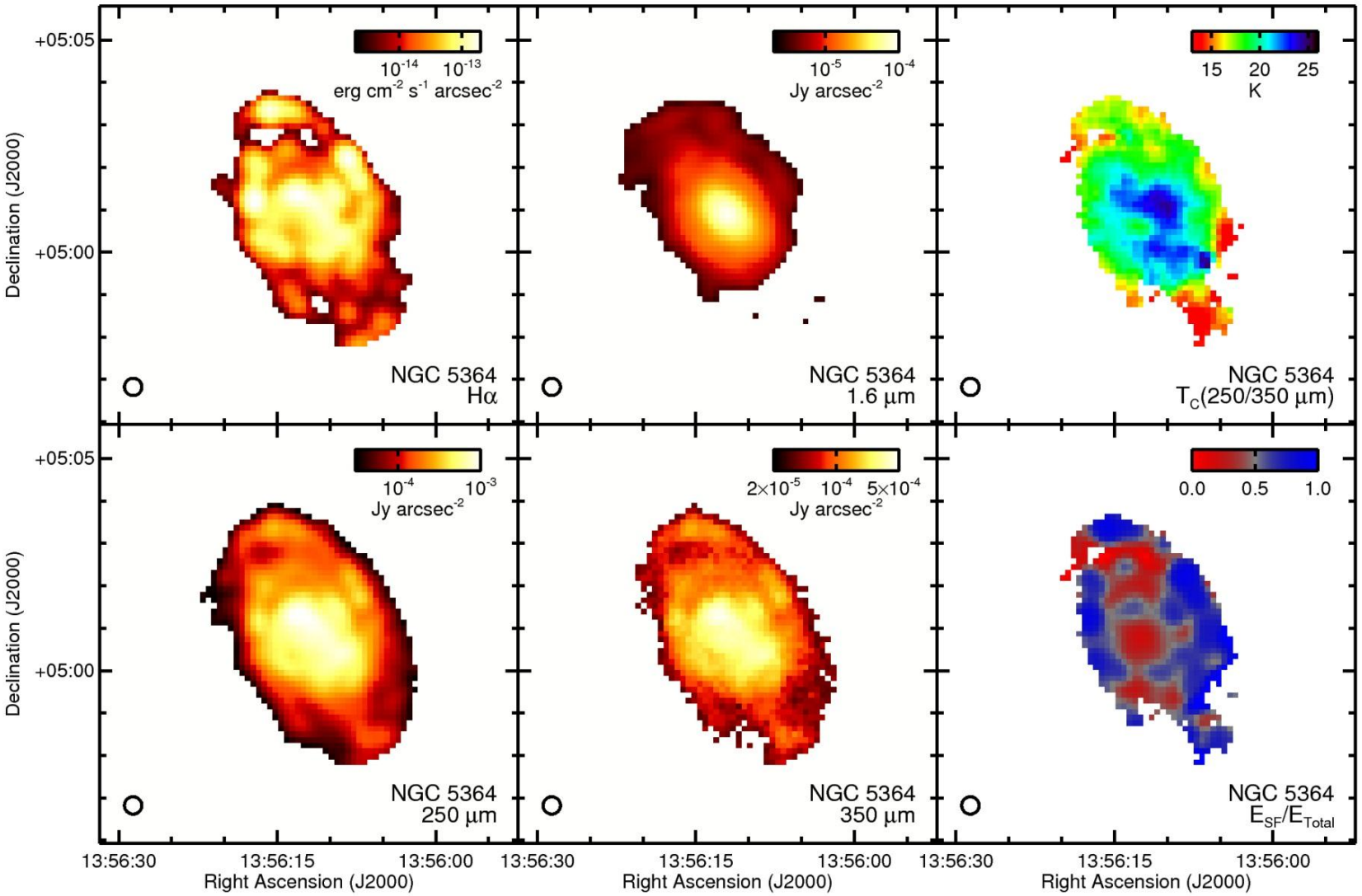
+05:05
+05:00
Declination (J2000)
10^{-14} 10^{-13}
erg cm^{-2} s^{-1} arcsec^{-2}
NGC 5364
Hα
10^{-5} 10^{-4}
Jy arcsec^{-2}
NGC 5364
1.6 μm
15 20 25
K
NGC 5364
T_C(250/350 μm)
10^{-4} 10^{-3}
Jy arcsec^{-2}
NGC 5364
250 μm
2×10^{-5} 10^{-4} 5×10^{-4}
Jy arcsec^{-2}
NGC 5364
350 μm
0.0 0.5 1.0
NGC 5364
E_{SF}/E_{Total}
13:56:30 13:56:15 13:56:00
Right Ascension (J2000)

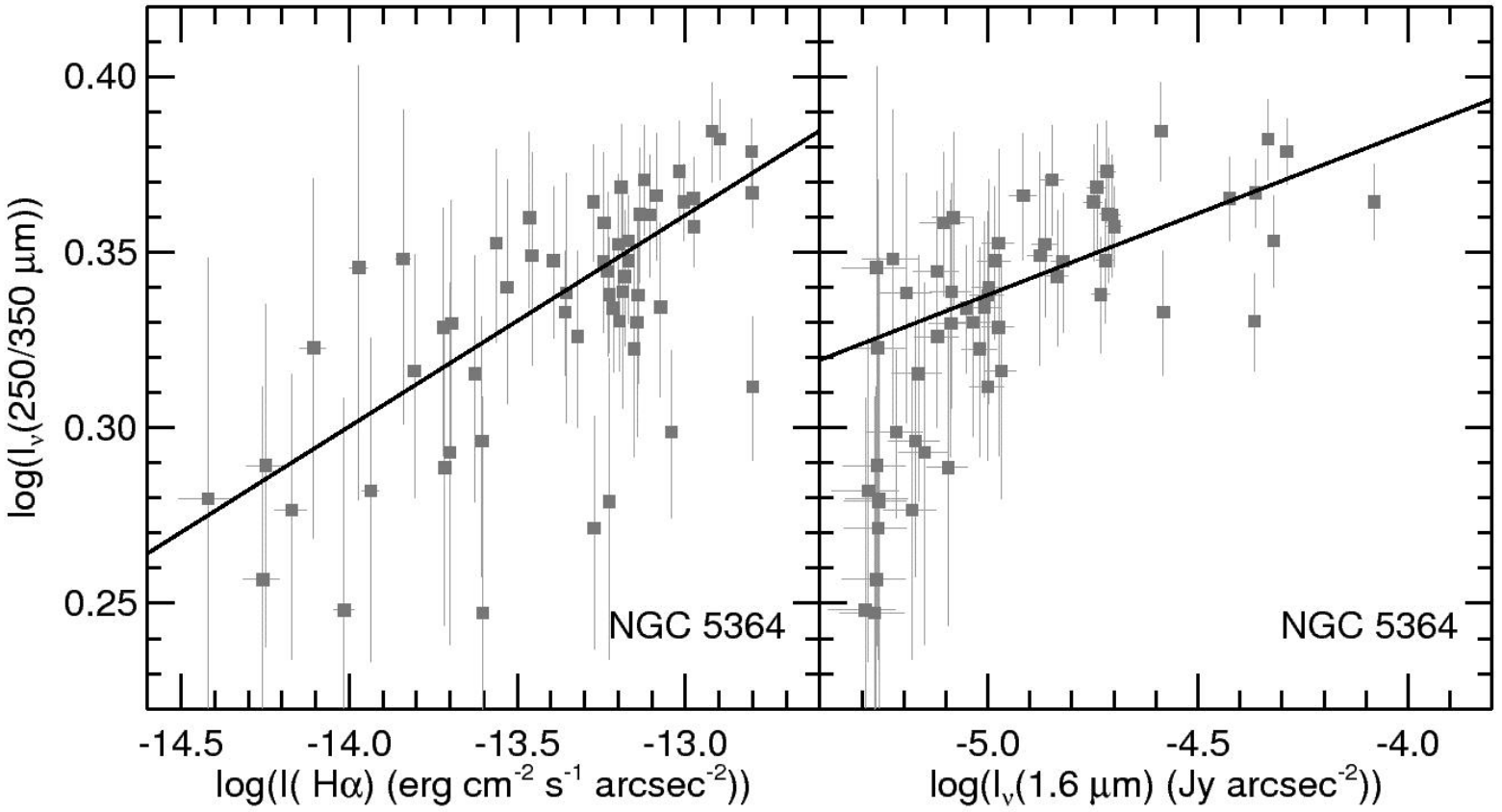
0.40
0.35
0.30
0.25
log(I$_\nu$(250/350 μm))
NGC 5364
NGC 5364
-14.5
-14.0
-13.5
-13.0
log(I(Hα) (erg cm^{-2} s^{-1} arcsec^{-2}))
-5.0
-4.5
-4.0
log(I$_\nu$(1.6 μm) (Jy arcsec^{-2}))

Observational results

- In most field galaxies, 250/350 μm ratio is more dependent on 1.6 μm emission.

- In Virgo Cluster galaxies and NGC 5364, 250/350 μm ratio is more dependent on Hα emission.

We tried associating E_{SF}/E_{total} with other galaxy properties and had limited success with finding any meaningful relations in the data.

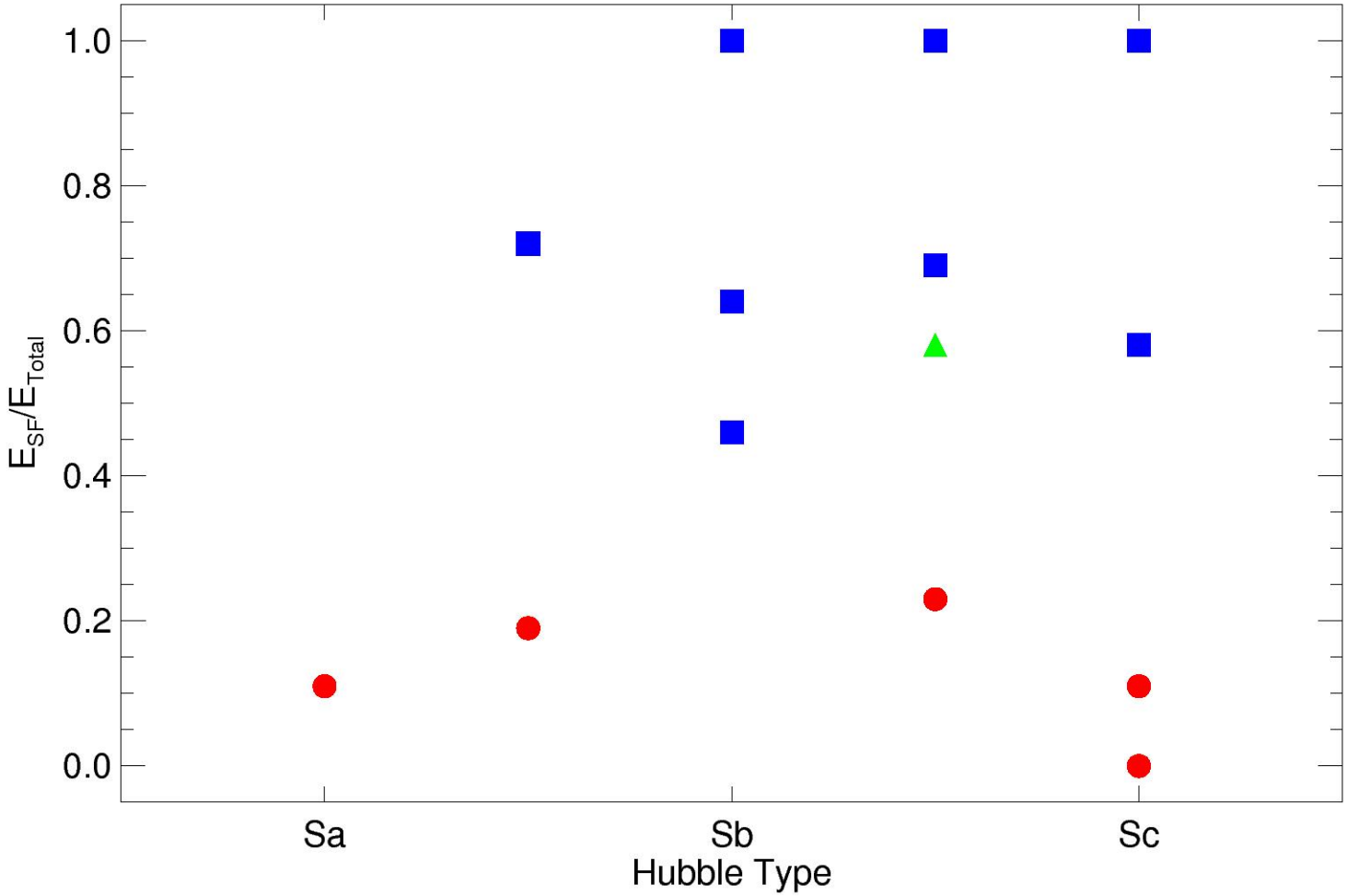
1.0
0.8
0.6
0.4
0.2
0.0
E_{SF}/E_{Total}
Sa
Sb
Sc
Hubble Type

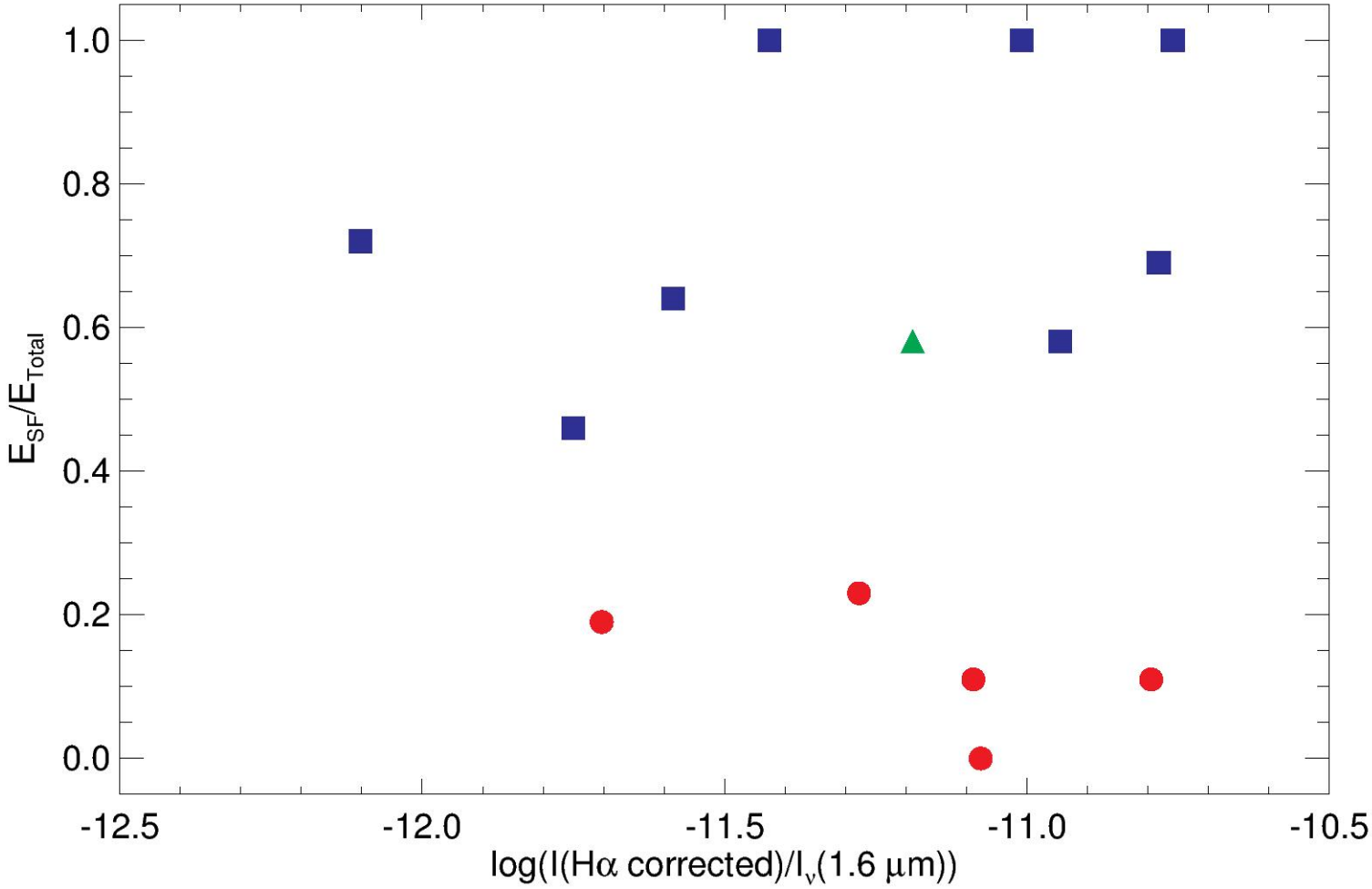
1.0
0.8
0.6
0.4
0.2
0.0
E_{SF}/E_{Total}
-12.5
-12.0
-11.5
-11.0
-10.5
log(I(Hα corrected)/I_ν(1.6 μm))

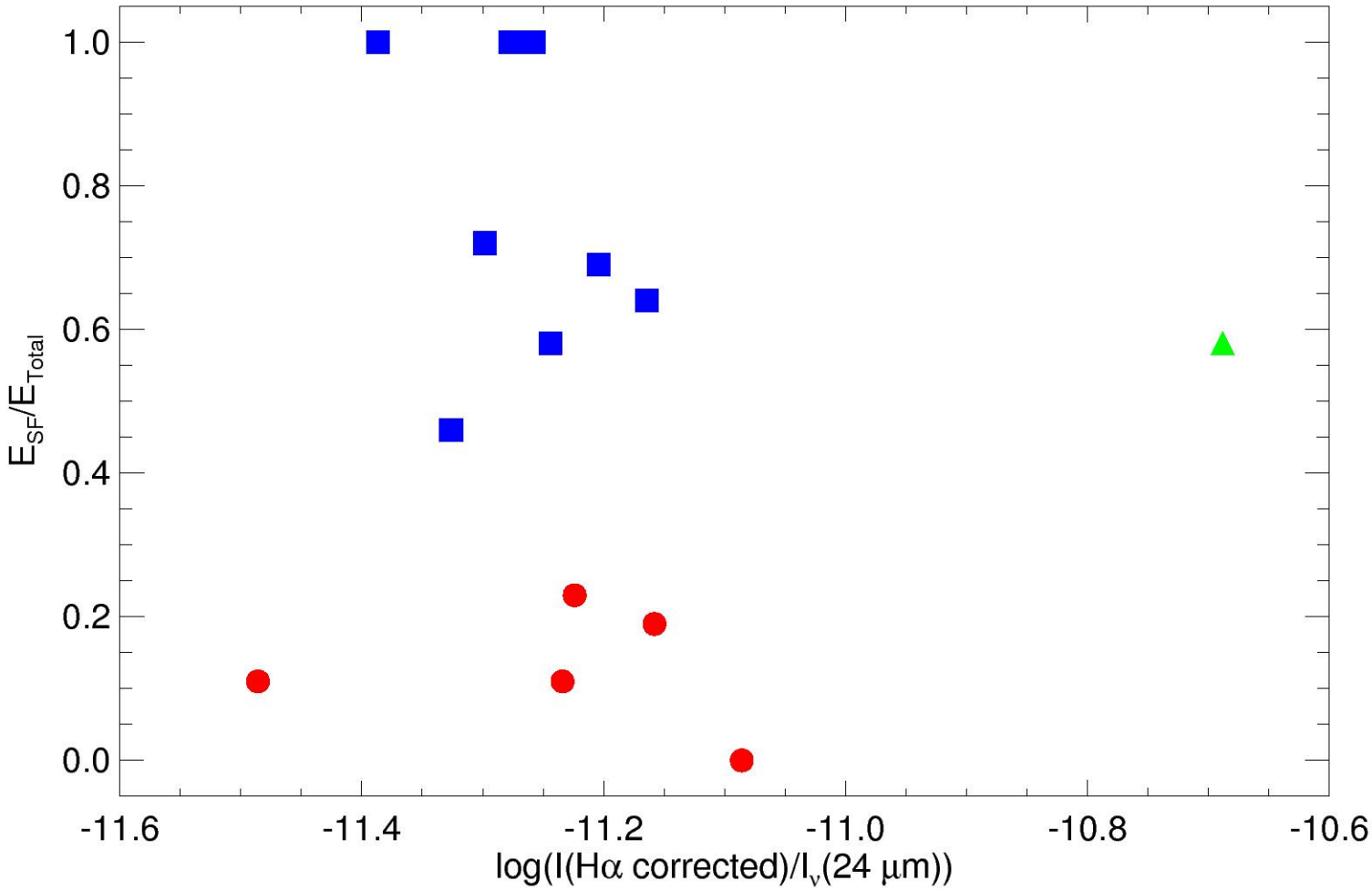
1.0
0.8
0.6
0.4
0.2
0.0
E_{SF}/E_{Total}
-11.6
-11.4
-11.2
-11.0
-10.8
-10.6
log(I(Hα corrected)/I_ν(24 μm))

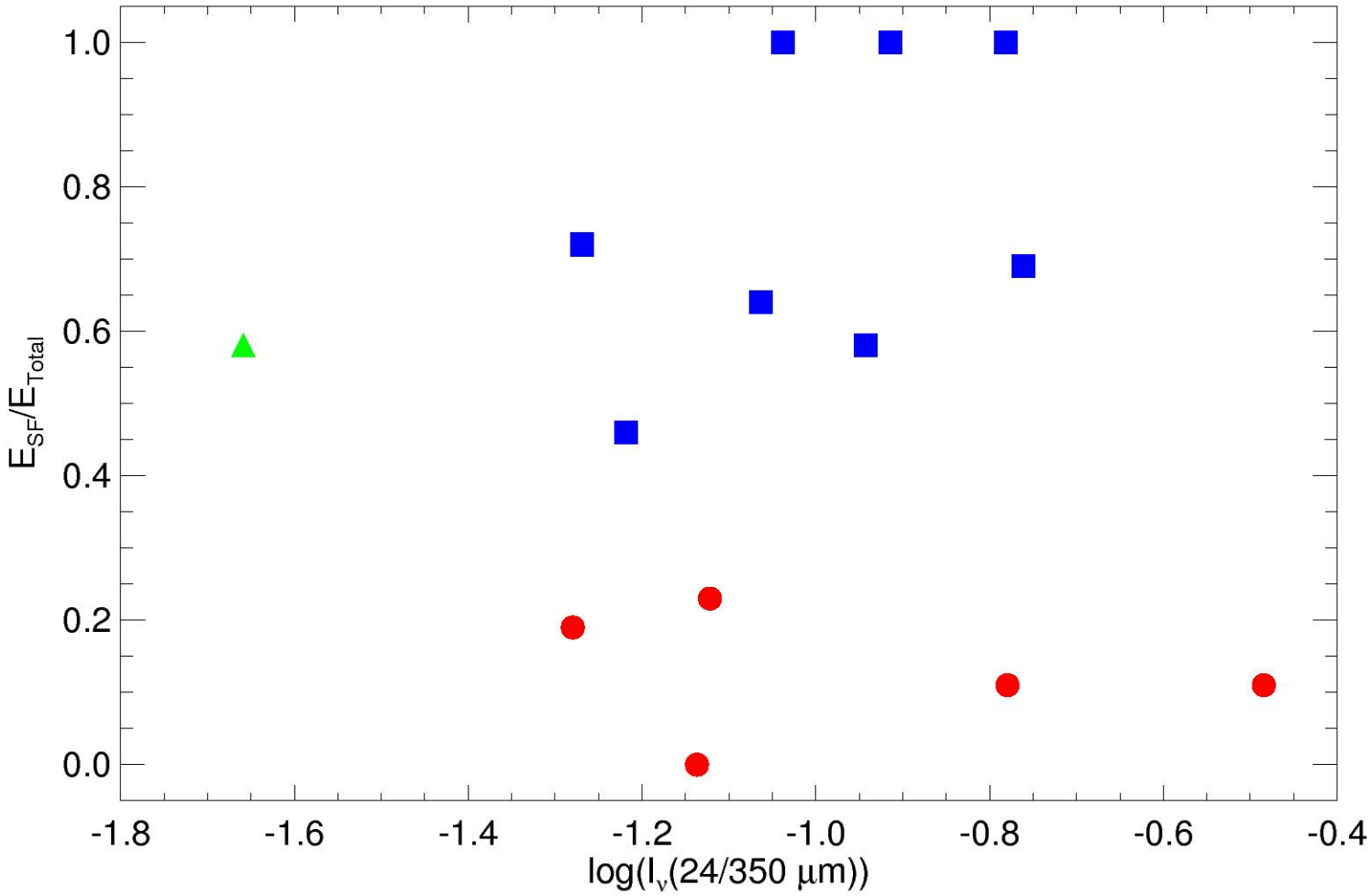
1.0
0.8
0.6
0.4
0.2
0.0
E_{SF}/E_{Total}
-1.8
-1.6
-1.4
-1.2
-1.0
-0.8
-0.6
-0.4
$\log(I_\nu(24/350\ \mu m))$

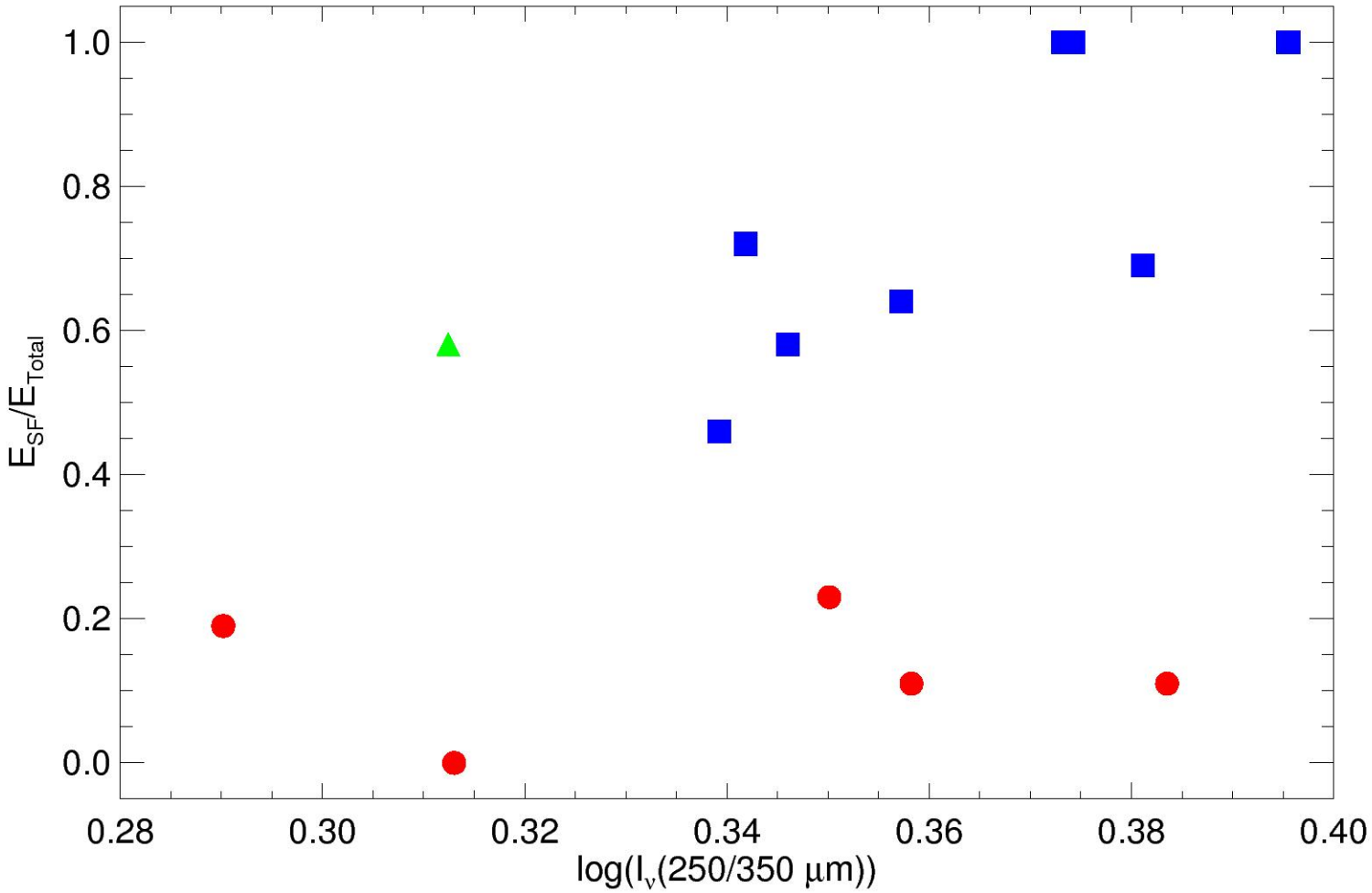
1.0
0.8
0.6
0.4
0.2
0.0
E_{SF}/E_{Total}
0.28
0.30
0.32
0.34
0.36
0.38
0.40
$\log(I_\nu(250/350\ \mu m))$

Troubleshooting

Could it be an issue with the observing mode?

No. We checked this with NGC 4254.

Could it be an issue with distance?

No. The sample galaxies are at similar distances. We also checked this with M81, M83, and NGC 2403.

Could it be an issue with using an optical star formation tracer?

No. Using 24 μm as a substitute can produce the same results.

Conclusions

- Herschel is detecting a colder thermal component of dust emitting at >250 μm that was missed by prior telescopes.
- This colder dust is heated by the total stellar population, not star forming regions.
- The emission from the cold component can still be related to star formation through the Schmidt law.
- The component is present in most field spiral galaxies and some infrared-bright high-redshift sources.
- The component may be absent in dwarf galaxies and cluster spiral galaxies. It is unclear why.